Part I: Self-Assembly, Stability Quantification, Controlled Molecular Switching, and Sensing Properties of an Anthracene-Containing Dynamic [2]Rotaxane

Part II: Substituent Effect in Imine-Containing Molecular Tweezers

WONG, Wing Yan

A Thesis Submitted in Partial Fulfillment of
the Requirements for the Degree of
Master of Philosophy
in
Chemistry

The Chinese University of Hong Kong
August 2010

Thesis Committee

Professor Tony Kung-Ming Shing (Chair)
(Department of Chemistry, The Chinese University of Hong Kong)

Professor Ken Cham-Fai Leung (Thesis Supervisor)
(Centre of Novel Functional Molecules,
Department of Chemistry, The Chinese University of Hong Kong)

Professor Pui-Chi Lo (Committee Member)
(Department of Chemistry, The Chinese University of Hong Kong)

Professor Wing-Hong Chan (External Examiner)
(Department of Chemistry, Hong Kong Baptist University)

Contents

Part II: Substituent Effect in Imine-Containing Molecular Tweezers

Acknowledgements

I would like to give my sincere thanks to my supervisor, Prof. Ken Cham-Fai Leung for his continuous guidance and kind suggestions during my M. Phil. project. He is not only an enthusiastic researcher, but also a mentor who demonstrates great patience and forgiveness and offers encouragement during my study.

I especially present my gratitude to my seniors, Dr. Siu-Yin Cheung, Mr. Chun-Ho Wong and Dr. Kwun-Ngai Lau for their enlightenment and invaluable teaching throughout my summer research in 2006 and 2007 and thereafter M. Phil. study. Thanks are also given to my fellow group members, including Dr. Shouhu Xuan, Mr. Chun-Pong Chak, Mr. Long-Ho Chau and Mr. Siu-Fung Lee for their helpful discussion and support.

Lastly, I wish to thank my parents, brothers and NaCl for their endless love and tolerance, especially during the preparation of this thesis.

July 2010,

Wing-Yan Wong

Department of Chemistry,

The Chinese University of Hong Kong,

Hong Kong, HKSAR

Abstract

This thesis is divided into two sections. The first part of the thesis includes the self-assembly and characterization of an anthracene-containing dynamic [2]rotaxane. By appealing to the ability of the anthracene ring system (one of the two stoppers associated with the dumbbell) to act as a fluorescent probe, the fluorescence and fluorescence-quenching nature of the dynamic rotaxane in an equilibrium mixture has been investigated and quantified in the presence of external stimuli such as water, acids, salts, and an amine. The stability, as expressed by the hydrolysis of the dynamic rotaxane has been monitored by following (i) the anthracene fluorescence and (ii) the movements of the signals in the ^{1}H NMR spectrum. Furthermore, it has been established that the anthracene fluorescence of the dynamic rotaxane rises with an increasing concentration of acid. Two acid sensors have been identified with different operating modes—namely, logarithmic and linear. The combination of different inputs involving water, acids, salts and an amine leads to different fluorescence outputs from the dynamic rotaxane, hence producing a prototype for expressing molecular logic.

The second section of the thesis illustrates complexations between two different ammonium threads and a series of diimine-containing molecular tweezers with various substituents. The substituent effect in the molecular tweezers towards

selected threads *via* multiple supramolecular interactions was studied. The binding constants of the complexes were determined by NMR and UV/visible absorption spectroscopies. Stoichiometries of the complexes were determined by their Job plots.

摘要

本論文分成兩部份。論文的首部份敘述了以蒽為封端基的動態[2]輪烷的自組裝及表徵。由於蒽環系統的感應特性，該動態輪烷可以用作各種化學環境的螢光探針。本工作通過蒽的螢光及氫譜中訊號的移動，監測動態輪烷對抗水解的穩定性。探討了在不同外界刺激如水、酸、鹽及胺類條件下動態輪烷的螢光發射和螢光淬滅特性，並得到了相應的量化結果。研究發現，當酸類的濃度增加，動態輪烷中蒽的螢光也相繼增強。根據結果，我們可以建立線性及對數性運作模式的兩個酸感應器。由於輸入不同水、酸、鹽及胺類組合，動態輪烷能輸出不同螢光，這為分子邏輯學研究提供了非常合適的雛型。

論文第二部份介紹了由一系列雙亞胺分子鉗及兩個銨鹽啞鈴組成的複合物，並研究分子鉗的取代基對於以多樣超分子相互作用生成的複合物的影響。通過氫譜及紫外線/可見光譜計算複合物的錯合常數，並以Job Plot推算出其化學計量比。

Abbreviations and Acronyms

Δ	Change; Heating
2D	Two-dimensional
Å	Ångström
Ar	Aromatic
a.u.	Arbitrary unit(s)
br	Broad (spectral)
^{t}Bu	*tert*-Butyl
^{t}BuOMe	*tert*-Butyl methyl ether
°C	Degree Celsius
calcd	Calculated
CB[6]	Cucurbit[6]uril
$CBPQT^{4+}$	Cyclobis(paraquat-*p*-phenylene)
CT	Charge-transfer
CV	Cyclic voltammetry
δ	Chemical shift in parts per million
δ_{obs}	Observed chemical shift in parts per million
δ_c	Chemical shift of complex in parts per million
D	Density
d	Day(s); Doublet (spectral)
DB24C8	Dibenzo[24]crown-8
DCM	Dichloromethane
DMF	*N*,*N*-Dimethylformamide
DMSO	Dimethyl sulfoxide
DNP	1,5-Dioxynaphthalene
EDC	1-Ethyl-3-(3-dimethyl-aminopropyl)carbodiimide
equiv.	Equivalent
ESI	Electrospray ionization
Et	Ethyl
Et_2O	Diethyl ether
EtOAc	Ethyl acetate
EtOH	Ethanol
g	Gram(s)
h	Hour(s)
HOSu	*N*-Hydroxysuccinimide
HRMS	High-resolution mass spectrometry
Hz	Hertz
J	Coupling constant
K	Kelvin
K_a	Binding constant
λ_{max}	Maximum wavelength
L	Liter(s)
LAH	Lithium aluminum hydride
μ	Micro
m	Multiplet (spectral); Meter (s)
M	Molar (moles per liter); Mega
M	Formula weight
M^+	Parent molecular ion
Me	Methyl
MeCN	Acetonitrile
mL	Milliliter(s)
$MeNO_2$	Nitromethane
MeOH	Methanol
MHz	Megahertz
min	Minute(s)
mM	Millimole(s) per liter
mmol	Millimole(s)
MNPs	Metal nanoparticles
mol	Mole(s)
m.p.	Melting point (range)
MS	Mass spectrometry
MS4A	Molecular sieve (4 Å)
*m*SAMS	*mixed* Self-assmbled monolayers
mV	Millivolt(s)
m/*z*	Mass-to-charge ratio
n.a.	Not available

n.d.	Not determined
NEMS	Nanoelectromechanical system
nm	Nanometer(s)
NMR	Nuclear magnetic resonance
NOE	Nuclear overhauser effect
NOESY	Nuclear overhauser effect spectroscopy
NP	Nanoparticle
OMe	Methoxy
p	*para*
PET	Photoinduced electron transfer
PhMe	Toluene
ppm	Part(s) per million
^{i}Pr	*iso*-Propyl
q	Quartet (spectral)
quin	Quintet (spectral)
R	Substituent(s)
R^2	Correlation coefficient
R_f	Retention factor
r.t.	Room temperature
s	Singlet (spectral); Second(s)
t	Triplet (spectral); *tert*
$t_{1/2}$	Half-life
TCNB	1,2,4,5-Tetracyanobenzene
TFA	Trifluoroacetate / Trifluoroacetic acid
TfOH	Triflic acid
THF	Tetrahydrofuran
TLC	Thin layer chromatography
Tol	Tolyl, 4-methylphenyl
TTF	Tetrathiafulvalene
UV	Ultraviolet
vis	Visible light

Publications Originated from the Work of this Thesis

1. Leung, K. C.-F.; Chak, C.-P.; Lo, C.-M.; Wong, W.-Y.; Xuan, S.; Cheng, C. H. K., "pH-Controllable Supramolecular Systems", *Chem. Asian J.* **2009**, *4*, 364–381.
2. Leung, K. C.-F.; Wong, W.-Y.; Aricó, F.; Haussmann, P. C.; Stoddart, J. F., "The Stability of Imine-Containing Dynamic [2]Rotaxanes to Hydrolysis", *Org. Biomol. Chem.* **2010**, *8*, 83–89.
3. Wong, W.-Y.; Leung, K. C.-F.; Stoddart, J. F., "Self-Assembly, Stability Quantification, Controlled Molecular Switching, and Sensing Properties of an Anthracene-Containing Dynamic [2]Rotaxane", *Org. Biomol. Chem.* **2010**, *8*, 2332–2343.
4. Leung, K. C.-F.; Lau, K.-N.; Wong, W.-Y., "Stabilities of Novel [2]Pseudorotaxanes Synthesized *via* Competitive Slippage Approach", submitted.
5. Wong, W.-Y.; Leung, K. C.-F., "Self-Assembly, Stability Quantification, Controlled Molecular Switching, and Sensing Properties of an Anthracene-Containing Dynamic [2]Rotaxane", *Abstract of "The Seventeenth Symposium on Chemistry Postgraduate Research in Hong Kong"* **2010**, Hong Kong SAR, China, p. O-26.

Part I

Self-Assembly, Stability Quantification, Controlled Molecular Switching, and Sensing Properties of an Anthracene-Containing Dynamic [2]Rotaxane

Chapter 1 – Introduction

1.1 Definition of Rotaxane

The idea of a rotaxane was first reported in 1961[1] and was synthetically realized in 1967.[2] A rotaxane (Latin: *rota*: wheel; *axis*: axle)[3] consists of a dumbbell (I-, H-, X-, Y- or bar-shaped) interlocked in one or more macrocycles (Figure 1-1). The bulkiness of the end groups prevents the extrusion of the macrocycles from the dumbbell. The number of molecular sub-entities participating in mechanical bonding in a rotaxane is given in square bracket at the beginning of the name. If one or more molecular elements are connected by a covalent bond (Figure 1-1c), the numbers of building blocks, in the order of wheel then axle, is used instead, with a hyphen symbolizing the covalent linkage.[4]

The components are mechanically linked together unless any covalent bond on either the dumbbell or macrocycle is broken. This structure allows large amplitude sub-molecular motions, including translation and pirouetting of the macrocycle along the thread.[5]

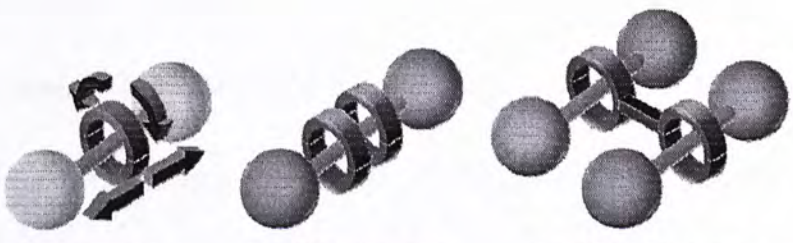

(a) [2]Rotaxane (b) [3]Rotaxane (c) [2-2]Rotaxane

Figure 1-1. Schematic representation of a [2]rotaxane, [3]rotaxane, and [2-2]rotaxane. The arrows show the possible motions of the macrocycle.

The first rotaxane synthesis (a [2]rotaxane, Scheme 1-1a) was reported by Harrison and Harrison in 1967.[2] Their method has been named as "threading-followed-by-stoppering". To begin with, a macrocycle was threaded through statistically to a linear molecule to give a [2]pseudorotaxane. [2]Pseudorotaxane is a compound that is similar to a [2]rotaxane except that the thread is free to move into or out from the macrocycle. Then, the two ends of the [2]pseudorotaxane was reacted with two "stopper" bulky molecules,[6] resulting in the formation of the first [2]rotaxane with a low yield (6 %). Another traditional method, on the other hand, is called "clipping"[6] (Scheme 1-1b), whereas a dumbbell is preorganized with an acyclic precursor, followed by macrocyclization with covalent bonds. Since these rotaxane syntheses involve kinetically controlled and covalent bond-forming processes, undesired and irreversible side-products are inevitably formed that would greatly reduce the overall product efficiency.

In contrast, rotaxanes can be prepared by a thermodynamically-controlled slippage approach[7] (Scheme 1-1c), in which a size-complementary dumbbell thread squeezes through a macrocycle upon heating and remains interlocked after cooling down to ambient temperature. In the absence of an efficient template, however, rotaxane was obtained in a very low yield.[7a] High-yield slippage approach can be achieved by stabilization by multiple noncovalent interactions between the rod and

ring components.[7b] Noticeably, rotaxanes formed by slippage are only stable in appropriate conditions.[8] They are susceptible to dissociation at elevated temperature or upon the change of solvent's polarity or acidity.

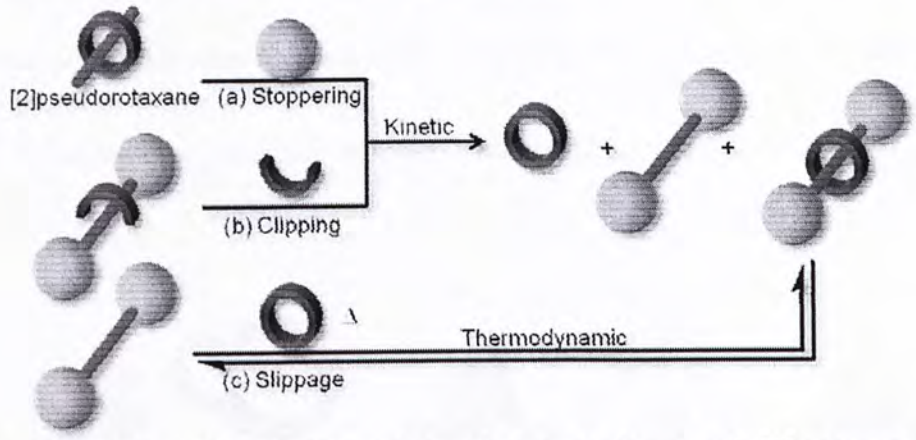

Scheme 1-1. Schematic representation of the syntheses of [2]rotaxane by (a) threading-followed-by-stoppering, (b) clipping under kinetic control, and (c) slippage under thermodynamic control.

After a long-lasting 30 years or so development of rotaxane synthesis, new methods have been recently appeared. Asakawa reported a new synthetic method namely, threading-followed-by-shrinking (Scheme 1-2a).[9] This method first involves a threading process between a relatively large macrocycle and a dumbbell to form a [2]pseudorotaxane complex. Subsequently, the macrocycle's void cavity was shrunk through coordination of an additional transition metal cation. A [2]rotaxane was formed in good yield.

Recently, Chiu's group reported another method for rotaxane synthesis, namely, threading-followed-by-swelling (Scheme 1-2b).[10] Two components, (i) a regular macrocycle; and (ii) a thread that contains a bulky stopper at one end and a smaller

stopper (but enlargeable) at another end, were mixed. The macrocycle was threaded through the smaller stopper of the thread to form a [2]pseudorotaxane complex. Subsequent elevation of temperature of the pseudorotaxane mixture triggered the activation of the kinetically controlled swelling process that enlarged the smaller stopper to become an effective stopper. Thus, a [2]rotaxane was formed in good yield.

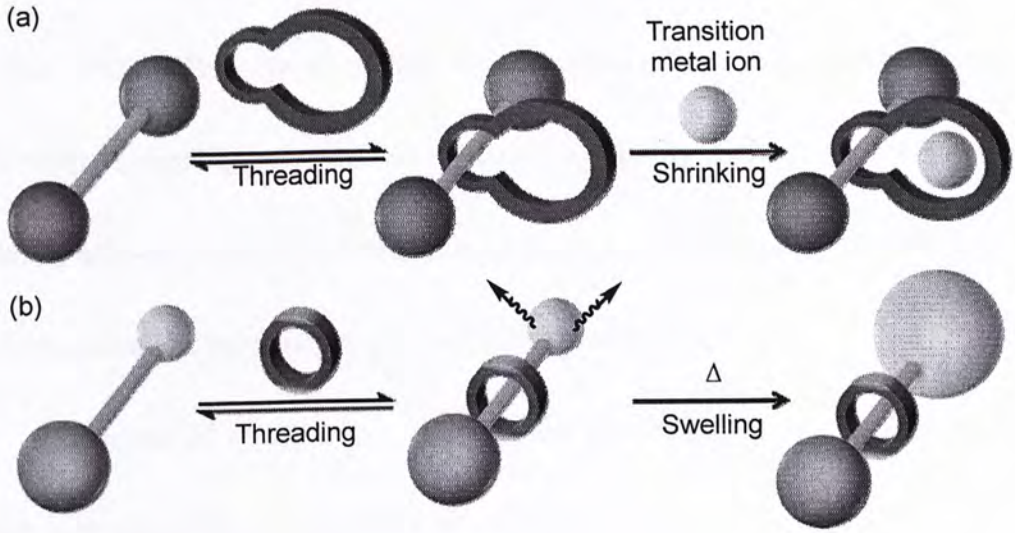

Scheme 1-2. Schematic representation of the syntheses of [2]rotaxane by (a) threading-followed-by-shrinking, and (b) threading-followed-by-swelling.

1.2 Dynamic Covalent Chemistry in Rotaxane Synthesis

Dynamic covalent chemistry (DCC)[11] opens the way of efficient syntheses of complicated macrocyclic and interlocked molecular compounds. The word "dynamic" highlights the reversibility of covalent bonds to be formed, broken and reformed under thermodynamic control. In such reactions, product distributions depend only

on the relative stabilities of final products. By (i) introducing complementary steric and electronic structural features into the starting components to stabilize the desired product; and (ii) driving the reaction equilibrium towards the desired product with the addition of excess amount of any starting component or subsequent removal of the product, the proportion of desired product(s) can be significantly amplified. Eventually, undesired products can be recycled back into the equilibrating mixture. Thus, DCC offers "proof-reading" and "error-checking" in organic synthesis. Another fascinating advantage of DCC over kinetically controlled reactions is the ability to re-adjust the product distribution by changing the reaction conditions, such as concentration, temperature, presence or absence of a template.

Examples of versatile reversible covalent functionalities used in DCC include esters, imines, hydrazones, oximes, disulfides and olefin functionalities.[12]

1.3 Thermodynamic Template

A template takes up an essential role in the syntheses of well-defined macrocycles and interlocked molecules. It coordinates separate components in a desired configuration and promotes a chemical reaction out of the numerous possible ones that leads to the target molecule. The templating strategy can be used under kinetic or thermodynamic control, yet showing a significant distinction (Scheme

1-3).[11] A kinetic template influences the mechanistic pathway by binding with the separate species, bringing the reaction sites into proximity and thus accelerating the formation of a particular macrocycle. In contrast, a thermodynamic template biases and amplifies exclusively the formation of a specific macrocycle by binding it complementarily from an equilibrating mixture to form a relatively stable complex. The use of thermodynamic template allows precise control of molecular recognition, hence enables creation and discovery of complicated molecular and supramolecular architectures.

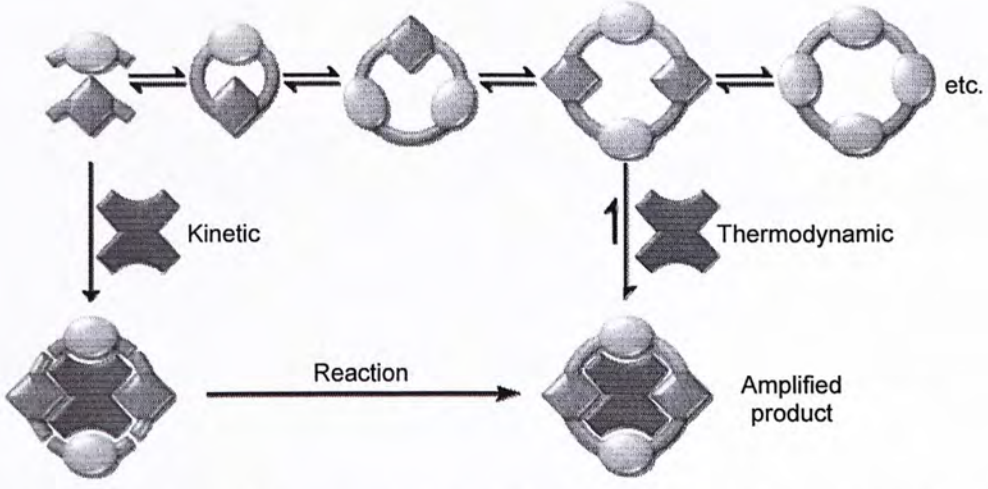

Scheme 1-3. A schematic representation of kinetic and thermodynamic templations.

In the context of thermodynamic templation,[13] noncovalent interactions are used as the glue between a template and precursors. Multiple hydrogen bonds by virtue of (i) [N^+–H···O] and [N^+C–H···O] in the case of secondary ammonium template and (ii) [N–H···O=C] in the case of amide template, are commonly occurred supramolecular

interactions. Other interactions may involve π–π stacking, π-donor/π-acceptor, and electrostatic interactions. Though some of the interactions are relatively weak, however, a precise molecular recognition between the template and the precursors can become feasible by cooperative, multiple supramolecular interactions.

With the aid of DCC and thermodynamic templation, extensive rotaxane syntheses were reported using the threading-followed-by-stoppering (Figure 1-2a),[14] clipping (Figure 1-2b)[15] and threading-stoppering-followed-by-clipping (Figure 1-2c)[16] methodologies under thermodynamic control.

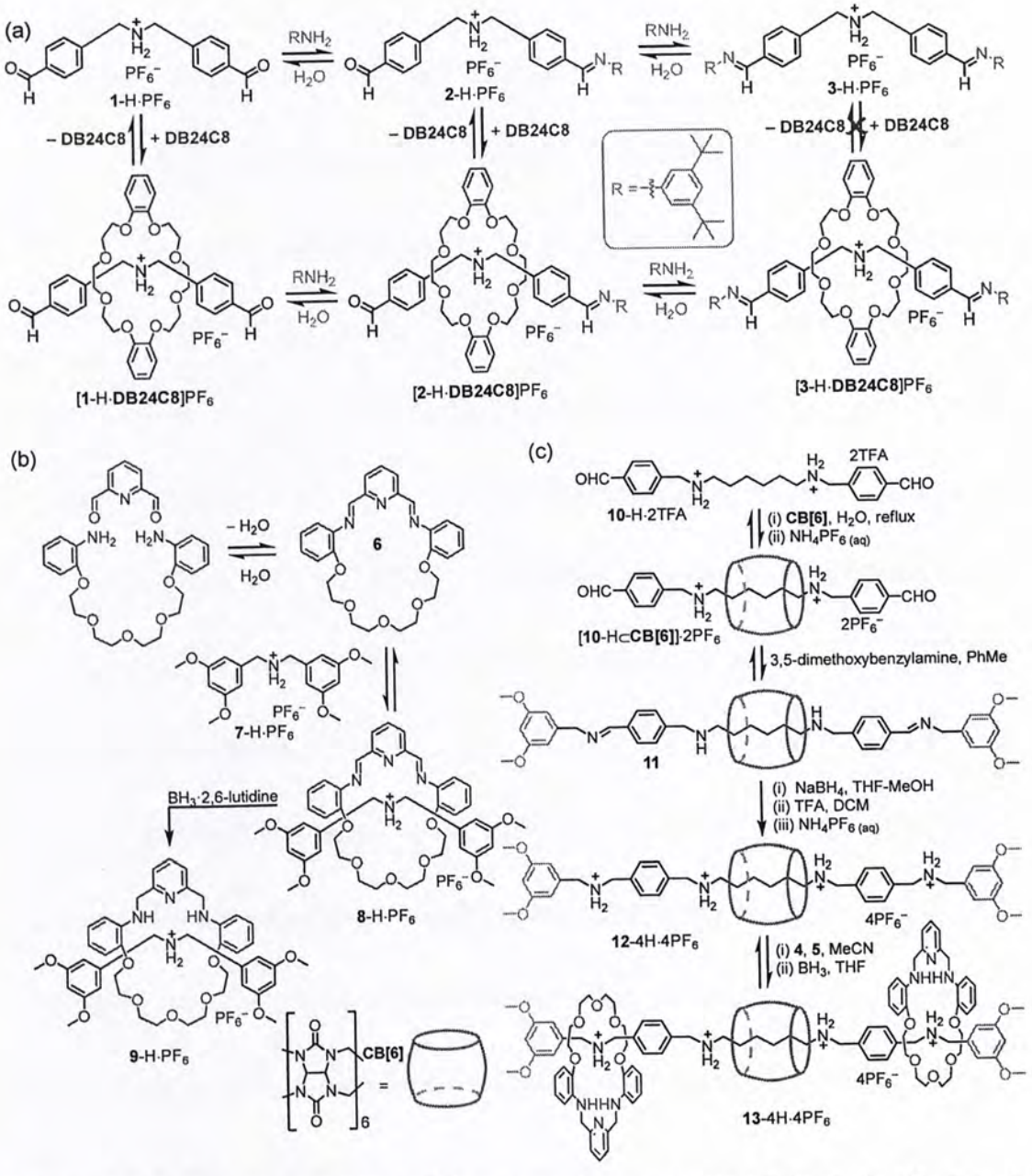

Figure 1-2. (a) Threading-followed-by-stoppering synthesis of dynamic [2]rotaxane [**3**-H·**DB24C8**]PF_6 using reversible imine formation/hydrolysis on the dumbbell with dibenzo[24]crown-8 (**DB24C8**); (b) Clipping synthesis of a [2]rotaxane using reversible imine formation/hydrolysis on the macrocycle with subsequent imine reduction to obtain kinetically stable [2]rotaxane **9**-H·PF_6; (c) Threading-stoppering-followed-by-clipping synthesis of hetero[4]rotaxane which involves (i) threading of a cucurbit[6]uril (**CB[6]**) onto the hexyl chain to form a [2]pseudorotaxane due to strong binding between the two dialkylammonium sites and **CB[6]**, (ii) stoppering through imine condensation followed by reduction/protonation to afford a kinetically stable [2]rotaxane and (iii) clipping of two macrocycles followed by reduction to afford a kinetically stable hetero[4]rotaxane **13**-4H·4PF_6.

1.4 Molecular Sensing Properties in Rotaxane

As discussed previously, most rotaxanes and pseudorotaxanes have been prepared by template-directed synthesis and that their intercomponent interactions can "live on" after self-assembly.[17] They can be manipulated to effect translational motion of the macrocycle (for rotaxanes), more accurately as co-conformational change,[18] or assembly/disassembly (for pseudorotaxanes) using external stimuli, both chemically (with acid/base, metal ions or redox reagents), photochemically and electrochemically, rendering the rotaxane-like molecules as an excellent candidate for molecular machines.[17]

Co-conformational change occurs explicitly in two-stationed [2]rotaxanes, also known as bistable [2]rotaxanes. An external stimulus chemically modifies the system and alters the noncovalent interactions such that the second station becomes energetically more favorable, causing translation of the macrocycle along the thread. This process can be achieved by either destabilizing the first station or increasing binding affinity of the second station. Application of a second chemical modification restores the initial co-conformation.[17] The shuttling of macrocycle can form the basis for devices that function through mechanical motion at molecular level. Usually, co-conformational change or assembly/disassembly switching processes are accompanied with fluorescence emission or visible color change,[19] for the sake of

convenient characerizations. Three examples of rotaxane with molecular sensing properties will be discussed.

Stoddart *et al.*[20] reported an anthracene-containing [2]pseudorotaxane [**14**-H⊂**DB24C8**]·PF_6 (Figure 1-3a) whose assembly and disassembly can be reversibly controlled with acid and base, showing fluorescence changes. Both the free amine thread **14** and **DB24C8** reveal their corresponding fluorescence emissions. Addition of acid such as trifluoroacetic acid (TFA) or triflic acid (TfOH) induces self-assembly between the ammonium thread [**14**-H]$^+$ and **DB24C8**, to form a [2]pseudorotaxane, due to significant [N^+–H···O] and [N^+C–H···O] hydrogen bond interactions. Upon excitation at 276 nm where most of the light was absorbed by **DB24C8**, the fluorescence of **DB24C8** was quenched due to electron transfer to the anthracene unit. Base treatment with quinuclidine deprontonated the [**14**-H]$^+$ and destroyed the prevalent hydrogen bond interactions, a process which released the amine thread **14** and retrieved the **DB24C8** fluorescence.

Figure 1-3b shows a redox-switchable [2]rotaxane[22] **15** which contains a benzylic amide macrocycle initially sitting on a succinamide station instead of a redox-active 3,6-di-*tert*-butyl-1,8-naphthalimide station. One-electron reduction of the naphthalimide resulted in an increase of hydrogen-bond accepting ability and that the macrocycle resided to the naphthalimide station, instead of the succinamide

station. Re-oxidation of the [2]rotaxane **15**$^{\bullet-}$ restored the original co-conformation of [2]rotaxane **15**. This switching process was observed by cyclic voltammetry (CV).

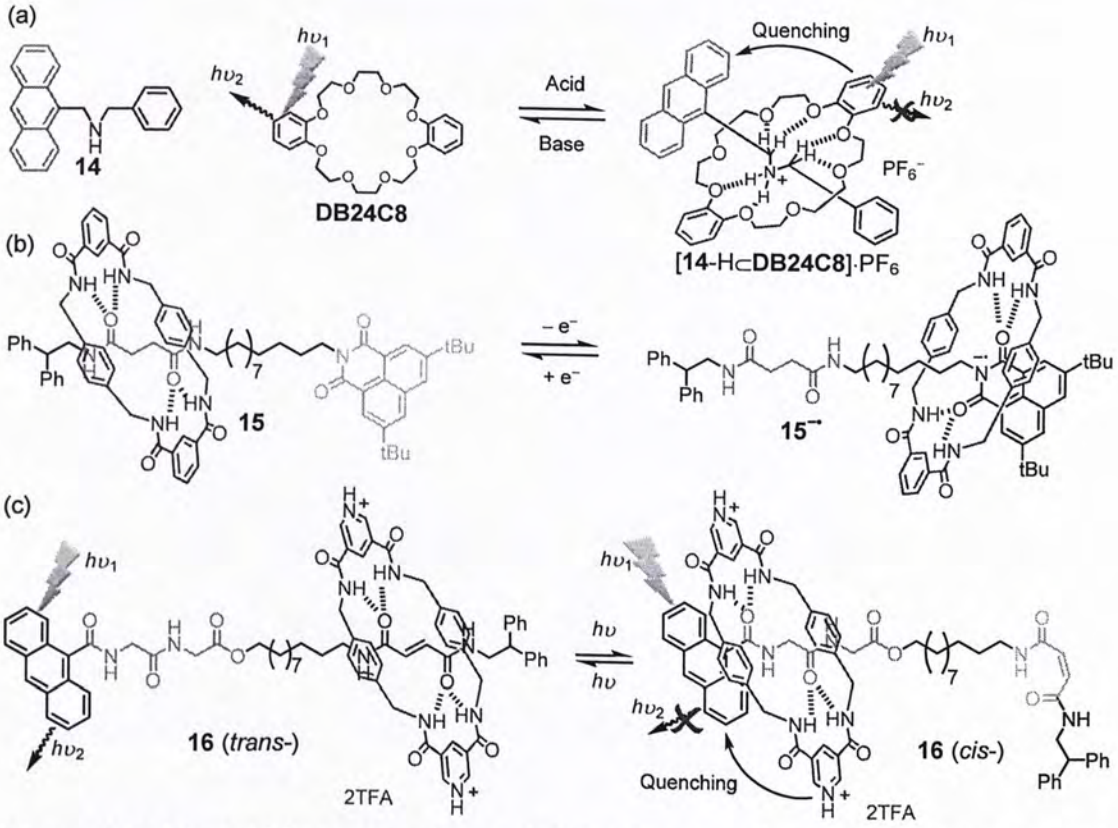

Figure 1-3. (a) Acid-base reversible switching between dialkylamine thread **14** and **DB24C8** to form [2]pseudorotaxane with photochemical properties; (b) Redox-induced shuttling of a [2]rotaxane **15** between a succinamide and naphthalimide station; (c) Light-driven shuttling of a [2]rotaxane **16** which exhibits fluorescence changes.

The Zerbetto group[21] reported a light-driven [2]rotaxane molecular switch **16** (Figure 1-3c) in which the macrocycle fits on the *trans*-fumaric diamide station due to strong [N–H···O=C] hydrogen bonding with structural complementary. The anthraceneamide fluorophore, also acts as a stopper, is far away from the pyridinium

units of the macrocycle so that photoinduced electron transfer (PET) was absent and that the fluorescence was "on". Isomerization of *trans*-fumaric diamide into *cis*-maleic diamide was induced upon irradiation, a process which disrupted the hydrogen-bond array. Subsequently, the macrocycle moved to the glycylglycine station that possessed relatively higher binding affinity, rendering the PET and "off" fluorescence.

1.5 Examples

After a few decades of enormous investigation on rotaxane synthesis, applications in nanoelectromechanical systems (NEMS), mechanized nanoparticles, and chemical sensors are now widely explored. Two selected, recent examples are discussed below.

The Stoddart group[23] reported a range (Au, Pt, Pd) of metal nanoparticles (MNPs) of varied diameters, covering with *mixed* self-assembled monolayers (*m*SAMS) and comprising "inert" background ligands and bistable [2]rotaxanes. For the rotaxanes, dumbbell **17** contained a 1,5-dioxynaphthalene (DNP) unit and a tetrathiafulvalene (TTF) unit stations whereas a cyclobis(paraquat-*p*-phenylene) ($CBPQT^{4+}$) ring was encircled exclusively onto the TTF station (Figure 1-4). The Au-MNP-immobilized rotaxanes demonstrated efficient reversible molecular

switching behavior, as observed in solution, using redox reagents as stimuli. First, the $CBPQT^{4+}$ ring preferentially bound to the TTF station with electrostatic and aromatic donor/acceptor interactions. Addition of an oxidant $Fe(ClO_4)_3$ caused oxidization of TTF into its radical cation $TTF^{\bullet+}$ and then dication TTF^{2+}, triggering a rapid shuttling of the $CBPQT^{4+}$ ring to the DNP station due to Coulombic repulsion. Conversely, the $CBPQT^{4+}$ ring could switch back to the TTF station after a reduction of TTF^{2+} to its neutral form by ascorbic acid. Zeta(ζ)-potential and CV measurements reveal that the rate of switching from DNP to TTF unit can be accelerated when the surface composition and/or the particle diameter increases. This pioneering example of redox-induced molecular-mechanical switching on the surfaces of nanoparticle gives insight in adaptive materials, nanoelectronic devices and nanoparticle-based sensors.

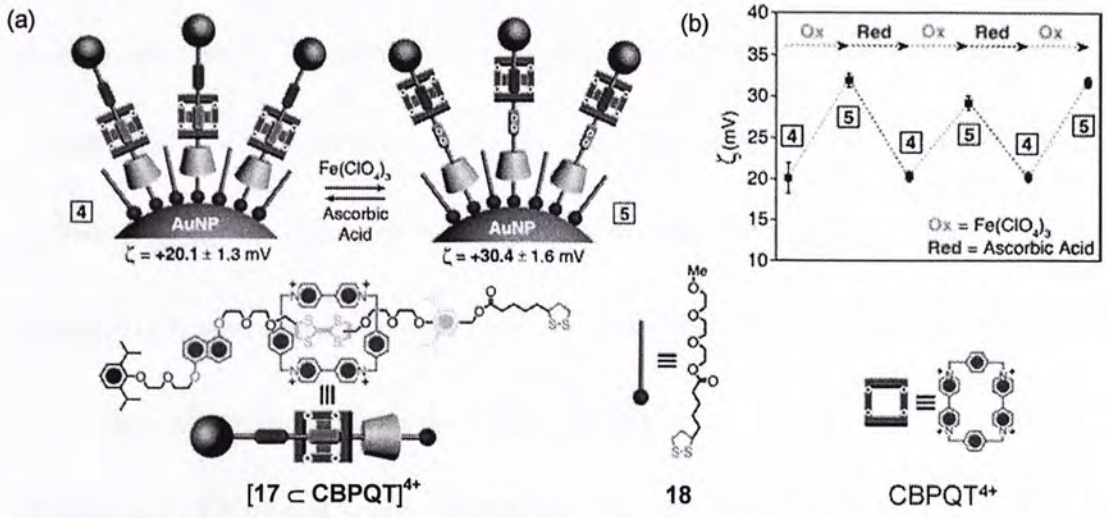

Figure 1-4. (a) Reversible switching and ζ-potential values for bistable [2]rotaxane-functionalized AuNP before (4) and after (5) oxidation; (b) Changes in ζ-potential as a function of reduction/oxidation processes (figures obtained from Ref. 23).

Recently, the Smith group reported a microwave-assisted slippage synthesis of squaraine rotaxane **19** as a fluorescence probe for bacterial imaging.[24] Squaraine dyes have been investigated over the years for potential applications in many photonic-based technologies owing to its narrow absorption band, small substituent effect on absorption maxima and remarkably high quantum yields in selected organic solvents. Yet, they are easily quenched by solvent molecules and form non-fluorescent aggregates in aqueous solution which is undesirable for bioimaging. The research group prepared a squaraine rotaxane which consisted of an anthracene-containing macrocycle and a squaraine-based thread with two zinc dipicolylamine ligands which selectively bind with the surface of bacterial cells. In terms of synthesis, a 1:1 mixture of the ring **20** and rod components **21** gave the desired rotaxane **22** in quantitative yield under microwave heating (slippage). By encapsulation of a macrocycle onto the squaraine group of the dumbbell, the squaraine group was insulated from solvent quenching. Even under a condition (1:9 DMSO/H_2O) which easily formed squaraine aggregates, the squaraine [2]rotaxanes were free from interchromophore energy transfer. Moreover, the squaraine [2]rotaxane **19** exhibited several advantages. They possess excellent water solubility, same absorption-emission wavelengths compared as a common cyanine dye Cy-5.5, and effective cell labeling properties for Gram-positive and Gram-negative bacteria.

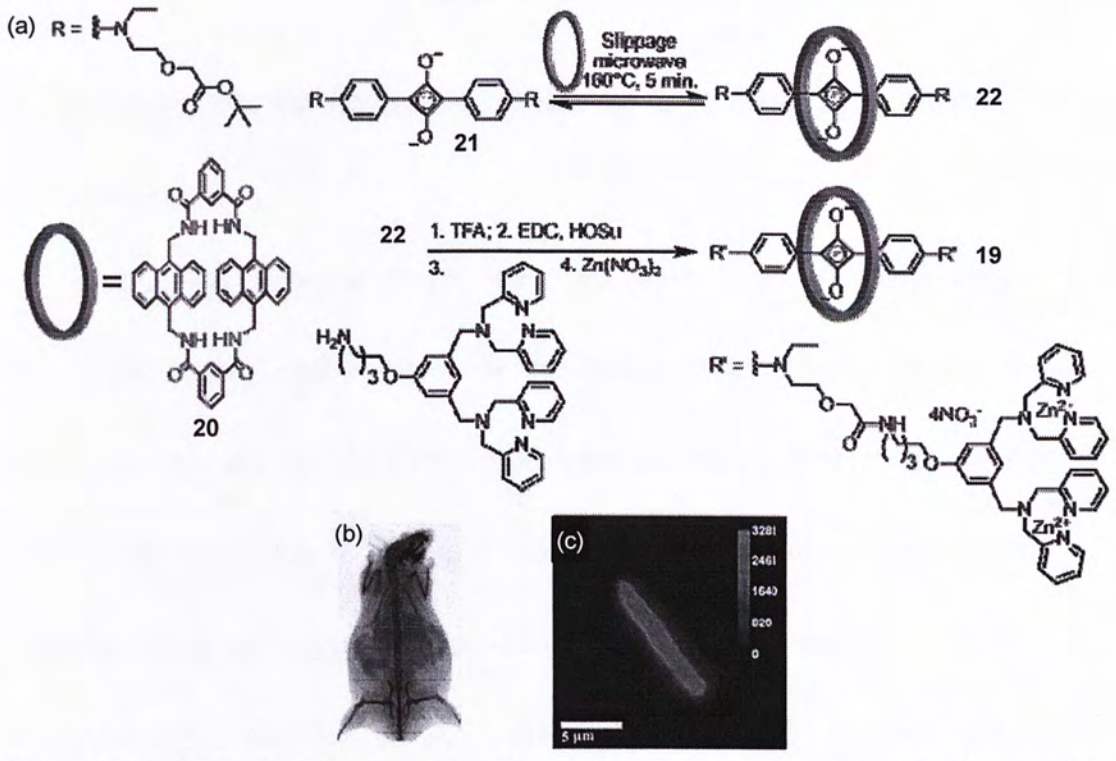

Figure 1-5. (a) Synthetic scheme of rotaxane using microwave-assisted slippage; (b) X-ray and fluorescence emission overlay of a living mouse with **19**-prelabeled *S. typhimurium* AM3 injected into right rear leg (red); (c) fluorescence micrograph of *S. typhimurium* AM3 after treatment with **19** (figures obtained from Ref. 24).

Chapter 2– Anthracene-Containing Dynamic [2]Rotaxane

2.1 Background

Imines—also known as Schiff bases—are relatively unstable since they are susceptible to rapid hydrolysis in the presence of water. Despite of this fact, imine-containing macrocycles possess remarkable stabilities in the presence of water. Other molecular systems,[25] involving dative bonds between imines and transition metal ions,[26] can also experience increased imine stabilities in water.

Previously, Stoddart *et al.*[15] described a clipping synthesis of an imine-containing dynamic [2]rotaxane (Scheme 2-1), which comprised of a [24]crown-8 imino macroring templated by a dibenzylammonium ion dumbbell. By condensation between the three separate components (**4**, **5a/b**, and **7**-H·PF_6) in 1:1:1 ratio in dry MeCN (60 mM), the resulting [2]rotaxanes **8a/b**-H·PF_6 were self-assembled in over 90 % yield. With electrostatic interaction, π–π stacking, and strong [N^+–H···O] and [N^+–C–H···O] hydrogen bonds between the macrocycle and dibenzylammonium dumbbell, large amounts (over 100 mole equivalents) of water were required to hydrolyze and partially disassemble the [2]rotaxane. The integrity of the [2]rotaxane could be restored by removing the water molecules with the addition of a drying reagent such as $MgSO_4$ or Na_2SO_4.

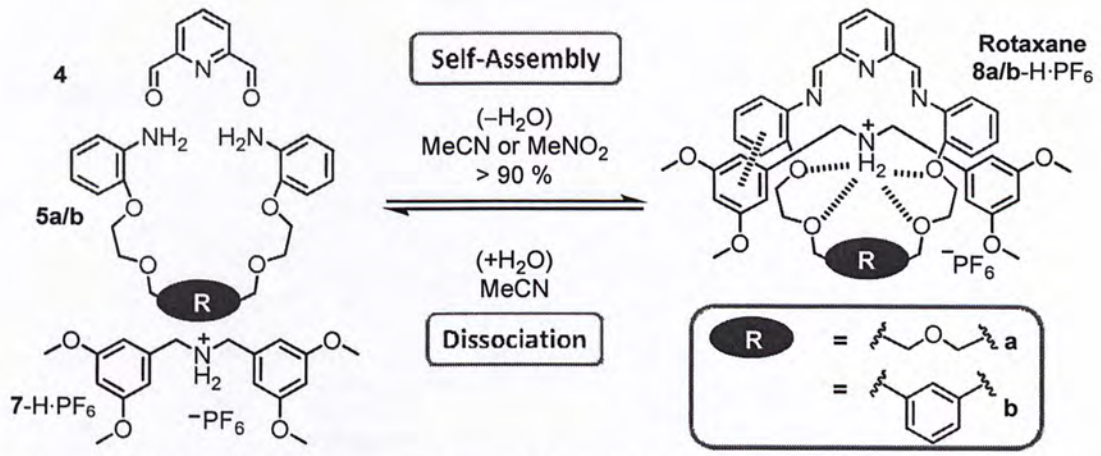

Scheme 2-1. Equilibrium for self-assembly and dissociation of dynamic [2]rotaxanes and their components.

2.2 Modification and Design of Dynamic [2]Rotaxane

To further investigate (i) the stability, (ii) detailed hydrolysis mechanism and dynamics, and (iii) switching of these dynamic [2]rotaxanes in the presence of various stimuli—e.g., water, acids, salts, and amines, a dynamic [2]rotaxane **23**-H·PF_6 (Figure 2-1) was synthesized with an anthracene moiety integrated to the dumbbell as a fluorescent probe. It is well known[27] that the anthracene fluorescence can be quenched by a nearby amino group through electron transfer. Herein, the imine and pyridine units in the macrocycle are reckoned as the basis of fluorescence quenching. The fluorescence and fluorescence-quenching nature of **23**-H·PF_6 in the rotaxane equilibrium mixture were monitored. In order to confirm that the quenching process was due to intramolecular electron transfer, a podand **24** which is an analogue (Figure 2-1) to the diimino-macrocycle, was prepared as a control

compound.

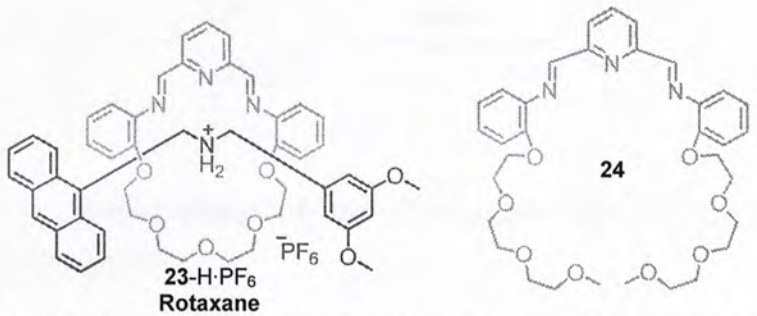

Figure 2-1. Structures of the anthracene-containing [2]rotaxane **23**-H·PF_6 and diimine **24**.

2.3 Self-Assembly of Rotaxane and Synthesis of Components

The [2]rotaxane **23**-H·PF_6 (Scheme 2-2) was formed by condensation of 2,6-diformylpyridine **4,** diamine **5** and an anthracene-containing ammonium thread **25**-H·PF_6 in 1:1:1 ratio in MeCN (60 mM) using the dynamic clipping approach. The ammonium thread acts as the thermodynamic template which stabilizes and amplifies the [1+1] condensation of diamine and dialdehyde to form the [24]crown-8 macrocycle. The macrocycle was encircled to the thread to form the [2]rotaxane **23**-H·PF_6. The thermodynamic stability of **23**-H·PF_6 arises as a result of complementary recognition associated with [N^+–H···X] hydrogen bonds (X = O or N), [N^+–C–H···O], electrostatic and C–H···π interactions between the macrocycle and the dumbbell thread.

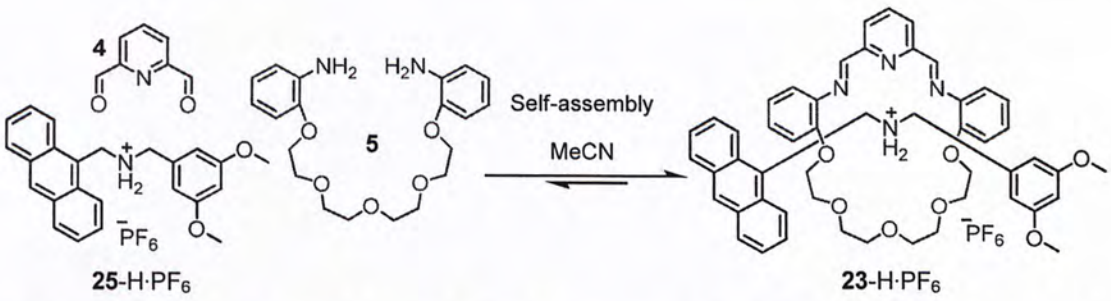

Scheme 2-2. Self-assembly of the [2]rotaxane **23**-H·PF_6 by clipping under thermodynamic control.

The syntheses of the diimine **24** and ammonium thread **25**-H·PF_6 are depicted in Scheme 2-3. The nitro compound **26**[28] was reduced into an aniline derivative **27** in the presence of hydrazine hydrate under catalytic amount of wet palladium on charcoal, with a reaction yield of 93 %. Then, a solution of 2,6-diformylpyridine **4** and 2 equivalents of **27** was stirred with molecular sieve (4 Å) for a day to obtain the diimine control compound **24** in 94 % yield. On the other hand, amine thread **25** was synthesized by a reductive amination in 88 % yield. Commercially available 3,5-dimethoxybenzylamine **28** and 9-anthraldehyde **29** were condensed with a Dean-Stark apparatus under reflux, followed by a subsequent reduction with sodium borohydride ($NaBH_4$). Finally, addition of aqueous hexafluorophosphoric acid (HPF_6) to the amine thread **25** resulted in the formation of ammonium dumbbell **25**-H·PF_6 in 75 % yield.

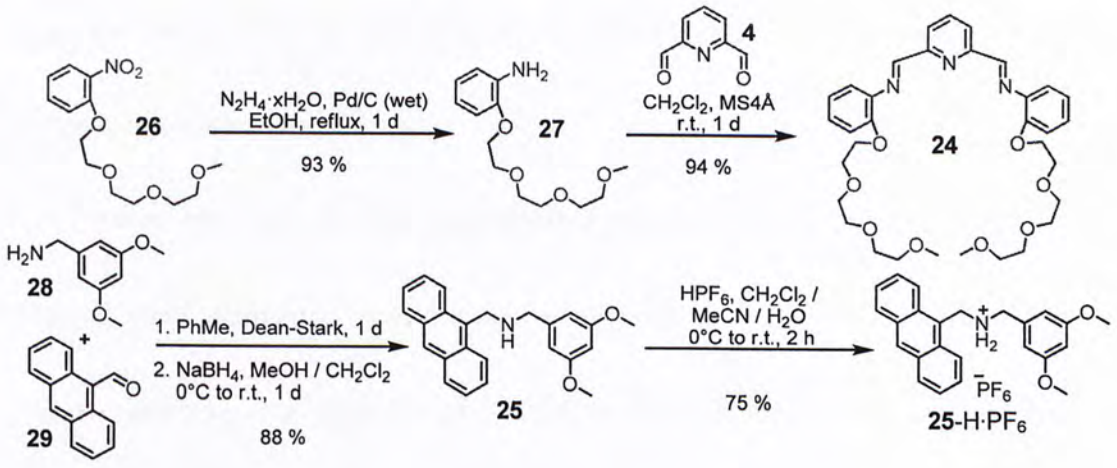

Scheme 2-3. Syntheses of diimine **24** and ammonium dumbbell **25**-H·PF_6.

2.4 Characterization

2.4.1 ^{1}H NMR Spectroscopy

[2]Rotaxane **23**-H·PF_6 in CD_3CN was appeared as an equilibrating equimolar mixture of the three components **4**, **5** and **25**-H·PF_6, in ^{1}H NMR spectrum. Stacked NMR spectra of the components and **23**-H·PF_6 are shown in Figure 2-2. New sharp proton signals were observed, which suggested that the [2]rotaxane **23**-H·PF_6 was the most thermodynamically stable product. In particular, the formyl proton (C*H*O) at δ = 10.1 ppm diminishes while the imine proton H_i at δ = 7.9 ppm prevails in the spectrum of **23**-H·PF_6. Also, benzylic methylene protons, H_d and H_e, that are adjacent to the ammonium centre, are remarkably shifted from δ = 4.4 and 5.2 ppm in **25**-H·PF_6 to δ = 5.1 and 5.8 ppm in **23**-H·PF_6, respectively. The sharpness of proton signals suggests that **23**-H·PF_6 is relatively kinetically stable on the NMR time scale.

From the integrations of the signals, the self-assembly of [2]rotaxane **23**-H·PF_6 proceeds in over 90 % yield.

Further evidence for the equilibrating dynamic [2]rotaxane **23**-H·PF_6 was obtained from analyzing its two-dimensional NOESY ^{1}H NMR spectrum (Figure 2-3). Cross-peaks arise from protons in the macrocycle and dumbbell of **23**-H·PF_6, for example, (i) imine proton H_i and anthracyl proton H_n, (ii) pyridyl proton H_k and anthracyl proton H_n and (iii) phenyl proton H_m and anthracyl proton H_g. These results support the fact that **23**-H·PF_6 is our desired [2]rotaxane.

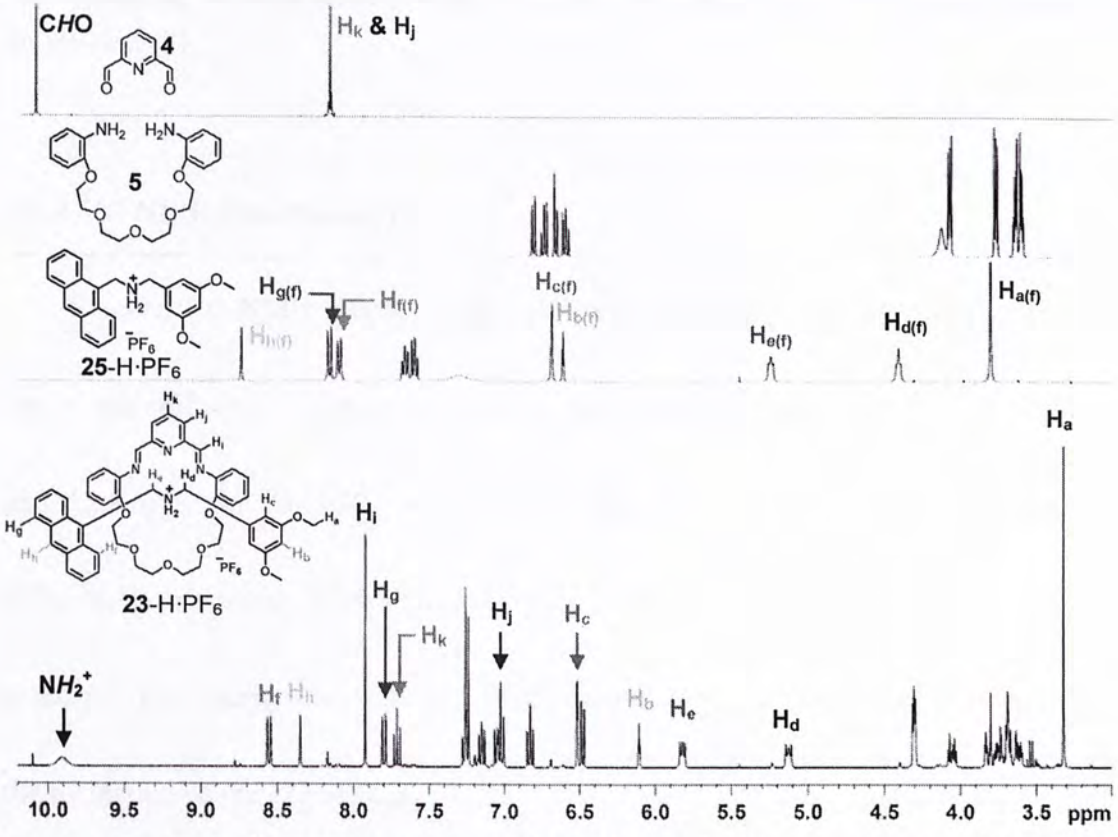

Figure 2-2. Partial ^{1}H NMR spectra of **23**-H·PF_6 and its free components: dialdehyde **4**, diamine **5** and dumbbell **25**-H·PF_6 in CD_3CN (f = free).

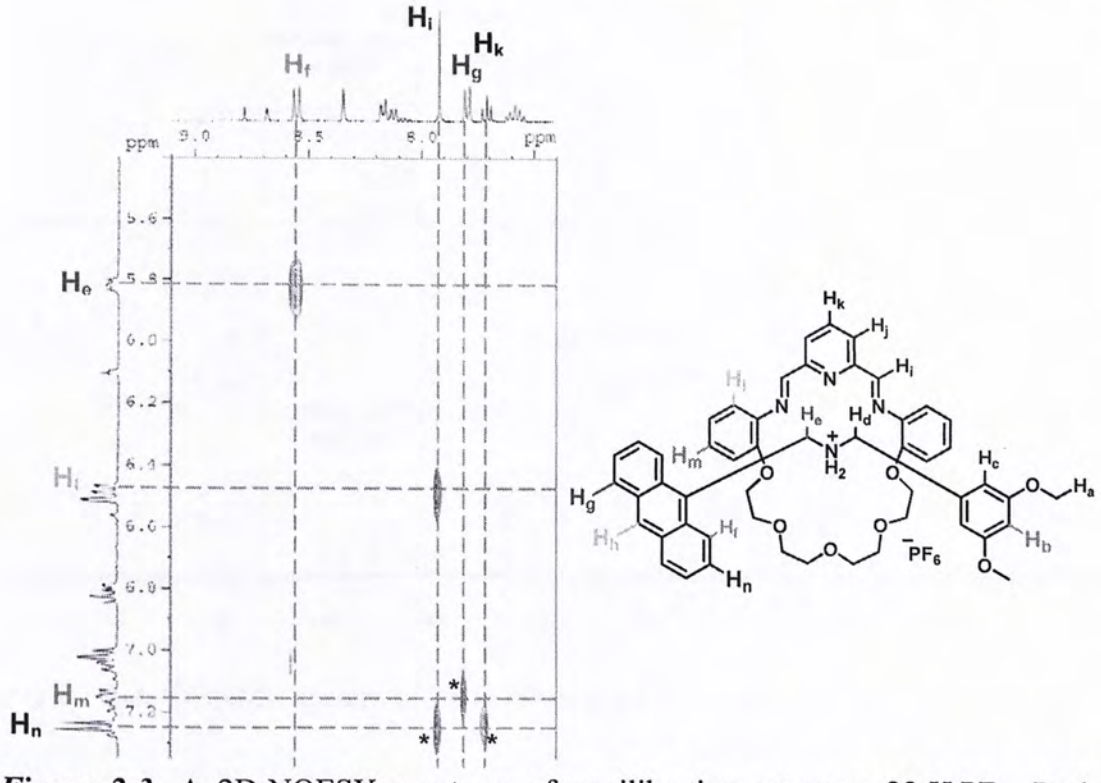

Figure 2-3. A 2D-NOESY spectrum of equilibrating rotaxane **23**-H·PF_6. Peaks corresponding to correlation between the dumbbell and macrocycle are marked with an asterisk (*).

2.4.2 ^{13}C NMR Spectroscopy

Stacked ^{13}C NMR spectra of **25**-H·PF_6 and **23**-H·PF_6 are shown in Figure 2-4. The slight shifts of ^{13}C signals of benzylic methylene carbons (N^+–*C*) from δ = 43.9 and 52.8 ppm in **25**-H·PF_6 to δ = 45.3 and 53.3 ppm in **23**-H·PF_6 reveal the differences in chemical environment before and after the self-assembly of the rotaxane. The emergence of imine (N=*C*) carbon signal at δ = 160.1 ppm supports the formation of the [2]rotaxane.

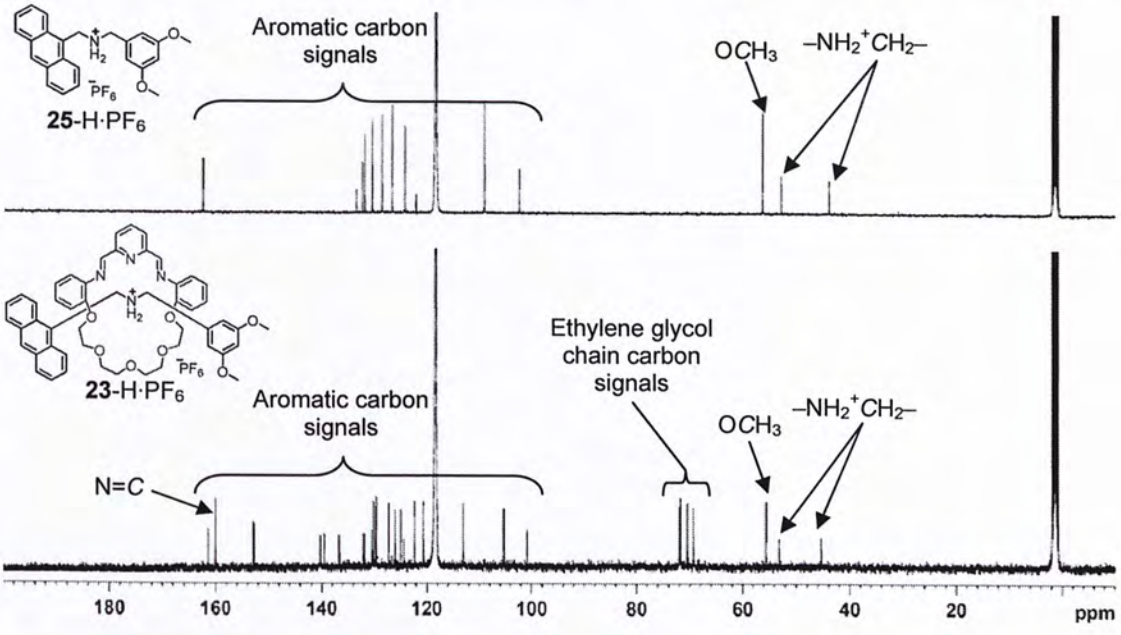

Figure 2-4. ^{13}C NMR spectra of **25**-H·PF_6 and **23**-H·PF_6 in CD_3CN.

2.4.3 Mass Spectrometry

The [2]rotaxane **23**-H·PF_6 was analyzed by using high resolution electrospray ionization mass spectrometry (ESI-MS). The mass spectrum (Figure 2-5) reveals a singly charged molecular ion base peak (*m/z*) of 833 as a predominant species which is corresponded to the $[M-PF_6]^+$ molecular ion of the [2]rotaxane. The absence of significant higher mass signals indicates that no other higher-order macrocylic homo-oligomers or related acyclic oligomers were formed. In addition, the [2]rotaxane **23**-H·PF_6 showed superior stability in gas phase.

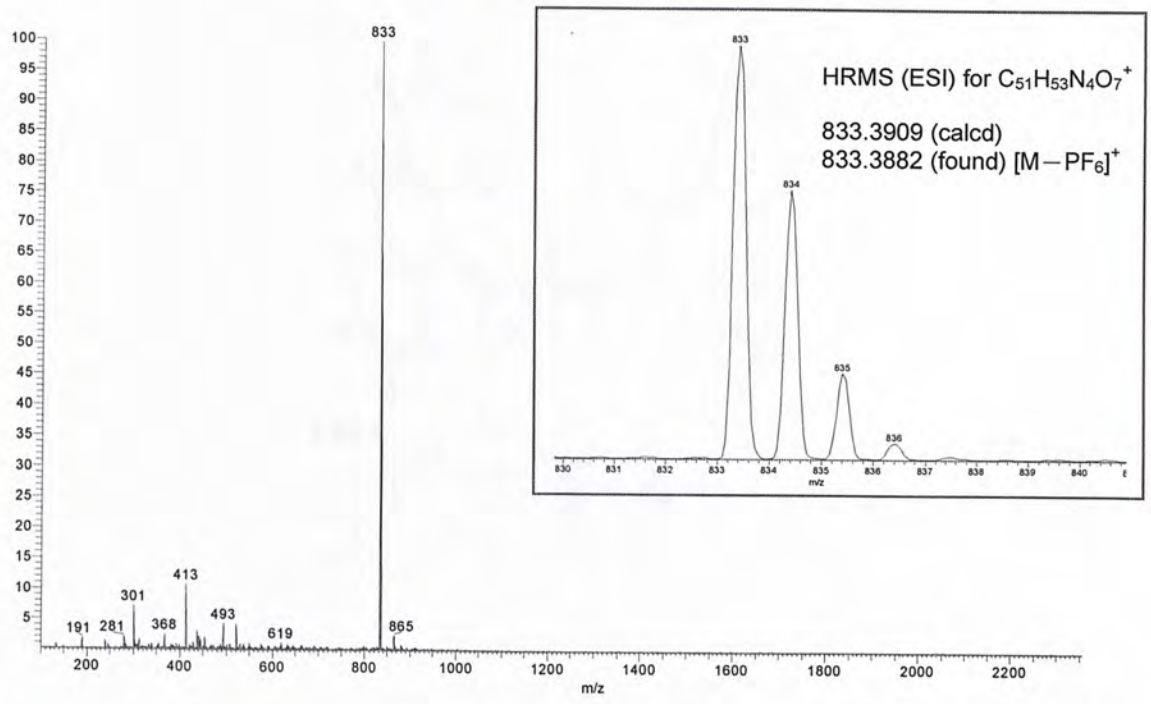

Figure 2-5. ESI-mass spectrum of [2]rotaxane **23**-H·PF_6 showing a $[M-PF_6]^+$ molecular ion peak.

2.4.4 X-Ray Crystallography

Single crystals of the dumbbell **25**-H·PF_6 were obtained by slow vapor diffusion of *tert*-butyl methyl ether into a solution of **25**-H·PF_6 in 1,2-dichloroethane. The crystal contained two dumbbell molecules with the two anthracene planes lying nearly perpendicular to each other (Figure 2-6). The shortest distance between a hydrogen atom of the anthracene moiety and the plane of another anthracene moiety is 2.986 Å, giving evidence of moderate C–H···π interaction.[13c]

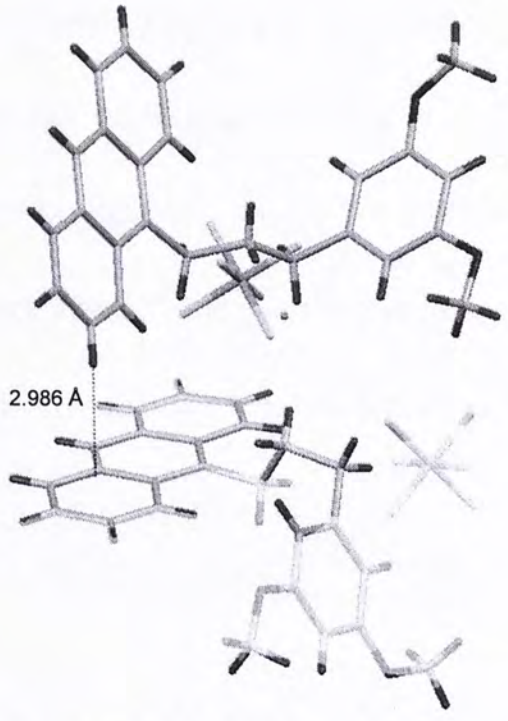

Figure 2-6. Solid-state structure of the dumbbell **25**-H·PF_6.

2.4.5 UV/Visible Absorption and Fluorescence Spectroscopies

The UV/visible absorption spectra of the [2]rotaxane **23**-H·PF_6 and its free components are shown in Figure 2-7. Absorption spectrum of **23**-H·PF_6 demonstrates the sum of absorption bands of its components and shares the characteristic band of anthracene moiety at 300–400 nm.

Upon excitation at 290 nm, where most of the light is absorbed by the components, **25**-H·PF_6 gives anthracene fluorescence at λ_{max} = 418 nm while **5**, **24** and **23**-H·PF_6 give aminophenolic fluorescence at λ_{max} = 334 nm (Figure 2-8a). In particular, the absence of anthracene fluorescence in **23**-H·PF_6 suggests that the imine and pyridine moieties quenched the anthracene fluorescence *via* intramolecular

electron transfer. Intermolecular quenching is ruled out due to the extremely dilute nature of the solutions and the fact that fluorescence of **25**-H·PF_6 could not be quenched by **4**, **5** and **24** separately (Figure 2-8b). Based on the fluorescence spectrum of the rotaxane **23**-H·PF_6, the threshold intensity at 418 nm is 5 (a.u.). Solution with intensity at 418 nm below 5 (a.u.) is defined as fluorescence quenched.

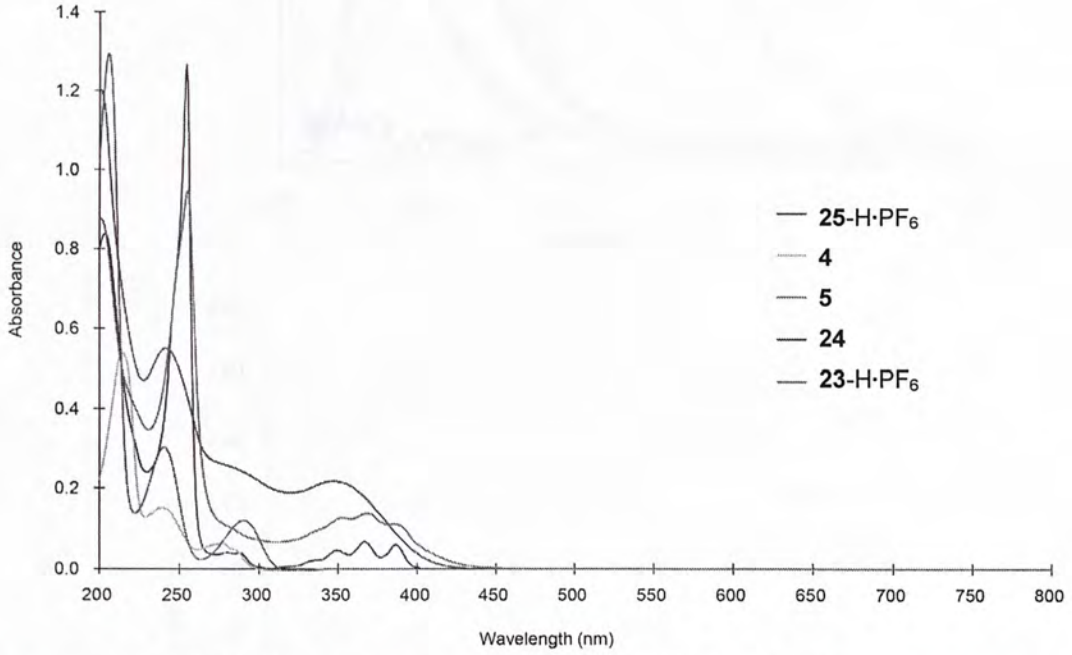

Figure 2-7. UV/visible absorption profiles of **23**-H·PF_6, its free components and diimine **24** (conc. = 0.02 mM in MeCN).

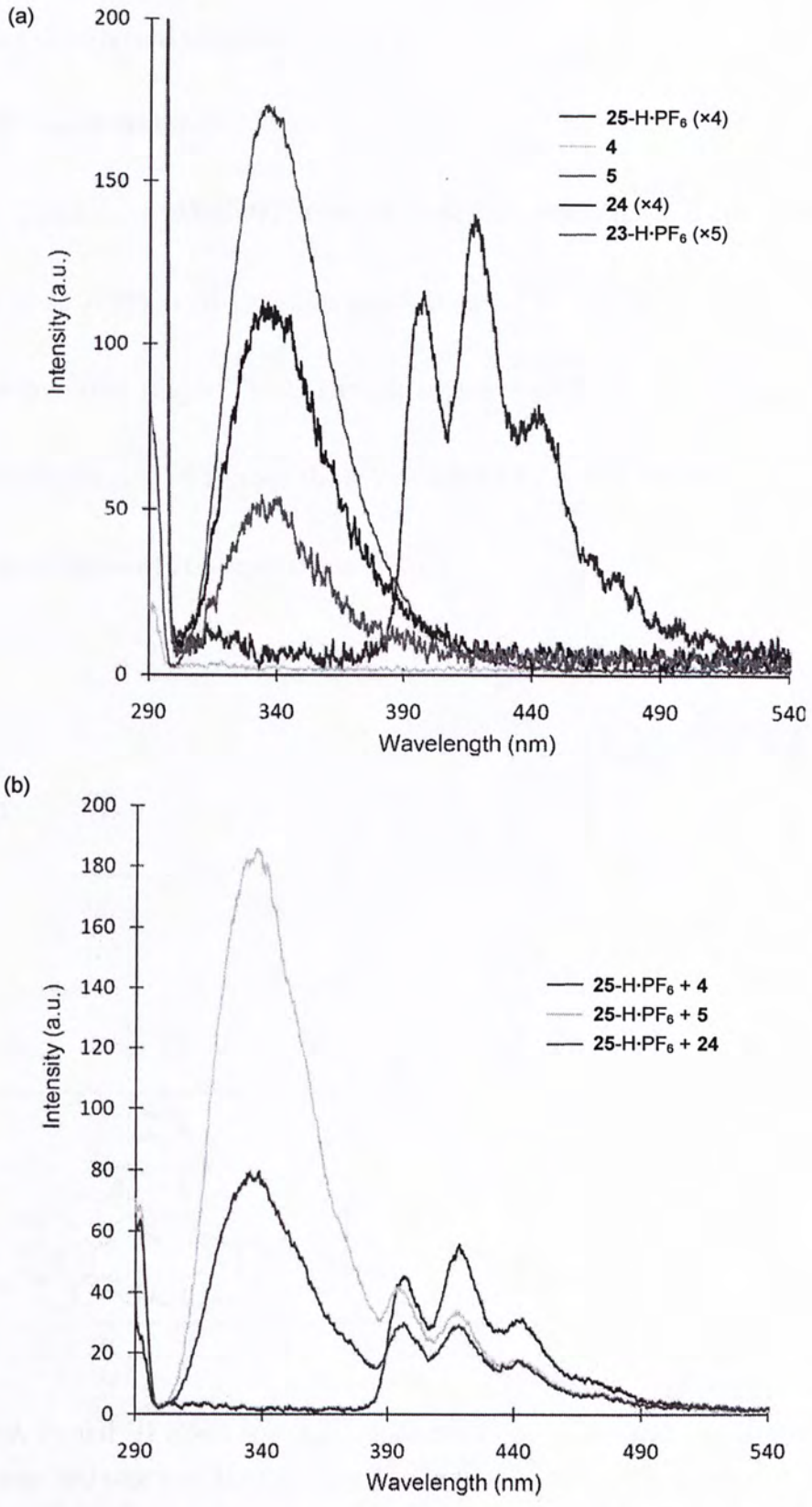

Figure 2-8. Fluorescence emission spectra (excitation wavelength = 290 nm) of (a) components and (b) mixture of **25**-H·PF_6 with **4**, **5** and **24** separately (conc. = 0.02 mM in MeCN).

2.5 Effect of External Stimuli

2.5.1 Addition of Water

The [2]rotaxane **23**-H·PF_6 showed excellent stability towards hydrolysis. Mixtures of **23**-H·PF_6 with 100, 200 and 500 equiv. of D_2O were probed using ^1H NMR spectroscopy (Figure 2-9). Though proton signals of free components are observed, integrations of signals show that **23**-H·PF_6 is still the dominant species even in the presence of 200 equivalents of D_2O.

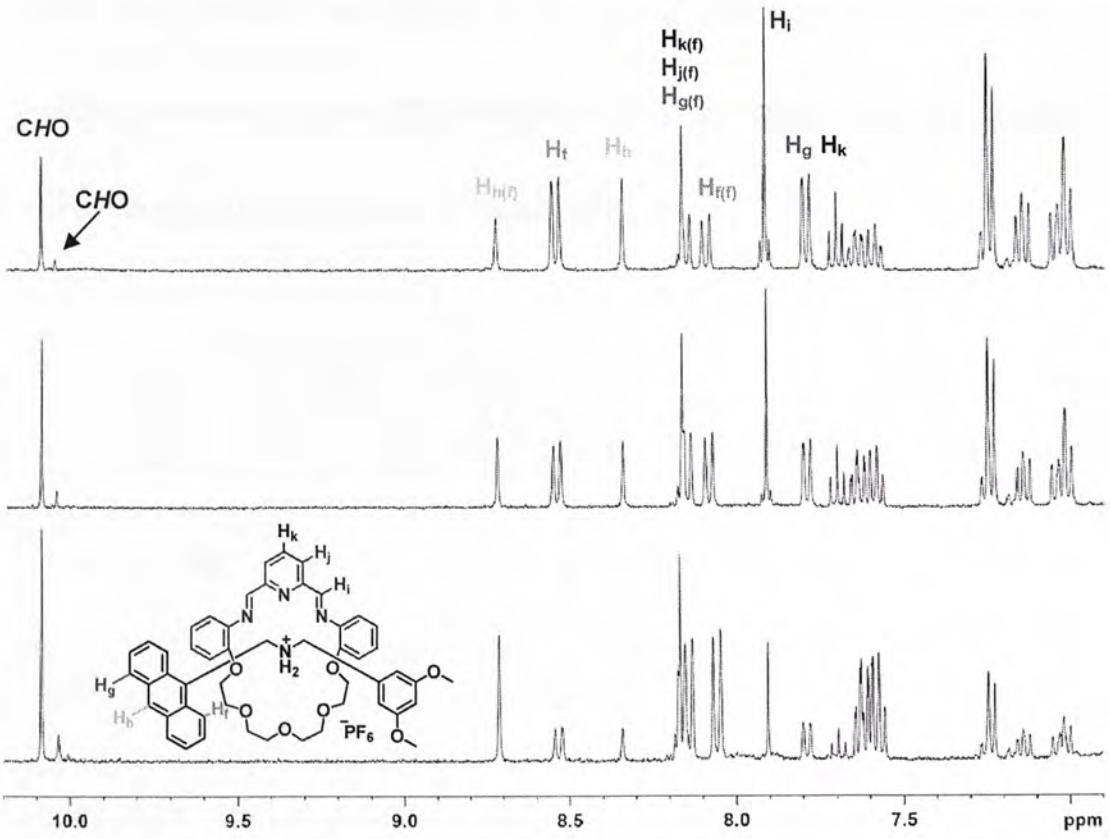

Figure 2-9. Partial ^1H NMR spectrum of **23**-H·PF_6 in the presence of (from the top) 100, 200 and 500 equiv. of D_2O in CD_3CN (f = free).

Furthermore, the dissociation rate of the [2]rotaxane **23**-H·PF_6 in the presence of excess water was monitored by observing ^1H NMR spectroscopy (Figure 2-10). As

the rotaxane dissociates, in particular, (i) the intensity of imine signal (δ = 7.92 ppm) gradually decreases with the consequent increase in intensity of aldehyde signal (δ = 10.10 ppm) and (ii) the shifts of N^+–C–H protons (H_d and H_e) from δ = 5.12 and 5.80 ppm to δ = 4.41 and 5.24 ppm, respectively. A plot of rotaxane concentration in the presence of D_2O or HCl/H_2O *versus* time is shown in Figure 2-11. The dissociations took place with second-order kinetics within the first hour. Since ^1H NMR signals of bound H_h (δ = 8.35 ppm) and free $H_{h(f)}$ (δ = 8.74 ppm) do not overlap with other peaks, their intensities are tracked for the kinetic study. Generally, equilibria were reached after about 5 h with 71, 54 and 24 % of the rotaxane remained at equilibrium in the presence of 100, 200 and 500 equiv. of D_2O.

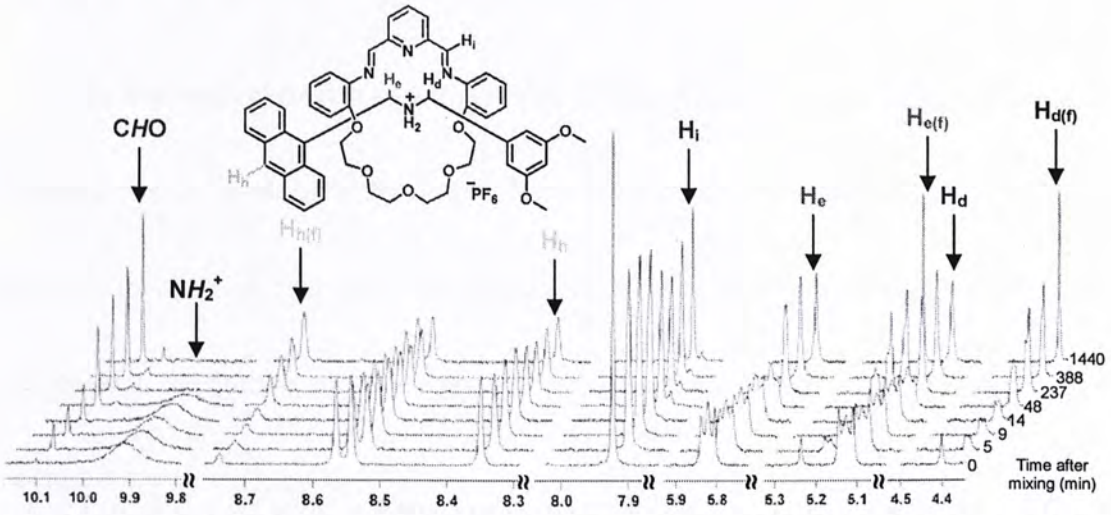

Figure 2-10. Stacked partial ^1H NMR plot of the [2]rotaxane **23**-H·PF_6 in the presence of 200 equiv. of D_2O in CD_3CN *versus* time (f = free).

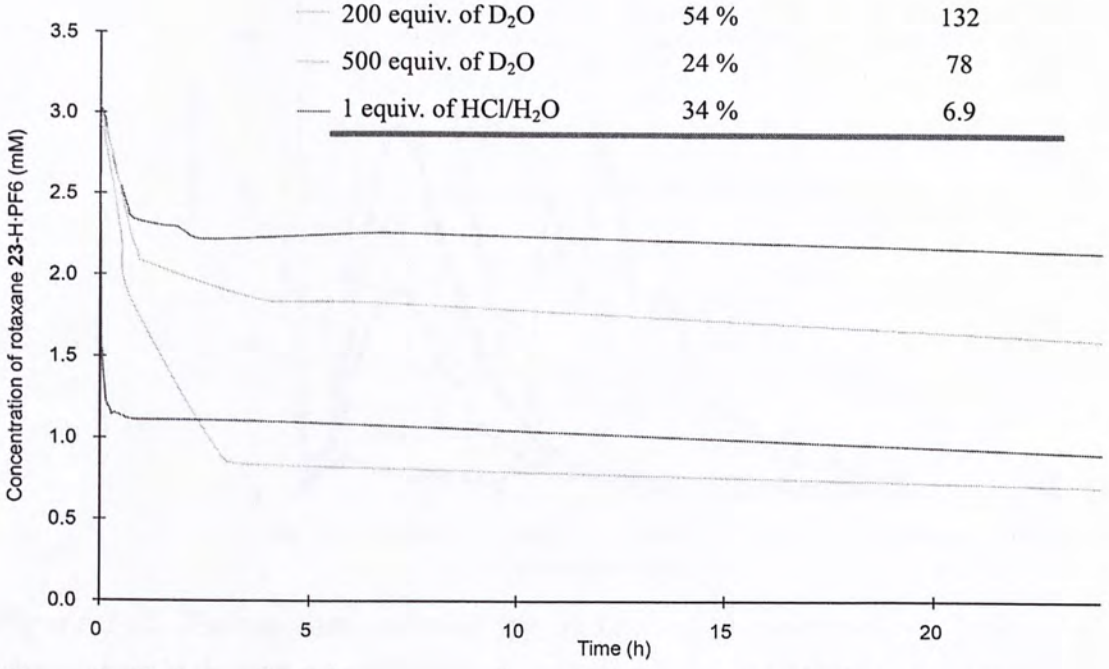

	[2]Rotaxane remained at equilibrium	Half-life $t_{1/2}$ (min)
100 equiv. of D_2O	71 %	149
200 equiv. of D_2O	54 %	132
500 equiv. of D_2O	24 %	78
1 equiv. of HCl/H_2O	34 %	6.9

Figure 2-11. A graph of the concentration of [2]rotaxane **23**-H·PF_6 in CD_3CN *versus* time (h) obtained by ^1H NMR spectroscopy and a table summarizing amounts of **23**-H·PF_6 remained and corresponding half-lives.

Fluorescence emission spectra (Figure 2-12) of **23**-H·PF_6 and other components in the presence of excess (200 equiv.) water were measured. Interestingly, they show similar emission spectra as in the absence of water. The [2]rotaxane **23**-H·PF_6 does not possess the anthracene characteristic band, meaning that fluorescence quenching occurred.

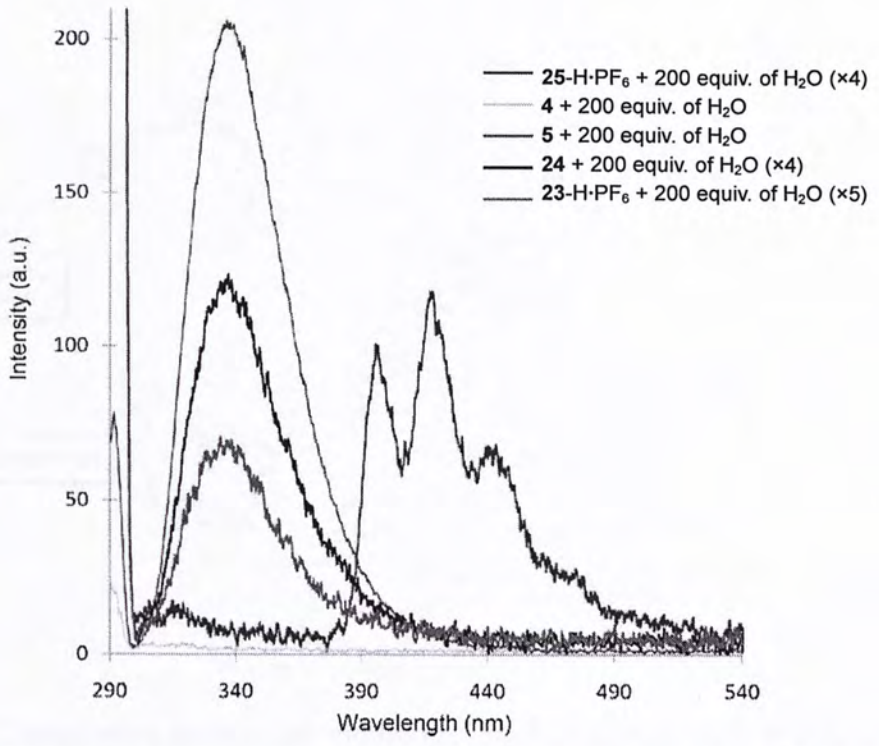

Figure 2-12. Fluorescence emission spectra (excitation wavelength = 290 nm) of components in the presence of 200 equiv. of water (conc. = 0.02 mM in MeCN).

With the NMR and fluorescence data in hand, a dissociation mechanism of the [2]rotaxane **23**-H·PF_6 in the presence of excess water is proposed (Scheme 2-4). The equilibria are biased to the rotaxane and intermediate I. Although intermediate I is partially dissociated, the close proximity between the dumbbell and mono-imine podand (open-chained crown ether) allows the quenching of anthracence fluorescence. A new mono-aldehyde signal at δ = 10.05 ppm in the NMR spectrum (Figure 2-9) also supports the presence of the intermediate I.

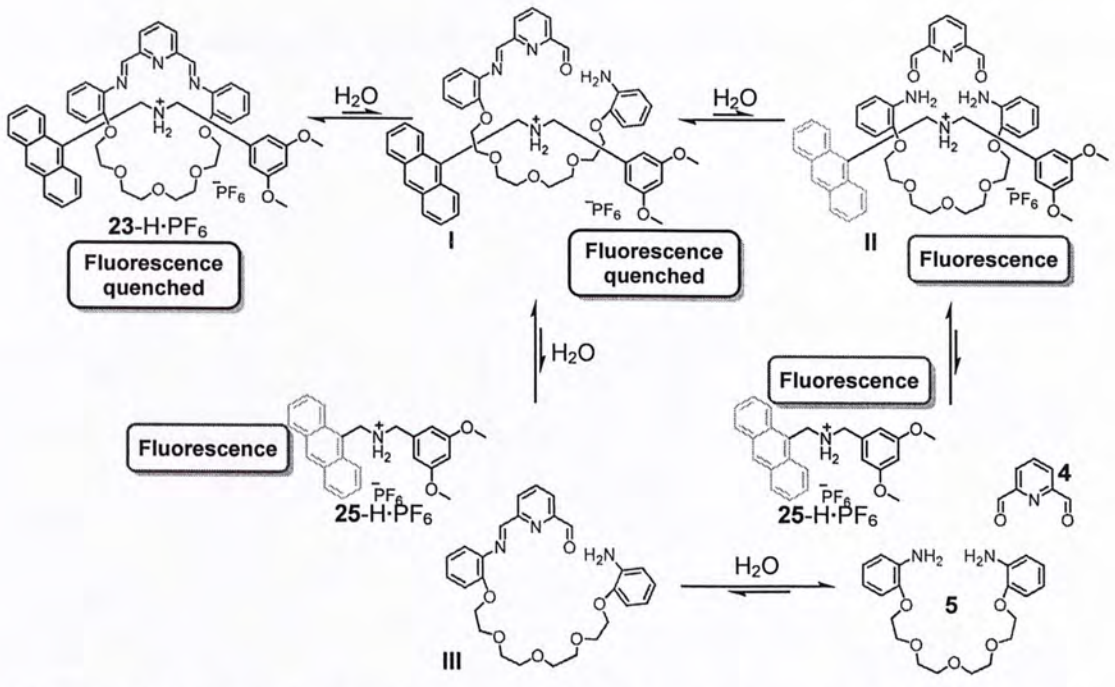

Scheme 2-4. Dissociation mechanism and fluorescence properties of **23**-H·PF_6 in the presence of excess water.

2.5.2 Addition of Acid

Upon addition of aqueous acid, imine bonds dissociate and so as the [2]rotaxane **23**-H·PF_6. Dissociations of separate mixtures of **23**-H·PF_6 in the presence of 1 equiv. of HCl/H_2O (0.1 M) and excess HPF_6/H_2O (0.1 M) were tracked by ^{1}H NMR spectroscopy. Sets of proton signals of all equilibrating components are observed in the NMR spectra (Figure 2-13) and that the [2]rotaxane **23**-H·PF_6 becomes the least dominant species. On account of counterion and acidity effect, the [2]rotaxane **23**-H·PF_6 partially dissociates into a mono-aldehyde intermediate from which the formyl proton resonances at δ = 10.12 ppm for the case of HCl/H_2O. On the other hand, the [2]rotaxane completely dissociates and shows a weak residual

mono-aldehyde signal at δ = 10.00 ppm for the case of HPF_6/H_2O.

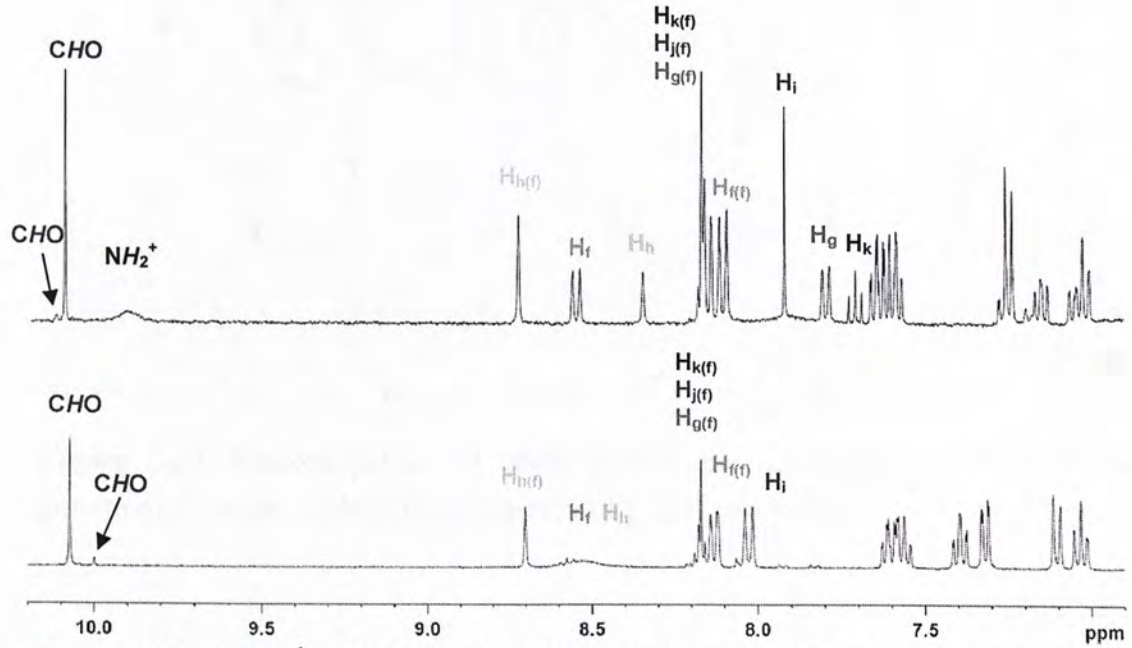

Figure 2-13. Partial ^{1}H NMR spectra of the [2]rotaxane **23**-H·PF_6 in the presence of (a) 1 equiv. of HCl/H_2O (0.1 M) and (b) excess HPF_6/H_2O (0.1 M) (f = free).

With the use of 1 equiv. of HCl/H_2O (0.5 M), the dissociation rate (half-life of 6.9 min) was much faster than employing water alone with 34 % of the [2]rotaxane remained in the mixture. The ^{1}H NMR signal (δ = 10.10 ppm) of aldehyde shows a drastic increase in intensity over time (Figure 2-14).

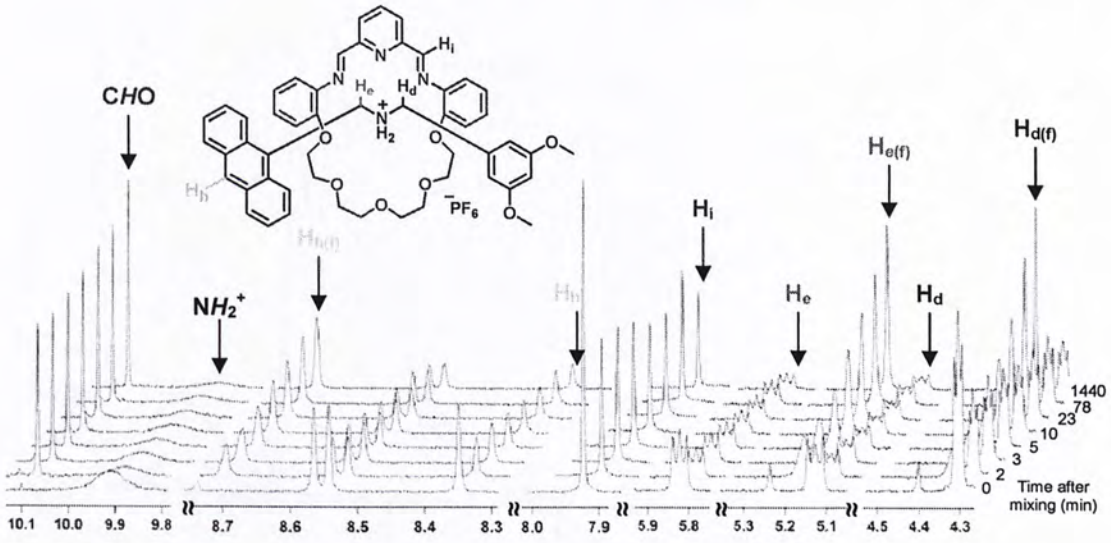

Figure 2-14. Stacked partial ^{1}H NMR plot of the [2]rotaxane **23**-H·PF_6 in the presence of 1 equiv. of HCl/H_2O (0.5 M) in CD_3CN *versus* time.

The fluorescence nature of [2]rotaxane **23**-H·PF_6 in the presence of excess acids was investigated. Treatment with an excess of acid (0.1 M HCl/H_2O and 0.1 M HPF_6/H_2O separately) resulted in dissociation of the rotaxane which subsequently induced anthracene fluorescence (Figure 2-15a). Surprisingly, the intensity of anthracene fluorescence varies with the amount of 0.1 M HCl/H_2O used. It shows a sharp increase in the range of 0–5 equiv. of 0.1 M HCl/H_2O and reaches a plateau, following a logarithmic curve (Figure 2-15b).

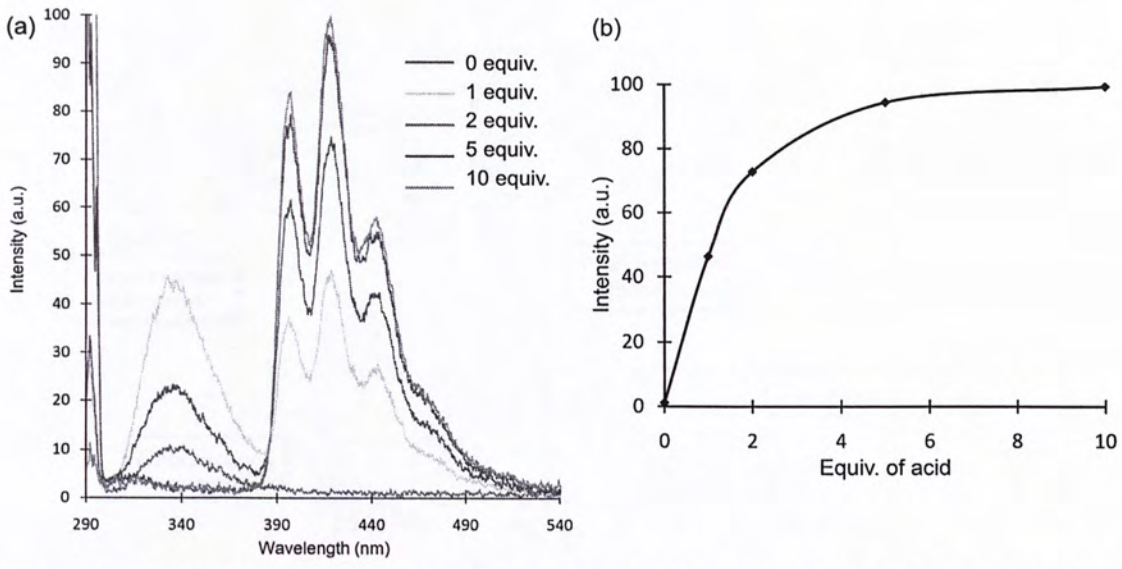

Figure 2-15. (a) Stacked fluorescence emission of [2]rotaxane **23**-H·PF_6 with various amount of 0.1 M HCl/H_2O; (b) a plot of fluorescence intensity at 418 nm against equiv. of acid used. Error = ±2 %.

Combining the ^{1}H NMR and fluorescence data, a reasonable dissociation mechanism is depicted in Scheme 2-5. By contrary to the use of excess water, the equilibria in the presence of acid favor the formation of the free components **4**, **5**, **25**-H·PF_6 and hence are responsible for the observation of anthracene fluorescence.

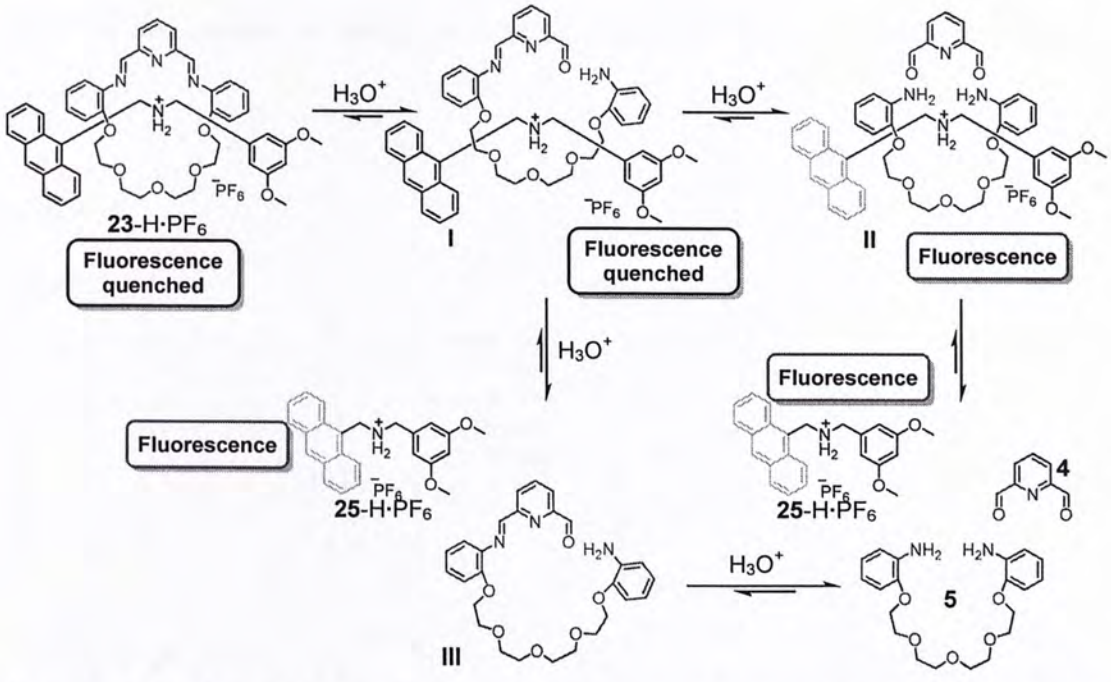

Scheme 2-5. Dissociation mechanism and fluorescence properties of **22**-H·PF_6 in the presence of aqueous acids (0.5 M HCl/H_2O or 0.1 M HPF_6/H_2O).

The stability of the [2]rotaxane **23**-H·PF_6 which dissolved in other organic solvents, was examined. Dissolutions of the [2]rotaxane in anhydrous MeOH, Me_2NCHO (DMF) and Et_2O showed insignificant, negligible dissociations. To further compare the importance of water and acid in the dissociation of rotaxane **23**-H·PF_6, excess anhydrous 0.1 M HCl/Et_2O was added to a solution of **23**-H·PF_6 in CD_3CN. ^1H NMR spectrum reveals a complete dissociation of rotaxane into its separate components. It is believed that small amounts of water molecules are inevitably present and responsible for the dissociation when the acid HCl/Et_2O is in excess. Fluorescence spectra were obtained from mixture of **23**-H·PF_6 in MeCN with various amount of anhydrous 0.1 M HCl/Et_2O. Anthracene fluorescence was

observed and showed a linear increase as increasing equiv. of acid used (Figure 2-16).

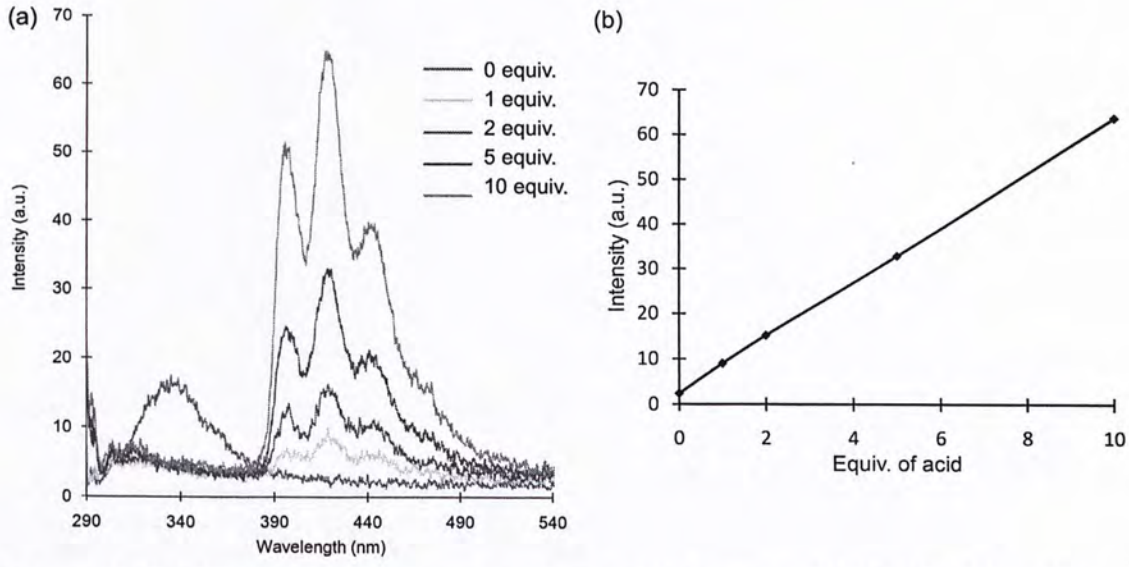

Figure 2-16. (a) Stacked fluorescence emission of [2]rotaxane **23**-H·PF_6 with various amount of anhydrous 0.1 M HCl/Et_2O; (b) a plot of fluorescence intensity at 418 nm against the equiv. of acid used. Error = ±2 %.

2.5.3 Addition of Salts

The use of salt in the dissociation of the rotaxane through competitive binding may offer a possibility of broadening the range of stimuli.[29] Potassium ion is known for universal binding with [24]crown-8-like macrocycle. The competitive binding will become feasible if the dynamic macrocycle of the rotaxane **23**-H·PF_6 preferentially complexes with K^+ ion and displaces out the dumbbell **25**-H·PF_6.

The effect of KPF_6 on dissociation of **23**-H·PF_6 was monitored by ^1H NMR spectroscopy (Figure 2-17). The intensity of aldehyde signal corresponding to free

dialdehyde **4** (δ = 10.10 ppm) shows insignificant increase after treatment of **23**-H·PF_6 with 1 equiv. of KPF_6 in CD_3CN. It follows that KPF_6 has no effect on dissociation of the rotaxane **23**-H·PF_6.

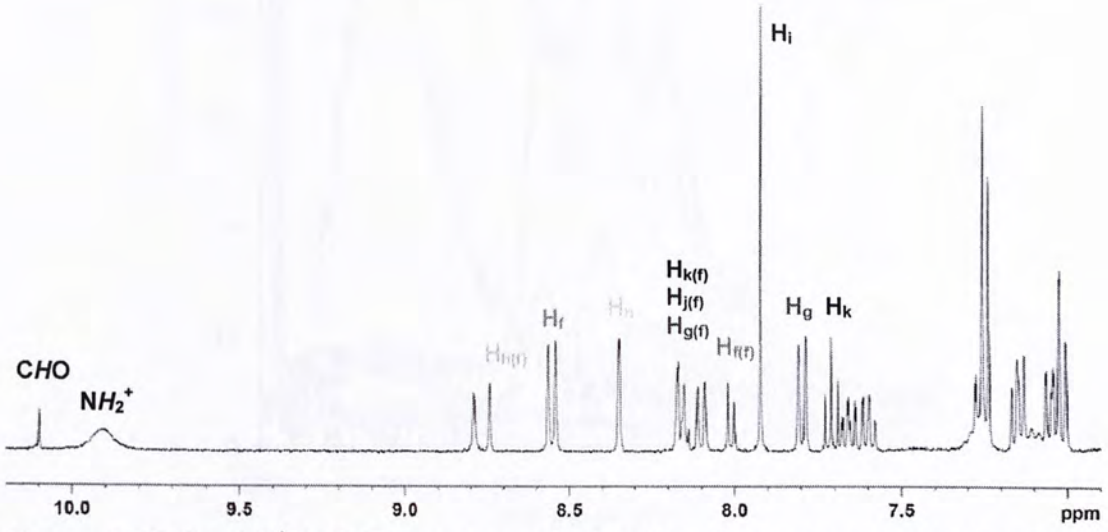

Figure 2-17. Partial ^{1}H NMR spectrum of **23**-H·PF_6 after treatment with 1 equiv. of KPF_6 in CD_3CN (f = free).

The fluorescence quenching ability of KPF_6 was also verified. The [2]rotaxane **23**-H·PF_6 and dumbbell **25**-H·PF_6 were treated successively with excess KPF_6, H_2O and 1.0 M HCl/H_2O. Fluorescence spectra (Figure 2-18) reveal that anthracene fluorescence was observed only after the addition of acid. Neither addition of KPF_6 nor that of KPF_6/H_2O can restore anthracene emission. The anthracene emission was observed in the presence of HCl (1.0 M) and KPF_6, suggesting that acid is essential in disruption of fluorescence quenching.

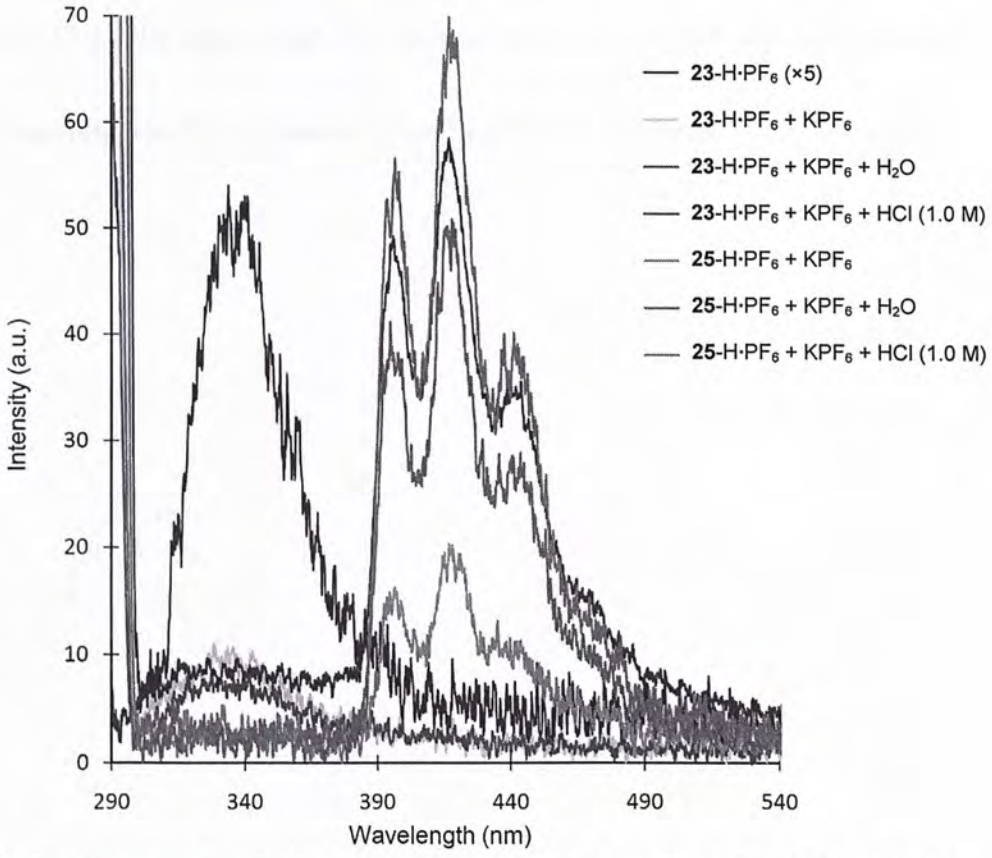

Figure 2-18. Fluorescence emission spectra (excitation wavelength = 290 nm) of **23**-H·PF_6 and **25**-H·PF_6 after successive addition of KPF_6, water and 1.0 M HCl/H_2O (conc. = 0.02 mM in MeCN).

2.5.4 Addition of Amines

The stability of [2]rotaxane **23**-H·PF_6 was further explored with a competitive imine exchange reaction. It is expected that, upon addition of an amine—toluidine (Tol-NH_2 or *p*-$MeC_6H_4NH_2$)—imine exchange interferes the imine formation of the macrocycle, hence cleaves the diimino-macrocycle and inhibits the production of rotaxane. After treatment of **23**-H·PF_6 with 2 equiv. of toluidine, ^{1}H NMR spectrum (Figure 2-19) disclosed new signals at δ = 8.63, 8.21 and 8.01 ppm, corresponding to new imine (H'_i) and pyridine aryl (H'_j and H'_k) protons, respectively. Signals of the

free dumbbell **25**-H·PF_6 were found. The absence of formyl signal suggested that the imine exchange reaction has a dynamic faster than NMR time scale.

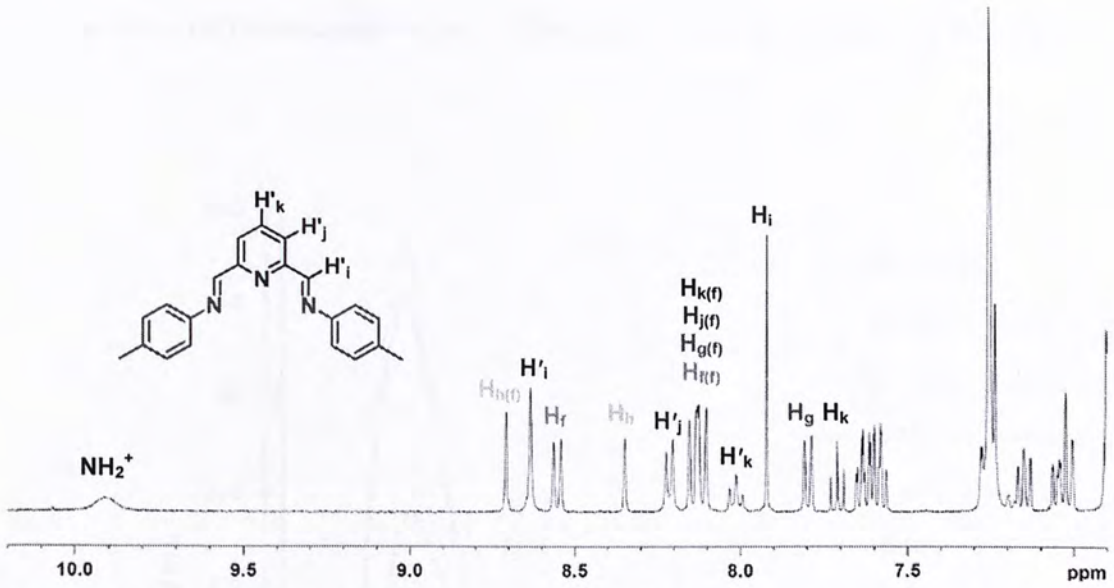

Figure 2-19. Partial ^{1}H NMR spectrum of **23**-H·PF_6 after treatment with 2 equiv. of toluidine in CD_3CN (f = free).

Since toluidine can successfully displace the dumbbell **25**-H·PF_6 from the [2]rotaxane **23**-H·PF_6, it may be a potential candidate for controlling fluorescence properties of **23**-H·PF_6. Fluorescence emission spectra (Figure 2-20) reveal that the anthracene fluorescence is quenched when [2]rotaxane **23**-H·PF_6 was mixed with 10 equiv. of toluidine in MeCN. However, anthracene fluorescence was observed after subsequent addition of water or acid. A control experiment demonstrated that anthracene fluorescence of the dumbbell **25**-H·PF_6 cannot be quenched by addition of 1 equiv. of toluidine. Therefore, it is reasonable to propose a dissociation

mechanism as shown in Scheme 2-6. The competitive imine exchange reaction leads to dissociation of the rotaxane **23**-H·PF_6 and formation of a new diimine compound **30** which exhibits additional supramolecular interactions with the dumbbell **25**-H·PF_6 and quenches its fluorescence when in close proximity (intermediates IV and V).

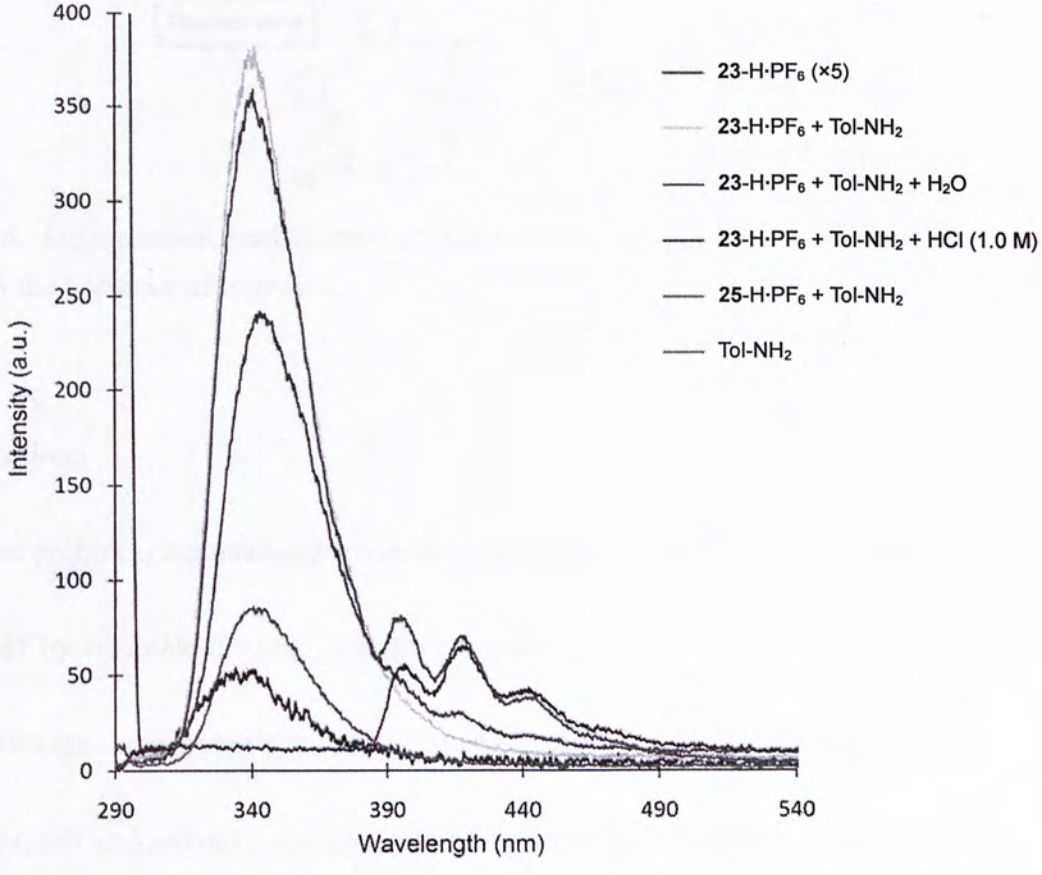

Figure 2-20. Fluorescence emission spectra (excitation wavelength = 290 nm) of components (conc. = 0.02 mM in MeCN).

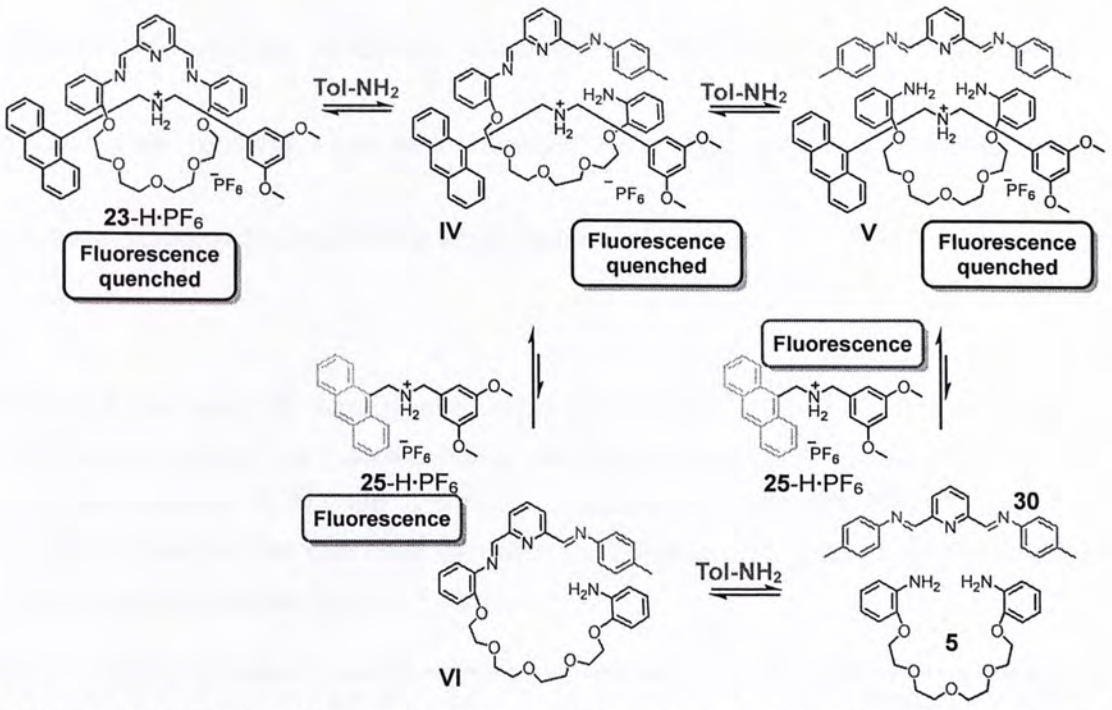

Scheme 2-6. Dissociation mechanism and fluorescence properties of [2]rotaxane **23**-H·PF_6 in the presence of toluidine.

2.6 Conclusions

A novel anthracene-containing dynamic [2]rotaxane **23**-H·PF_6 was synthesized in high yield by template-directed, thermodynamic self-assembly. The dissociation rate and anthracene quenching nature of [2]rotaxane **23**-H·PF_6 under external stimuli (water, acids, salt and amine) were investigated by using ^{1}H NMR spectroscopy and fluorescence spectrophotometry. The rotaxane dissociates much faster in the presence of acid than in the presence of excess water. Also, two acid sensors with linear and logarithmic modes of dimmer control were identified. The use of combinations of stimuli were investigated and summarized in Table 2-1 using a binary notation. In particular, entries C, I, J and O are somehow uncertain as it is nearly impossible to

maintain thoroughly dry conditions. The outputs (as bracketed values) are valid if the residual water molecules can be overlooked. As a result, different molecular logic can be acquired by rational selections of input combinations.

Table 2-1. Summary of fluorescence output of the rotaxane **23**-H·PF_6 in the presence of different stimuli. The fluorescence is measured under excitation at 290 nm. The threshold intensity at 418 nm is 5 (a.u.). Solution with intensity below 5 (a.u.) is defined as fluorescence quenched (output = 0). Solution with intensity above 5 (a.u.) is defined as fluorescent (output = 1).

Entry	Input				Output	
	H_2O	H^+	KPF_6	Tol-NH_2	Anthracene fluorescence at 418 nm	Fluorescence at 330 nm
A	0	0	0	0	0	1
B	1	0	0	0	0	1
C	0	1	0	0	(1)	0
D	0	0	1	0	0	1
E	0	0	0	1	0	1
F	1	1	0	0	1	0
G	1	0	1	0	0	1
H	1	0	0	1	0	1
I	0	1	1	0	(1)	0
J	0	1	0	1	(1)	0
K	0	0	1	1	0	1
L	1	1	1	0	1	0
M	1	1	0	1	1	0
N	1	0	1	1	0	1
O	0	1	1	1	(1)	0
P	1	1	1	1	1	0

Part II

Substituent Effect in Imine-Containing Molecular Tweezers

Chapter 3 – Molecular Tweezers

3.1 Introduction

Molecular tweezers (also known as molecular clips), a term coined by Whitlock,[30] is a class of synthetic receptors developed since 1980 which contain two preorganized aromatic chromophores covalently linked by a single spacer. A proper spacer allows a molecular tweezer to form sandwich complex with an aromatic substrate *via* π-π stacking interaction. More sophisticated molecular tweezers carry additional functional groups oriented towards the aromatic cleft so that hydrogen bonding can provide synergic effect in binding appropriate substrates. These noncyclic receptors possess distinct advantages over their cyclic relatives (cyclophanes) owing to their flexible cavities and topology, rendering them effective receptors for neutral and cationic aromatic substrates.[31]

In 2001, Park *et al.*,[32] reported a Schiff base molecular tweezer **31**, that forms a 1:1 complex with salicylaldehyde **32**, with an association constant (log K_a) of 1.10 (Figure 3-1a). The complex formation was monitored by ^{1}H NMR titration of the Schiff base **31** with salicylaldehyde **32**. During the complex formation, intramolecular hydrogen bonding of salicylaldehyde gets weaker, while the intermolecular hydrogen bonding between the tweezers and salicylaldehyde gets stronger. The driving forces for the complex formation are the hydrogen bonding and

π-π stacking interactions between the aromatic planes. Moreover, the pH-dependent reversible binding of the complex was demonstrated.

Recently, photochemistry has been utilized in complexation between molecular tweezers and substrates. The Klärner group[33] reported a luminescent host/guest complex involving a molecular tweezer **33** and 1,2,4,5-tetracyanobenzene (**TCNB**) (Figure 3-1b). Free molecular tweezer **33** and **TCNB** are colorless in $CHCl_3$. Equimolar mixture of both species is yellow and gives out luminescence due to the charge-transfer (CT) nature of the complex.

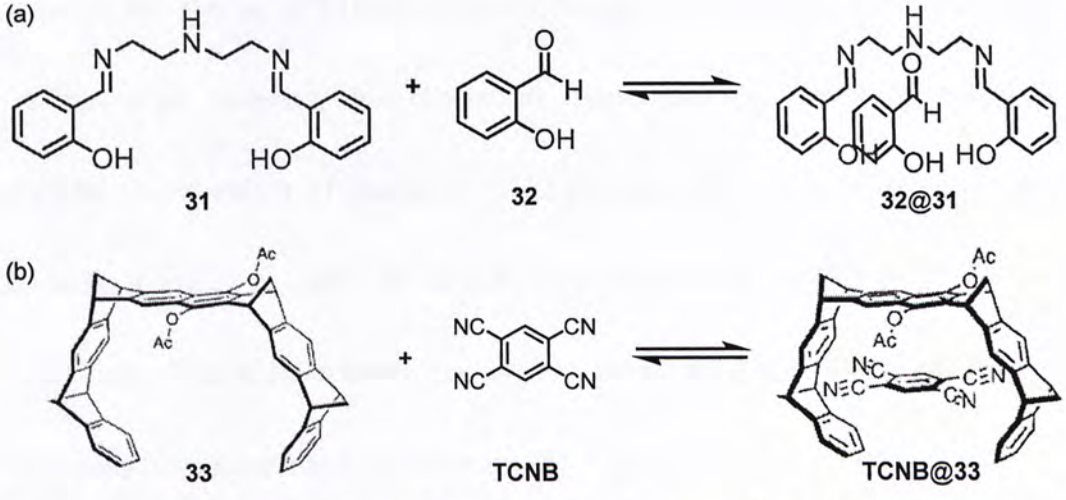

Figure 3-1. (a) Reversible complex formation between the Schiff base molecular tweezer **31** and salicylaldehyde **32** to form a 1:1 complex **32@31**; (b) Luminescent complex formed from a colorless molecular tweezer **33** and **TCNB** (figure obtained from Ref. 33).

In Chapter 2, the effect of external stimuli towards dissociation of the dynamic [2]rotaxane **23**-H·PF_6 was investigated. It was found that addition of toluidine can displace out the dumbbell **25**-H·PF_6 from the [2]rotaxane through competitive imine

exchange. Moreover, the newly formed diimine **30** exerts some supramolecular interactions on the dumbbell and quenches anthracene fluorescence when the two species are in close proximity. We are interested in understanding the binding characteristics and to investigate how substituents on the diimine can affect the binding affinity and fluorescence-quenching ability.

3.2 Synthesis

Two dumbbells, **7**-H·PF_6 and **25**-H·PF_6 (Figure 3-2), were selected for our investigation. The use of **7**-H·PF_6 allows the formation of symmetric complexes with the molecular tweezers, for convenient characterization and comparison of steric/electronic effects of dumbbell on the binding event. A series of symmetric diimine molecular tweezers **34**–**40** with different substituents (Figure 3-2) were synthesized. The stoichiometries and binding constants of the tweezers with two dumbbells were determined by monitoring the changes of chemical shift in their ^{1}H NMR spectra. Fluorescence properties of the complexes formed between the tweezers and dumbbell **25**-H·PF_6 were also monitored.

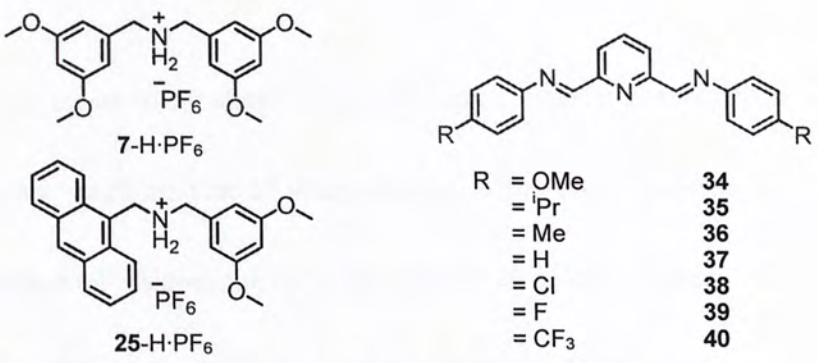

Figure 3-2. Structures of dumbbells and molecular tweezers.

Dumbbell **7**-H·PF_6 was prepared according to the literature procedure[4] while **25**-H·PF_6 was prepared as stated in Chapter 2. The molecular tweezers **34–40** were synthesized in high yield (Scheme 3-1) by a condensation of 2,6-diformylpyridine **4** with the corresponding aniline (1:2 molar ratio) in the presence of molecular sieves (4 Å).

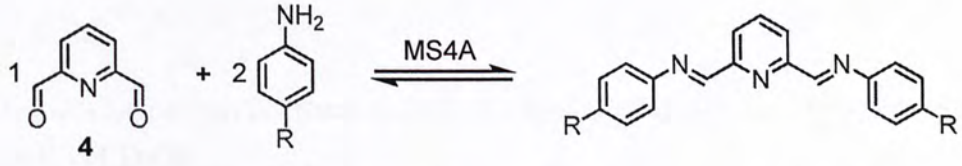

Scheme 3-1. General synthetic scheme for molecular tweezers **34–40** (R = OMe, ^{i}Pr, Me, H, Cl, F, and CF_3).

3.3 Characterization of Molecular Tweezers

3.3.1 ^{1}H NMR Spectroscopy

All diimine tweezers were characterized by ^{1}H NMR spectroscopy in CD_2Cl_2. The tweezers, dumbbells, and their complexes are well solvated in dichloromethane which is not acidic enough to hydrolyze imines, and is not a strong competitive

solvent in the presence of electron donor/acceptor species. Even though there is inevitably very small amount of water present in the NMR solution, all diimine tweezers showed no residual aldehyde signal at δ = 10.15 ppm in their NMR spectra, indicating that the tweezers are thermodynamically stable. Imine proton signals of the molecular tweezers show gradual changes in chemical shift according to the electron-withdrawing and electron-donating ability of the substituents. Compared to the reference compound **37** (R = H), imine protons of more electron-withdrawing group-substituted tweezers (R = Cl, F, CF_3) show upfield shift while more electron-donating substituted tweezers (R = OMe, ^{i}Pr, Me) show downfield shift (Table 3-1).

Table 3-1. Comparison of chemical shift of imine ^{1}H NMR signal of tweezers **34–40** at 296 K in CD_2Cl_2.

Tweezers	R	Chemical shift of imine proton δ (ppm)
34	OMe	8.68
35	^{i}Pr	8.68
36	Me	8.66
37	H	8.66
38	Cl	8.63
39	F	8.64
40	CF_3	8.64

3.3.2 Mass Spectroscopy

Molecular tweezers **35**, **38**, **39**, and **40** were analyzed by high resolution ESI-MS. All mass spectra show the presence of target molecular ion peaks (Table 3-2), without any fragment of hydrolyzed imine tweezers or dialdehyde **4**. It follows that these molecular tweezers show remarkable stability in gas phase.

Table 3-2. Summary of mass-to-charge ratios of tweezers from ESI-mass spectra.

Tweezers	R	Molecular ion	Calculated	Found
35	^{i}Pr	$[M+Na]^+$	392.2097	392.2100
38	Cl	$[M+Na]^+$	376.0376	376.0378
39	F	$[M+Na]^+$	344.0970	344.0965
40	CF_3	$[M+H]^+$	422.1086	422.1095

3.4 Characterization of Complexes

3.4.1 ^{1}H NMR Spectroscopy

The tweezers **34–40** and the two dumbbells **7**-H·PF_6 and **25**-H·PF_6 were mixed and matched (1:1 ratio, conc. = 20 mM) and stood for 6 h to reach equilibrium before obtaining the NMR data. From all NMR spectra, proton signals of free and complexed tweezers appeared as weighted-averages, suggesting that all complexations undergo fast exchange on the NMR timescale. Complex formation can be detected through the pronounced shifts of signals in the ^{1}H NMR spectra of dumbbells after addition of the tweezer. By way of an example, for an equimolar mixture of tweezer **34** and dumbbell **25**-H·PF_6 (Figure 3-3), significant shifts of

protons (H_d, H_e, H_i, H_l, and H_n) signify the emergence of noncovalent interactions ([N^+–H···N] and [N^+C–H···N] hydrogen bonding, π–π stacking, and electrostatic) after complexation. Noticeably, an aldehyde proton signal at δ = 10.09 ppm is present since small amount of the tweezer **34** was inevitably hydrolyzed into its separate components, in the presence of the acidic dumbbell **25**-H·PF_6.

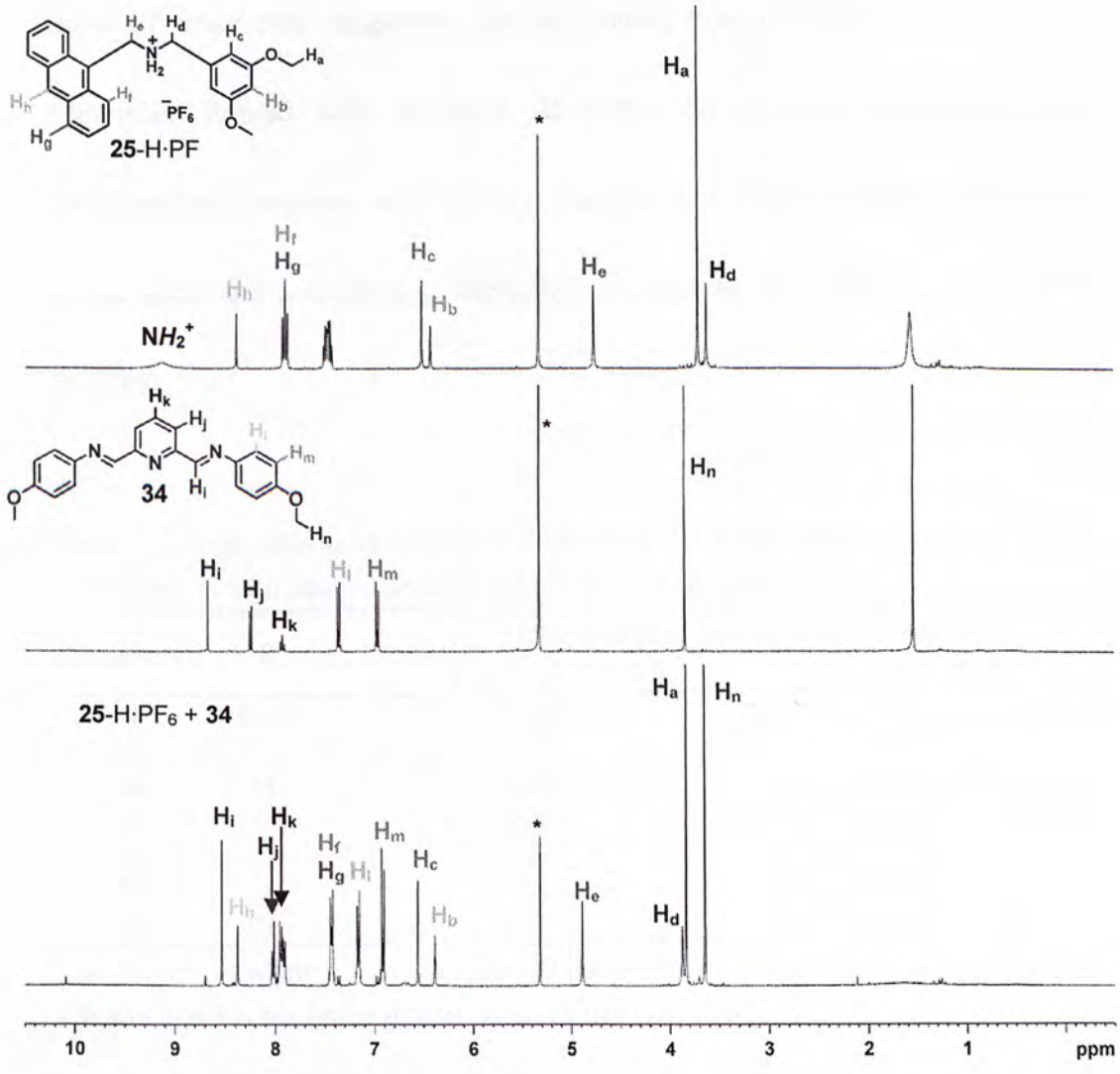

Figure 3-3. Stacked partial ^{1}H NMR spectra of dumbbell **25**-H·PF_6, tweezer **34** and their equimolar mixture in CD_2Cl_2.

Upon complexation, the imine nitrogen atoms and pyridine unit on the tweezers donate electron to the ammonium center of the dumbbells and, in return, disperse the electron density around the imine. Therefore, by monitoring the extent of upfield shift of imine proton, the binding strength between the tweezers and dumbbells can be estimated. From Table 3-3, the upfield shifts of imine proton reduce down the series of complexes, suggesting that the binding strength declines. Furthermore, complexes formed with dumbbell **25**-H·PF_6 show greater shifts than the corresponding complexes with **7**-H·PF_6. This greater binding strength may attribute to the additional π–π stacking interaction provided by the anthracene moiety of **25**-H·PF_6.

Table 3-3. Comparison of upfield shift of imine ^{1}H NMR signal of tweezers after complexation with equimolar of dumbbells **7**-H·PF_6 and **25**-H·PF_6.

Tweezers	R	Upfield shift of imine proton $\Delta\delta$ (ppm)[a]	
		Dumbbell **7**-H·PF_6	Dumbbell **25**-H·PF_6
34	OMe	0.06	0.13
35	^{i}Pr	0.06	0.13
36	Me	0.05	0.09
37	H	0.03	0.10
38	Cl	0.01	0.06
39	F	0.01	0.06
40	CF_3	0.01	0.03

[a] $\Delta\delta = \delta_{obs} - \delta$; where δ_{obs} is the observed imine proton signal in the fast equilibrating mixture and δ is the imine proton signal of free tweezers.

In order to determine the stoichiometries and binding constants (K) of the complexes formed between the tweezers **34–40** and dumbbells **7**-H·PF_6 and **25**-H·PF_6, ^{1}H NMR titration experiments were conducted. The total concentration of the solution was kept constant while the ratio between a tweezer and a dumbbell varied. The dependence of complexation-induced ^{1}H NMR shifts of methylene proton next to the ammonium centers (–N^+CH_2–) on the dumbbells (δ = 3.92 and 4.76 ppm for free **7**-H·PF_6 and **25**-H·PF_6 respectively) was monitored as the mole fraction of dumbbell varied. The stoichiometries were determined from the x-coordinate at the maximum in a Job plot[34] whereas the observed chemical shift times the concentration of dumbbell is plotted against the mole fraction of dumbbell. Complexation between tweezer **36** and dumbbell **7**-H·PF_6 was taken as an example (Figure 3-4). Extrapolations of data points near the mole fractions = 0 and 1 give an interception point at mole fraction = 0.51. Therefore, tweezer **36** and dumbbell **7**-H·PF_6 form a 1:1 complex. Since the chemical shift of the methylene proton next to the ammonium centers (–N^+CH_2–) of the complexed dumbbell δ_c cannot be obtained directly, therefore, Rose-Drago method[35] was applied to evaluate the complex concentration and hence the binding constant (K). By fitting the data into a 1:1 complexation model, δ_c and K were determined to be 4.10 ppm and 359 M^{-1} respectively. The δ_c and K values for other complexes were calculated (Table 3-4 and

3-5). However, some of the complexes, especially those with the dumbbell **25**-H·PF_6, are unstable and exists in several co-conformations. Thus, large errors arose during the calculation and that their Job plots could not be obtained. For complexes with stoichiometry other than 1:1, δ_c and K cannot be evaluated using the Rose-Drago method.

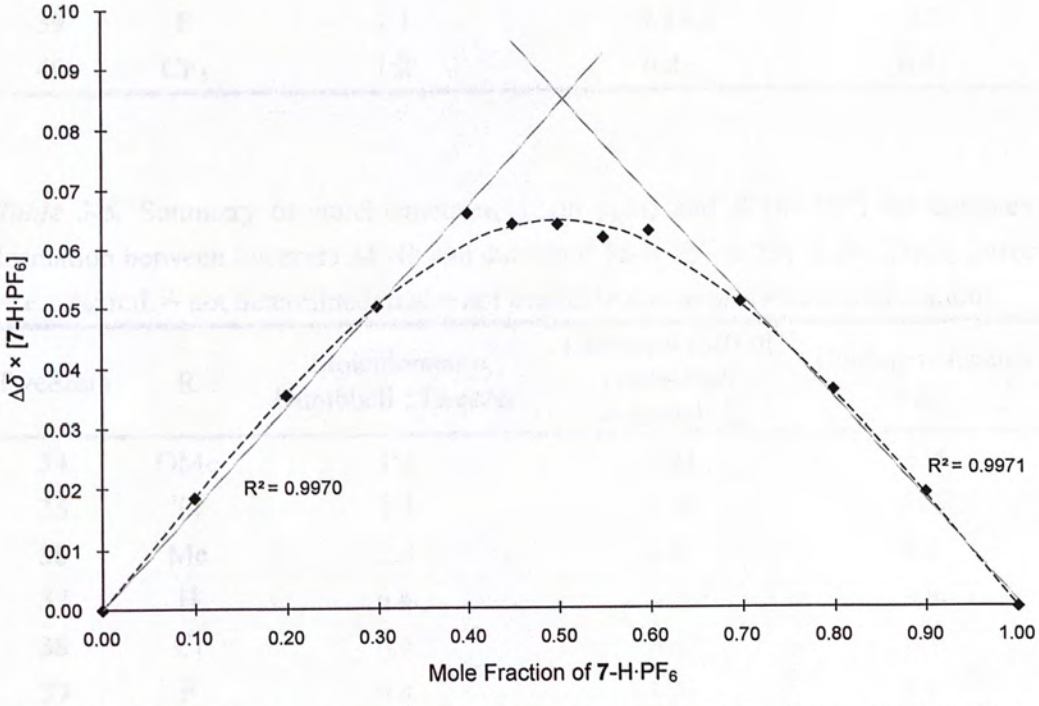

Figure 3-4. Job plot for complexation between tweezer **36** and dumbbell **7**-H·PF_6 (total conc. = 20 mM) based on NMR spectroscopic data (♦: observed; – – –: calcd).

Table 3-4. Summary of stoichiometries, δ_c (in ppm) and K (in M^{-1}) for complex formation between tweezers **34–40** and dumbbell **7**-H·PF_6 at 295 K in CD_2Cl_2 (error = ± 1 %; n.d. = not determined).

Tweezers	R	Stoichiometry Dumbbell : Tweezer	Chemical shift of complexed dumbbell δ_c	Binding constants K
34	OMe	2:1	n.d.	n.d.
35	^{i}Pr	1:1	4.13	399
36	Me	1:1	4.10	359
37	H	1:1	4.19	128
38	Cl	1:2	n.d.	n.d.
39	F	1:1	4.13	87
40	CF_3	1:2	n.d.	n.d.

Table 3-5. Summary of stoichiometries, δ_c (in ppm) and K (in M^{-1}) for complex formation between tweezers **34–40** and dumbbell **25**-H·PF_6 at 295 K in CD_2Cl_2 (error = ± 1 %; n.d. = not determined; n.a. = not available due to unstable complexation).

Tweezers	R	Stoichiometry Dumbbell : Tweezer	Chemical shift of complexed dumbbell δ_c	Binding constants K
34	OMe	1:1	5.04	238
35	^{i}Pr	1:1	5.04	178
36	Me	2:3	n.d.	n.d.
37	H	n.a.	n.a.	n.a.
38	Cl	n.a.	n.a.	n.a.
39	F	n.a.	n.a.	n.a.
40	CF_3	n.a.	n.a.	n.a.

For the complexes formed between tweezers **34–40** and dumbbell **7**-H·PF_6, in comparison, a more electron-donating group substituted tweezer (e.g., **34** with a –OMe group) can accommodate with more than one dumbbell molecule (i.e., higher dumbbell/tweezer ratio). The electron-donating group enhances the tweezer's binding affinity towards the dumbbell's ammonium center *via* an increased

ion-dipole interaction. As the electron-donating ability of the tweezers decreases, the stoichiometries of tweezer@dumbbell complexes as well as the binding constants decrease. This trend also occurs for complexes with dumbbell **25**-H·PF_6.

To further confirm the interactions between the molecular tweezers and the dumbbell, two-dimensional NOESY ^{1}H NMR spectroscopy was employed. From an equimolar mixture of tweezer **34** and dumbbell **25**-H·PF_6 in dry CD_2Cl_2 (Figure 3-5), strong NOE signals appear among the methylene proton (H_e) next to the ammonium center, anthracyl proton (H_h), and pyridine proton at *para* position (H_k). Protons (H_{a-c}) on the 3,5-dimethoxy group of the dumbbell show no correlation with protons of the tweezer. Therefore, it is reasonable to propose that the pyridine moiety of the tweezer should be assembled with the anthracene unit of the dumbbell, forming a face-to-face complex.

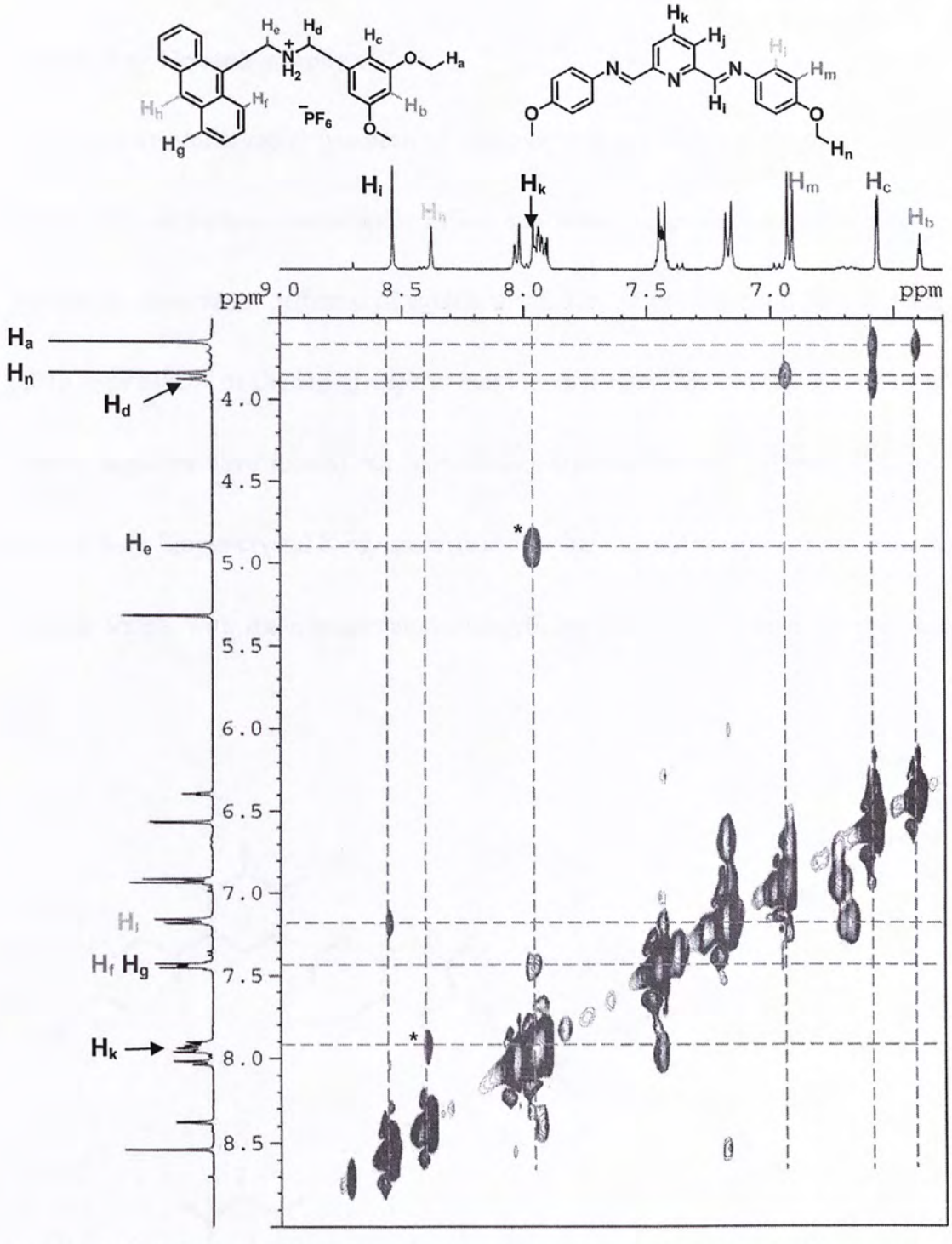

Figure 3-5. A 2D-NOESY spectrum of equilibrating mixture of molecular tweezers **34** and dumbbell **25**-H·PF_6 in 1:1 ratio. Peaks corresponding to correlation between the tweezers and dumbbell are marked with an asterisk (*).

3.4.2 X-Ray Crystallography

X-ray crystallography has been an efficient tool to characterize intermolecular interactions of various compounds. Effort was made to grow dumbbell@tweezer crystals by slow vapor diffusion of equimolar mixture of tweezers and dumbbells in (CH_2Cl_2 or MeCN or $ClCH_2CH_2Cl$)/*tert*-butyl methyl ether (^{t}BuOMe). No crystals of these complexes were formed but free tweezer crystals (**34** and **36**) were obtained (Figure 3-6). Single-crystal X-ray analysis shows that the molecular tweezers possess a linear shape, with the nitrogen atoms of pyridine and imines facing the opposite side.

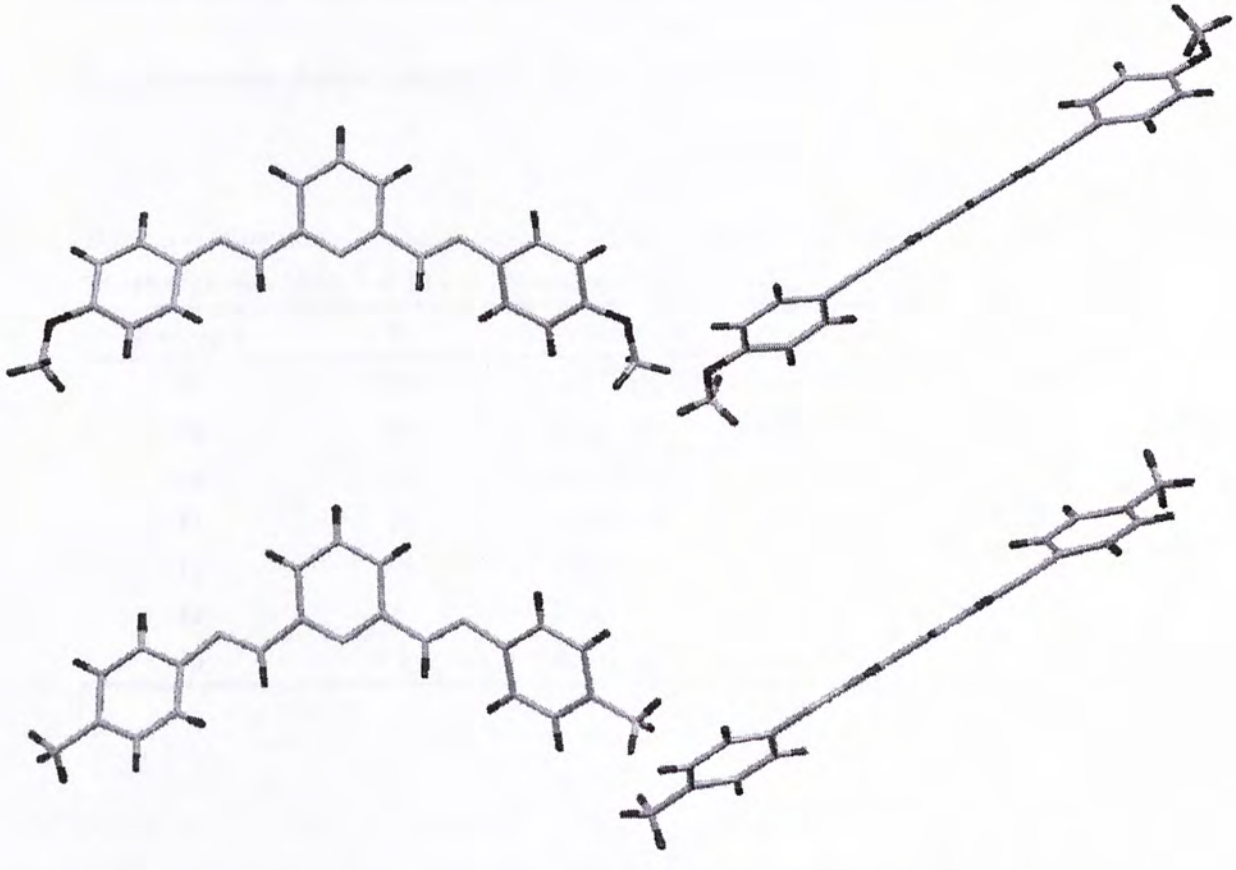

Figure 3-6. Solid-state structures of molecular tweezers **34** (top) and **36** (bottom).

3.4.3 Mass Spectroscopy

Mixtures of tweezers **34–40** with dumbbells **7**-H·PF_6 and **25**-H·PF_6 in dry CH_2Cl_2 (total conc. = 0.02 mM) were prepared according to the stoichiometries obtained from Job's plots and analyzed with high resolution ESI-MS (Table 3-6 and 3-7). Unfortunately, no molecular ion peaks with the determined complex stoichiometries were observed. It follows that the 1:1 molecular tweezers/dumbbell ratio is the most stable conformation in gas phase. Noticeably, an adduct with a general structure of $[Na@Tweezers_2]^+$ was found in all ESI-mass spectra. It is believed that the strong binding affinity of molecular tweezers with Na^+ disrupts the formation of the desired complexes—$[Dumbbell@Tweezers_2]^+$.

Table 3-6. Summary of mass-to-charge ratios of complexes formed from tweezers **34–40** with dumbbell **7**-H·PF_6 in ESI-mass spectra.

Tweezers	R	Molecular ion	Calculated	Found
34	OMe	[**34**@**7**-H]$^+$	663.3177	663.3184
35	^{i}Pr	[**35**@**7**-H]$^+$	687.3905	687.3922
36	Me	[**36**@**7**-H]$^+$	631.3279	631.3286
37	H	[**37**@**7**-H]$^+$	603.2966	603.2961
38	Cl	[**38**@**7**-H]$^+$	671.2186	671.2185
39	F	[**39**@**7**-H]$^+$	639.2777	639.2771
40	CF_3	[**40**@**7**-H]$^+$	739.2714	739.2713

Table 3-7. Summary of mass-to-charge ratios of complexes formed from tweezers **34–40** with dumbbell **25**-H·PF_6 in ESI-mass spectra.

Tweezers	R	Molecular ion	Calculated	Found
34	OMe	[**34**@**25**-H]$^+$	703.3279	703.3294
35	^{i}Pr	[**35**@**25**-H]$^+$	727.4007	727.3995
36	Me	[**36**@**25**-H]$^+$	671.3381	671.3376
37	H	[**37**@**25**-H]$^+$	643.3068	643.3067
38	Cl	[**38**@**25**-H]$^+$	711.2288	711.2312
39	F	[**39**@**25**-H]$^+$	679.2879	679.2886
40	CF_3	[**40**@**25**-H]$^+$	779.2815	779.2826

3.4.4 UV/Visible Absorption Spectroscopy

UV/Vis absorption spectra (Figure 3-7) of all tweezers show a broad imino residual band and that of the dumbbell **25**-H·PF_6 shows the characteristic anthracene absorption band at 300–400 nm. Fluorescence spectra (Figure 3-8) of equimolar mixture of tweezers **34–40** and dumbbell **25**-H·PF_6 show the characteristic anthracene emission (λ_{max} = 418 nm), yet, with lower intensities than that of the free **25**-H·PF_6. This result suggests that, though the binding strengths of tweezers are not strong enough to completely quench **25**-H·PF_6, they are capable to lower the anthracene emission. In addition, as the electron-donating ability decreases down along the tweezers **34–40**, the ability to lower the anthracene fluorescence also decreases. This result agrees well with the previous NMR studies wherein the binding strength decreases down the series.

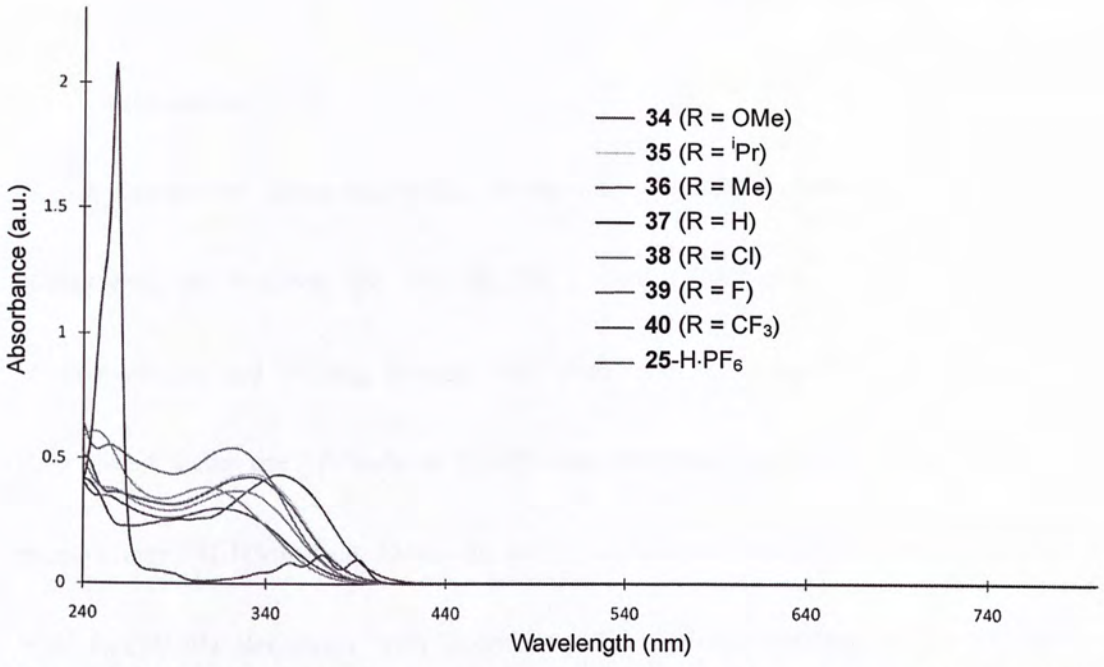

Figure 3-7. UV/vis absorption spectra of molecular tweezers **34**–**40** and dumbbell **25**-H·PF_6 (0.02 mM in CH_2Cl_2).

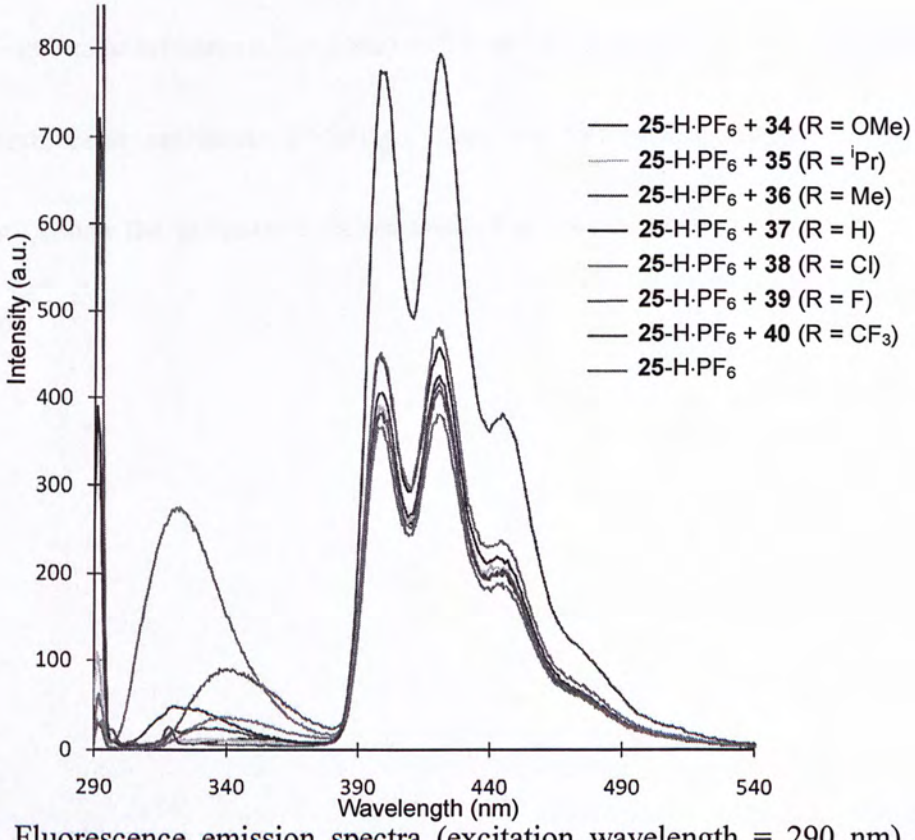

Figure 3-8. Fluorescence emission spectra (excitation wavelength = 290 nm) of dumbbell **25**-H·PF_6 and its equimolar mixture with molecular tweezers **34**–**40** (0.02 mM in CH_2Cl_2).

3.5 Conclusions

A series of imine-containing molecular tweezers **34–40** with different substituents (R = OMe, ^{i}Pr, Me, H, Cl, F, and CF_3) were synthesized. Their stoichiometries and binding strength with dumbbells **7**-H·PF_6 and **25**-H·PF_6 were determined using the Methods of Continuous Variations and Rose-Drago method based on the ^{1}H NMR data. Down the series of tweezers, the binding strength with both dumbbells decreases with decreasing the electron-donating ability of the substituents. Moreover, the tweezers generally show a stronger binding with the anthracene-containing dumbbell **25**-H·PF_6 than dumbbell **7**-H·PF_6. Fluorescence spectra of equimolar mixtures of the tweezers **34–40** and dumbbell **25**-H·PF_6 show a reduced anthracene emission. It follows that, the complexes formed cannot completely quench the anthracene fluorescence, but only weaken the intensity to some extent.

Chapter 4 – Experimental Procedures

4.1 General Information

^{1}H, ^{13}C, and ^{1}H NOESY NMR spectra for structural characterization were recorded on Bruker Avance 400 (^{1}H: 400 MHz; ^{13}C: 101 MHz) spectrometer at 296 K. NMR samples were dissolved in $CDCl_3$ unless otherwise stated. Chemical shifts were reported as parts per million (ppm) in δ scale and calibrated by using the solvent residual peak (e.g., for residual $CHCl_3$ in $CDCl_3$, ^{1}H: $\delta = 7.26$; ^{13}C: $\delta = 77.16$) as internal standard. Coupling constants (J) were reported in hertz. Electrospray ionization (ESI) mass spectra were obtained on a Thermo Finnigan MAT 95XL mass spectrometer using 1:1 CH_2Cl_2–MeOH as mobile phase. The reported molecular mass (m/z) values correspond to the most abundant monoisotopic masses. Melting points were measured on an Electrothermal 9100 digital melting point apparatus and were uncorrected. UV/Visible absorption spectra were obtained using a Cary 5G UV-Vis-NIR spectrophotometer. Excitation and fluorescence spectra were recorded using a Hitachi F-4500 Fluorescence spectrophotometer. The intensity data for crystals were collected with a Bruker APEX II X-ray diffractometer or a Bruker ASX CCD X-ray system.

All non-aqueous reactions were carried out under dry, high-purity N_2 with oven-dried (115 °C) glassware. Unless otherwise specified, all solvents and reagents

were purchased commercially with reagent quality and used without further purification. Tetrahydrofuran (THF) was freshly distilled from Na/benzophenone ketyl under N_2. Toluene (PhMe) was freshly distilled from Na spheres. Dichloromethane (CH_2Cl_2) was freshly distilled from CaH_2. Acetonitrile (MeCN) was pre-dried by stirring with CaH_2 for 24 h and distillation under N_2, and stored in the presence of molecular sieves (4 Å). Thin layer chromatography (TLC) was performed on silica gel 60 F_{254} (Merck). Column chromatography was performed on silica gel 60F (Merck 9385, 0.040–0.063 mm).

4.2 General Synthetic Procedures for Molecular Tweezers (34–40)

A solution of *p*-substituted aniline (2.0 equiv.) and 2,6-diformylpyridine **4** (1.0 equiv.) in anhydrous CH_2Cl_2 (1 mL/mmol) was stirred in the presence of 4 Å molecular sieves for 4 h. Molecular sieves were filtered off and washed with CH_2Cl_2. The excess of solvent of the filtrate was removed in *vacuo* to yield the product.

4.3 Experimental Procedures

Amino dumbbell 25. A solution of 9-anthraldehyde **29** (0.62 g, 2.99 mmol) and 3,5-dimethoxybenzylamine **28** (0.55 mL, 3.64 mmol) in PhMe (50 mL) was heated to reflux for 24 h using a Dean-Stark apparatus. The resulting solution was evaporated to

dryness. The residue was re-dissolved in a mixture of MeOH/CH_2Cl_2 (20 mL/ 10 mL) and then $NaBH_4$ (0.51 g, 13.40 mmol) was added at 0 °C. The reaction mixture was stirred at ambient temperature for 24 h. After that, the solvents were removed *in vacuo*, and the residue was partitioned between H_2O (50 mL) and CH_2Cl_2 (25 mL). The aqueous layer was further extracted with CH_2Cl_2 (3 × 25 mL). The combined organic extracts were dried ($MgSO_4$) and the resulting solution was evaporated to dryness. Flash column chromatography with hexane/EtOAc/Et_3N (150:50:1) on silica gel of the residue gave the amine **25** (0.94 g, 88 %) as a bright yellow powder. R_f: 0.26 (hexane/EtOAc/Et_3N = 150:50:1). M.p. 85.4–87.1 °C. ^{1}H NMR: δ = 3.82 (s, 6 H, OC*H*$_3$), 3.99 (s, 2 H, C*H*$_2$NH), 4.69 (s, 2 H, C*H*$_2$NH), 6.42 (t, J = 2.2 Hz, 1 H, Ar*H*), 6.62 (d, J = 2.2 Hz, 2 H, Ar*H*), 7.44–7.52 (m, 4 H, Ar*H*), 8.01 (d, J = 7.7 Hz, 2 H, Ar*H*), 8.25 (d, J = 8.8 Hz, 2 H, Ar*H*), 8.41 (s, 1 H, Ar*H*). ^{13}C NMR: δ = 44.9, 54.5, 55.5, 99.5, 106.1, 124.3, 125.0, 126.1, 127.3, 129.2, 130.4, 131.66, 131.74, 143.1, 161.1. HRMS (ESI): $C_{24}H_{23}NO_2$ $[M+H]^+$: calcd 358.1802; found 358.1799.

Ammonium dumbbell 25-H·PF$_6$. A solution of amine **25** (0.73 g, 2.05 mmol) in CH_2Cl_2/MeCN (30 mL/ 10 mL) was added dropwise with 60 wt. % HPF_6 in H_2O (0.60 mL, 7.28 mmol) at 0 °C over a period of 5 min and stirred at ambient temperature for 2 h. The solvents were removed *in vacuo* to give a yellow solid, which

was then dissolved in CH_2Cl_2 (40 mL), washed with H_2O (20 mL), further extracted with CH_2Cl_2 (3 × 10 mL) and dried (Na_2SO_4). The resulting solution was evaporated to give the product **25**-H·PF_6 as an off-white powder (0.78 g, 75%). M.p. > 194 °C (decomposed). ^{1}H NMR (CD_3CN): δ = 3.80 (s, 6 H, OCH_3), 4.41 (t, J = 5.2 Hz, 2 H, $CH_2NH_2^+$), 5.24 (t, J = 6.0 Hz, 2 H, $CH_2NH_2^+$), 6.61 (t, J = 2.2 Hz, 1 H, Ar*H*), 6.69 (d, J = 2.2 Hz, 2 H, Ar*H*), 7.12–7.50 (br, 2 H, NH_2^+), 7.58–7.68 (m, 4 H, Ar*H*), 8.10 (d, J = 8.8 Hz, 2 H, Ar*H*), 8.16 (d, J = 8.3 Hz, 2 H, Ar*H*), 8.74 (s, 1 H, Ar*H*). ^{13}C NMR (CD_3CN, one aromatic signal is missing/overlapping): δ = 43.9, 52.8, 56.3, 102.3, 109.1, 122.1, 124.1, 126.6, 128.6, 130.5, 131.8, 132.3, 133.4, 162.5. HRMS (ESI): $C_{24}H_{24}F_6NO_2P$ $[M-PF_6]^+$: calcd 358.1802; found 358.1795. Slow evaporation of a solution of **25**-H·PF_6 in CH_2Cl_2/^{t}BuOMe yielded single crystals of the dumbbell suitable for X-ray crystallography. X-ray diffraction: $[C_{48}H_{48}N_2O_4]Cl(PF_6)$, M = 897.30, triclinic, $P\bar{1}$, a = 12.0530(4), b = 12.8073(4), c = 16.0081(9) Å, α = 95.8310(10)°, β = 99.9830(10)°, γ = 114.1490(10)°, V = 2179.41(16) Å^3, Z = 2, D_{calcd} = 1.367 Mg/m^3, μ(Mo-K_α) = 0.197 mm^{-1}, F(000) = 936, T = 296 K, 0.50 × 0.40 × 0.30 mm, colorless prisms; 7855 independent measured reflections, full-matrix least-squares on F^2 refinement, R_1 = 0.0420, wR_2 = 0.1117, 6456, independent observed reflections, [$|F_o| > 4\sigma(|F_o|)$, $2\theta_{max}$ = 50.5°], 562 parameters.

Amine 27. 1-(2-(2-(2-methoxyethoxy)ethoxy)ethoxy)-2-nitrobenzene **26** was prepared as described in the literature.[28] A solution of nitrobenzene **26** (0.14 g, 0.50 mmol) in EtOH (10 mL) was mixed with wet Pd/C (catalytic amount) and hydrazine hydrate (0.10 mL, 3.21 mmol) and then heated to reflux for 24 h. The resulting mixture was filtered through a pad of Celite, washed with H_2O (5 mL) and extracted with CH_2Cl_2 (3 × 10 mL), dried ($MgSO_4$), and evaporated to dryness to give the product **27** as a faintly yellow liquid (0.12 g, 93%). ^{1}H NMR: δ = 3.38 (s, 3 H, OC*H*$_3$), 3.54–3.57 (m, 2 H, aliphatic *H*), 3.65–3.69 (m, 4 H, aliphatic *H*), 3.72–3.74 (m, 2 H, aliphatic *H*), 3.84–3.86 (m, 2 H, aliphatic *H*), 3.87–3.93 (br, 2 H, N*H*$_2$), 4.14–4.17 (m, 2 H, aliphatic *H*) 6.67–6.73 (m, 2 H, Ar*H*), 6.78–6.82 (m, 2 H, Ar*H*). ^{13}C NMR: δ = 58.7, 68.1, 69.5, 70.3, 70.38, 70.45, 71.7, 112.8, 114.9, 117.8, 121.6, 137.1, 146.0. HRMS (ESI): $C_{13}H_{21}NO_4$ $[M+Na]^+$: calcd 278.1363; found 278.1364.

Podand 24. A solution of 2,6-pyridinedicarboxaldehyde **4** (0.03g, 0.23 mmol) and amine **27** (0.12 g, 0.46 mmol) in CH_2Cl_2 (5 mL) was stirred with molecular sieve (4 Å) for 1 d. Removal of the molecular sieve and solvent gave the product (0.14 g, 94 %) as a yellow oil. ^{1}H NMR: 3.33 (s, 6 H, OC*H*$_3$), 3.49 (t, *J* = 4.6 Hz, 4 H, aliphatic *H*), 3.59–3.64 (m, 8 H, aliphatic *H*), 3.75 (t, *J* = 4.6 Hz, 4 H, aliphatic *H*), 3.89 (t, *J* = 4.8 Hz, 4 H, aliphatic *H*), 4.24 (t, *J* = 4.8 Hz, 4 H, aliphatic *H*), 7.00–7.02

(m, 4 H, Ar*H*), 7.13 (d, *J* = 7.2 Hz, 2 H, Ar*H*), 7.20 (t, *J* = 7.2 Hz, 2 H, Ar*H*), 7.92 (t, *J* = 7.7 Hz, 1 H, Ar*H*), 8.31 (d, *J* = 7.7 Hz, 2 H, Ar*H*), 8.70 (s, 2 H, Ar*H*). ^{13}C NMR: 59.0, 68.9, 69.7, 70.5, 70.7, 71.0, 71.9, 114.1, 121.0, 121.6, 122.9, 127.5, 137.1, 140.9, 151.6, 154.8, 161.2. HRMS (ESI): $C_{33}H_{43}N_3O_8$ $[M+Na]^+$: calcd 632.2942; found 632.2940.

[2]Rotaxane 23-H·PF$_6$. Diamine **5** was prepared as described in the literature procedure.[15] A solution of dialdehyde **4** (0.04 g, 0.28 mmol), diamine **5** (0.10 g, 0.28 mmol) and thread **25**-H·PF$_6$ (0.14 g, 0.28 mmol) in dry MeCN (0.46 mL, 60 mM) was stirred for 5 min at ambient temperature. Evaporation of the solvent yielded the product rotaxane **23**-H·PF$_6$ (94 %) as a yellow solid. M.p. > 163 °C (decomposed). ^{1}H NMR (CD_3CN): 3.32 (s, 6 H, OCH_3), 3.59–3.84 (m, 10 H, aliphatic *H*), 4.03–4.08 (m, 2 H, aliphatic *H*), 4.29–4.31 (m, 4 H, aliphatic *H*), 5.13 (t, *J* = 6.9 Hz, 2 H, CH_2NH$_2^+$), 5.82 (t, *J* = 6.7 Hz, 2 H, CH_2NH$_2^+$), 6.11 (t, *J* = 2.0 Hz, 1 H, Ar*H*), 6.48 (d , *J* = 7.7 Hz, 2 H, Ar*H*), 6.52 (d, *J* = 2.0 Hz, 2 H, Ar*H*), 6.83 (t, *J* = 7.7 Hz, 2 H, Ar*H*), 7.00–7.07 (m, 4 H, Ar*H*), 7.15 (t, *J* = 7.4 Hz, 2 H, Ar*H*), 7.24–7.28 (m, 4 H, Ar*H*), 7.71 (t, *J* = 7.7 Hz, 1 H, Ar*H*), 7.79 (d, *J* = 8.4 Hz, 2 H, Ar*H*), 7.92 (s, 2 H, Ar*H*), 8.35 (s, 1 H, Ar*H*), 8.55 (d, *J* = 8.9 Hz, 2 H, Ar*H*), 9.67–10.05 (br, 2 H, NH_2^+). ^{13}C NMR (CD_3CN): 45.3, 53.3, 55.6, 69.2, 70.4, 71.8, 72.0, 100.9, 105.3, 112.9,

120.6, 122.2, 124.4, 124.9, 126.0, 127.3, 129.5, 129.6, 130.1, 130.5, 131.8, 132.1, 136.6, 139.5, 140.2, 152.8, 153.0, 160.1, 161.4. HRMS (ESI): $C_{51}H_{53}F_6N_4O_7P$ $[M–PF_6]^+$: calcd 833.3909; found 833.3882.

Diimine 34 (R = OMe). Slow evaporation of an equimolar mixture of **34** and dumbbell **7**-H·PF_6 in $ClCH_2CH_2Cl$/^{t}BuOMe yielded only single crystals of the diimine **34** suitable for X-ray crystallography. X-ray diffraction: $[C_{21}H_{19}N_3O_2]$, M = 345.39, orthorhombic, *A*ba2, a = 7.1660(6), b = 40.204(3), c = 6.3427(5) Å, α = 90°, β = 90°, γ = 90°, V = 1827.4(3) Å^3, Z = 4, D_{calcd} = 1.255 Mg/m^3, μ(Mo-K_α) = 0.083 mm^{-1}, F(000) = 728, T = 296 K, 0.40 × 0.30 × 0.20 mm, colorless prisms; 2019 independent measured reflections, full-matrix least-squares on F^2 refinement, R_1 = 0.0439, wR_2 = 0.0920, 1226, independent observed reflections, [$|F_o| > 4\sigma(|F_o|)$, $2\theta_{max}$ = 55.9°], 119 parameters.

Diimine 35 (R = ^{i}Pr). Following the general procedure, a mixture of 4-isopropylaniline (0.49 g, 3.60 mmol) and 2,6-diformylpyridine **4** (0.24 g, 1.80 mmol) were stirred in anhydrous CH_2Cl_2 (5 mL) with molecular sieve (4 Å) for 4 h. After a filtration and subsequent removal of solvent, diimine **35** was obtained as a bright yellow solid (0.55 g, 83 %). R_f: 0.81 (hexane/EtOAc = 1:1). M.p. 126.8–127.2

°C. ^{1}H NMR (CD_2Cl_2): 1.28 (d, J = 6.9 Hz, 12 H, $CH(CH_3)_2$), 2.96 (quin, J = 6.9 Hz, 2 H, $CH(CH_3)_2$), 7.26–7.34 (m, 8 H, Ar*H*), 7.94 (t, J = 7.8 Hz, 1 H, Ar*H*), 8.27 (d, J = 7.8 Hz, 2 H, Ar*H*), 8.68 (s, 2 H, *H*C=N). ^{13}C NMR (CD_2Cl_2): 24.4, 34.3, 121.7, 123.2, 127.8, 137.8, 148.6, 149.1, 155.4, 159.9. HRMS (ESI): $C_{32}H_{27}N_3$ $[M+Na]^+$: calcd 392.2097; found 392.2100.

Diimine 36 (R = Me). Slow evaporation of an equimolar mixture of **36** and dumbbell **7**-H·PF_6 in CH_2Cl_2/MeCN yielded only single crystals of the diimine **36** suitable for X-ray crystallography. X-ray diffraction: [$C_{21}H_{19}N_3$], M = 313.39, monoclinic, $P2/c$, a = 4.7249(7), b = 6.2811(9), c = 28.965(4) Å, α = 90°, β = 94.639(3) °, γ = 90 °, V = 856.8(2) Å^3, Z = 2, D_{calcd} = 1.215 Mg/m^3, μ(Mo-K_α) = 0.073 mm^{-1}, F(000) = 332, T = 296 K, 0.50 × 0.40 × 0.30 mm, colorless prisms; 1566 independent measured reflections, full-matrix least-squares on F^2 refinement, R_1 = 0.1810, wR_2 = 0.6184, 1391, independent observed reflections, [$|F_o| > 4\sigma(|F_o|)$, $2\theta_{max}$ = 50.5°], 111 parameters.

Diimine 38 (R = Cl). Following the general procedure, a mixture of 4-chlorolaniline (0.33 g, 2.60 mmol) and 2,6-diformylpyridine **4** (0.18 g, 1.30 mmol) were stirred in anhydrous CH_2Cl_2 (4 mL) with molecular sieve (4 Å) for 4 h. After a filtration and

subsequent removal of solvent, diimine **38** was obtained as a yellow powder (0.66 g, quantitative). R_f: 0.59 (hexane/EtOAc = 1:1). M.p. > 198.4 °C (decomposed). ^{1}H NMR (CD_2Cl_2): 7.27 (d, J = 8.7 Hz, 4 H, Ar*H*), 7.41 (d, J = 8.7 Hz, 4 H, Ar*H*), 7.97 (t, J = 7.8 Hz, 1 H, Ar*H*), 8.29 (d, J = 7.8 Hz, 2 H, Ar*H*), 8.63 (s, 2 H, *H*C=N). ^{13}C NMR (CD_2Cl_2): 123.1, 123.7, 129.9, 132.8, 138.0, 150.0, 155.1, 161.2. HRMS (ESI): $C_{19}H_{13}Cl_2N_3$ $[M+Na]^+$: calcd 376.0376; found 376.0378.

Diimine 39 (R = F). Following the general procedure, a mixture of 4-fluorolaniline (0.30 g, 2.72 mmol) and 2,6-diformylpyridine **4** (0.18 g, 1.36 mmol) were stirred in anhydrous CH_2Cl_2 (4 mL) with molecular sieve (4 Å) for 4 h. After a filtration and subsequent removal of solvent, diimine **39** was obtained as a light yellow powder (0.27 g, 62 %). R_f: 0.72 (hexane/EtOAc = 1:1). M.p. 172.3–173.0 °C. ^{1}H NMR (CD_2Cl_2): 7.10–7.18 (m, 4 H, Ar*H*), 7.29–7.37 (m, 4 H, Ar*H*), 7.95 (t, J = 7.8 Hz, 1 H, Ar*H*), 8.27 (d, J = 7.8 Hz, 2 H, Ar*H*), 8.64 (s, 2 H, *H*C=N). ^{13}C NMR (CD_2Cl_2): 116.4, 116.6, 123.3, 123.4, 123.4, 137.9, 147.46, 147.49, 155.2, 160.52, 160.53, 161.1, 163.6. HRMS (ESI): $C_{19}H_{13}F_2N_3$ $[M+Na]^+$: calcd 344.0970; found 344.0965.

Diimine 40 (R = CF_3). Following the general procedure, a mixture of 4-(trifluoromethyl)aniline (0.37 g, 2.28 mmol) and 2,6-diformylpyridine **4** (0.15 g,

1.14 mmol) were stirred in anhydrous CH_2Cl_2 (3 mL) with molecular sieve (4 Å) for 4 h. After a filtration and subsequent removal of solvent, diimine **40** was obtained as an off-white powder (0.54 g, quantitative). R_f: 0.68 (hexane/EtOAc = 1:1). M.p. 149.1–149.7 °C. ^{1}H NMR (CD_2Cl_2): 7.37 (d, J = 8.3 Hz, 4 H, Ar*H*), 7.70 (d, J = 8.3 Hz, 4 H, Ar*H*), 8.02 (t, J = 7.8 Hz, 1 H, Ar*H*), 8.33 (d, J = 7.8 Hz, 2 H, Ar*H*), 8.64 (s, 2 H, *H*C=N). ^{13}C NMR (CD_2Cl_2): 121.8, 124.2, 125.2 (q, J = 215.5 Hz), 127.0 (m), 128.8 (q, J = 32.7 Hz), 138.1, 154.7, 154.9, 162.7. HRMS (ESI): $C_{21}H_{13}F_6N_3$ $[M+H]^+$: calcd 422.1086; found 422.1095.

4.4 Determination of Binding Constant *K*

With regard to the ^{1}H NMR spectroscopic method, binding constant determination is classified into two categories, slow and fast exchanges, depending on the rate of equilibrium relative to NMR timescale. For slow-exchange equilibria, free and complexed hosts give separate signals. Stoichiometry, concentration of complex [C] and binding constant K can be calculated from peak integrations. For fast exchanging system, free and complexed hosts appear as a weighted average. The stoichiometry can be determined from Job plot. A titration experiment and regression (Rose-Drago method) are required to evaluate [C]. Then, K can be calculated by curve-fitting.

For a host-guest complexation:

$a \cdot H + b \cdot G \rightleftharpoons C$ where H = Host, G = Guest, C = complex

$$K = \frac{[C]}{[H]^a \cdot [G]^b} \quad \ldots(1)$$

$$[H]_0 = [H] + a \cdot [C] \quad \ldots(2)$$

$$[G]_0 = [G] + b \cdot [C] \quad \ldots(3)$$

K: binding constant

a, b: stoichiometry

$[H]_0$: initial (total) concentration of host molecule

$[G]_0$: initial (total) concentration of guest molecule

[H], [G], [C]: equilibrium concentrations of host, guest, and complex, respectively

Substitution of (2), (3) into (1) gives

$$K = \frac{[C]}{([H]_0 - a \cdot [C])^a \cdot ([G]_0 - b \cdot [C])^b} \quad \ldots(4)$$

For a fast-exchange equilibrium on NMR timescale

$$[H]_0 \cdot (\delta_{obs} - \delta_h) = a \cdot [C] \cdot (\delta_c - \delta_h) \quad \ldots(5)$$

where δ_{obs} = observed chemical shift

δ_h = chemical shift of free host

δ_c = chemical shift of complexed host

The stoichiometry is determined from the x-coordinate at the maximum in the Job plot where $[H]_0 \cdot (\delta_{obs} - \delta_h)$ is plotted against mole fraction of host $\left(\frac{[H]_0}{[H]_0 + [G]_0}\right)$.

To evaluate the complex concentration [C], simple transformation of (5) gives

$$[C] = \frac{1}{a} \cdot \frac{\delta_{obs} - \delta_h}{\delta_c - \delta_h} \cdot [H]_0 \quad \ldots(6)$$

Rose-Drago method is applied using a 1:1 complexation model ($a = b = 1$).

Substitution of (6) into (4) gives

$$\frac{1}{K} = \frac{(\delta_{obs} - \delta_h) \cdot [H]_0}{(\delta_c - \delta_h)} - ([H]_0 + [G]_0) + \frac{(\delta_c - \delta_h)}{(\delta_{obs} - \delta_h)} \cdot [G]_0 \quad \ldots(7)$$

From ^{1}H NMR titration experiment with n different combinations of $[H]_0$ and $[G]_0$, a

matrix of { δ_{obs}, $[H]_{0n}$, $[G]_{0n}$ } with 3 elements was obtained in which

δ_{obs} = observed chemical shift
$[H]_{0n}$ = initial concentration of host molecule for n-th measurement
$[G]_{0n}$ = initial concentration of guest molecule for n-th measurement

Using the following definitions:

$$Y = \frac{1}{K}$$

$$X = (\delta_{obs} - \delta_h)$$

$$a_n = [H]_{0n} \cdot (\delta_{obs\,n} - \delta_h)$$

$$b_n = [H]_{0n} + [G]_{0n}$$

$$c_n = \frac{[G]_{0n}}{\delta_{obs\,n} - \delta_h}$$

(7) is then expressed as $Y = \frac{a_n}{X} - b_n + c_n \cdot X$.

A combination of data gives a matrix of answers { X, Y }. The maximum numbers of obtainable answer pairs { X, Y } is ${}_nC_2$ pairs for n combinations of concentration conditions. The binding constant K and chemical shift of complexed host δ_c can then be obtained. Values differed by more than 2.5 standard deviations from the mean are eliminated and a new mean is determined. The calculated K and δ_c are fitted back into the Job plot for optimization.

References

1. (a) Frisch, H. L.; Wasserman, E. *J. Am. Chem. Soc.* **1961**, *83*, 3789–3795; (b) Schill, G. *Catenanes, Rotaxanes, and Knots*; Academic Press: New York, U. K., **1971**; (c) Lindoy, L. F.; Atkinson, I. M. *Self-assembly in Supramolecular Systems*; Stoddart, J. F., Ed.; Royal Society of Chemistry: Cambridge, U. K., **2000**; pp 47–86.
2. Harrison, I. T.; Harrison, S. *J. Am. Chem. Soc.* **1967**, *89*, 5723–5724.
3. (a) Schill, G.; Zöllenkopf, H. *Nachr. Chem. Tech.* **1967**, *15*, 149; (b) Schill, G.; Zöllenkopf, H. *Justus Liebigs Ann. Chem.* **1969**, *721*, 53–74.
4. Safarowsky, O.; Windisch, B.; Mohry, A.; Vögtle, F. *J. Prakt. Chem.* **2000**, *342*, 437–444.
5. Kay, E. R.; Leigh. D. A. *Top. Curr. Chem.* **2005**, *262*, 133–177.
6. Philp, D.; Stoddart, J. F. *Synlett* **1991**, 445–458.
7. (a) Harrison, I. T. *J. Chem. Soc., Chem. Commun.* **1972**, 231–232; (b) Ashton, P. R.; Bělohradský, M.; Philp, D.; Stoddart, J. F. *J. Chem. Soc., Chem. Commun.* **1993**, 1269–1274; (c) Ashton, P. R.; Bělohradský, M.; Philp, D.; Spencer, N.; Stoddart, J. F. *J. Chem. Soc., Chem. Commun.* **1993**, 1274–1277; (d) Amabilino, D. B.; Stoddart, J. F. *Pure & Appl. Chem.* **1993**, *65*, 2351–2359; (e) Raymo, F. M.; Stoddart, J. F. *Pure & Appl. Chem.* **1997**, *69*, 1987–1997.
8. Aricó, F.; Badjic, J. D.; Cantrill, S. J.; Flood, A. H.; Leung, K. C.-F.; Liu, Y.; Stoddart, J. F. *Top. Curr. Chem.* **2005**, *249*, 203–259.
9. Yoon, I.; Narita, M.; Shimizu, T.; Asakawa, M. *J. Am. Chem. Soc.* **2004**, *126*, 16740–16741.
10. Chiu, C.-W.; Lai, C.-C.; Chiu, S.-H. *J. Am. Chem. Soc.* **2007**, *129*, 3500–3501.
11. Rowan, S. J.; Cantrill, S. J.; Cousins, G. R. L.; Sanders, J. K. M.; Stoddart, J. F.

Angew. Chem. Int. Ed. **2002**, *41*, 898–952.

12. (a) Otto, S.; Furlan, R. L. E.; Sanders, J. K. M. *Drug Discovery Today* **2002**, *7*, 117–125; (b) Lehn, J.-M. *Chem. Eur. J.* **1999**, *5*, 2455–2463.
13. (a) Lindoy, L. F.; Atkinson, I. M. *Self-assembly in Supramolecular Systems*; Stoddart, J. F., Ed.; Royal Society of Chemistry: Cambridge, U. K., **2000**; pp 7–18; (b) Hubin, T. J.; Busch, D. H. *Coord. Chem. Rev.* **2000**, *200–202*, 5–52; (c) Jeffrey, J. A. *An Introduction to Hydrogen Bonding*; Oxford University Press: Oxford, U. K., **1997**.
14. Cantrill, S. J.; Rowan, S. J.; Stoddart, J. F. *Org Lett.* **1999**, *1*, 1363–1366.
15. Glink, P. T.; Oliva, A. I.; Stoddart, J. F.; White, A. J. P.; Williams, D. J. *Angew. Chem. Int. Ed.* **2001**, *40*, 1870–1875.
16. Yin, J.; Chi, C.; Wu, J. *Org. Biomol. Chem.* **2010**, *8*, 2594–2599.
17. (a) de Silva, A. P.; McClenaghan, N. D. *Chem. Eur. J.* **2004**, *10*, 574–586; (b) Callan, J. F.; de Silva, A. P.; Magri, D. C. *Tetrahedron* **2005**, *61*, 8551–8588; (c) Kay, E. R.; Leigh, D. A.; Zerbetto, F. *Angew. Chem. Int. Ed.* **2007**, *46*, 72–191; (d) Leung, K. C.-F.; Chak, C.-P.; Lo, C.-M.; Wong, W.-Y.; Xuan, S.; Cheng, C. H. K. *Chem. Asian J.* **2009**, *4*, 364–381; (e) Rescifina, A.; Zagni, C.; Iannazzo, D.; Merino, P. *Curr. Org. Chem.* **2009**, *13*, 448–481.
18. Fyfe, M. C. T.; Glink, P. T.; Menzer, S.; Stoddart, J. F.; White, A. J. P.; Williams, D. J. *Angew. Chem. Int. Ed. Engl.* **1997**, *36*, 2068–2070.
19. Mullen, K. M.; Davis, J. J.; Beer, P. D. *New J. Chem.* **2009**, *33*, 769–776.
20. Ashton, P. R.; Ballardini, R.; Balzani, V.; Gómez-López, M.; Lawrence, S. E.; Martínez-Díaz, V.; Montalti, M.; Piersanti, A.; Prodi, L.; Stoddart, J. F.; Williams, D. J. *J. Am. Chem. Soc.* **1997**, *119*, 10641–10651.
21. Pérez, E. M.; Dryden, D. T. F.; Leigh, D. A.; Teobaldi, G.; Zerbetto, F. *J. Am. Chem. Soc.* **2004**, *126*, 12210–12211.

22. (a) Brouwer, A. M.; Frochot, C.; Gatti, F. G.; Leigh, D. A. Mottier, L.; Paolucci, F.; Roffia, S.; Wurpel, G. W. H. *Science* **2001**, *291*, 2124–2128; (b) Altier, A.; Gatti, F. G.; Kay, E. R.; Leigh, D. A.; Martel, D.; Paolucci, F.; Slawin, A. M. Z.; Wong, J. K. Y. *J. Am. Chem. Soc.* **2003**, *125*, 8644–8654.

23. Coskun, A.; Wesson, P. J.; Klajn, R.; Trabolsi, A.; Fang, L.; Olson, M. A.; Dey, S. K.; Grzybowski, B. A.; Stoddart, J. F. *J. Am. Chem. Soc.* **2010**, *132*, 4310–4320.

24. (a) Gassensmith, J. J.; Baumes, J. M.; Smith, B. D. *Chem. Commun.* **2009**, 6329–6338; (b) Lee, J.-J.; White, A. G.; Baumes, J. M.; Smith, B. D. *Chem. Commun.* **2010**, *46*, 1068–1069.

25. Simion, A.; Simion, C.; Kanda, T.; Nagashima, S.; Mitoma, Y.; Yamada, T.; Mimura, K.; Tashiro, M. *J. Chem. Soc., Perkin Trans. 1* **2001**, 2071–2078.

26. Hutin, M.; Schalley, C. A.; Bernardinelli, G.; Nitschke, J. R. *Chem. Eur. J.* **2006**, *12*, 4069–4076.

27. Bissell, R. A.; de Silva, A. P.; Gunaratne, H. Q. N.; Lynch, P. L. M.; Maguire, G. E. M.; McCoy, C. P.; Sandanayake, K. R. A. S. *Top. Curr. Chem.* **1993**, *168*, 223–264.

28. Kimura, M.; Kajita, K.; Onoda, N.; Morosawa, S. *J. Org. Chem.* **1990**, *55*, 4887–4892.

29. (*a*) Leung, K. C.-F.; Nguyen, T. D.; Stoddart, J. F.; Zink, J. I. *Chem. Mater.* **2006**, *18*, 5919–5928; (*b*) Liu, R.; Zhang, Y.; Feng, P. *J. Am. Chem. Soc.* **2009**, *131*, 15128–15129.

30. Chen, C.-W.; Whitlock, H. W. *J. Am. Chem. Soc.* **1978**, *100*, 4921–4922.

31. (a) Zimmerman, S. C.; VanZyl, C. M. *J. Am. Chem. Soc.* **1987**, *109*, 7894–7896; (b) Klärner, F.-G.; Kahlert, B. *Acc. Chem. Res.* **2003**, *36*, 919–932.

32. Kim, Y.; Park, M. *Synth. Met.* **2001**, *117*, 297–299.

33. Marchioni, F.; Juris, A.; Lobert, M.; Seelbach, U. P.; Kahlert, B.; Klärner, F.-G. *New J. Chem.* **2005**, *29*, 780–784.

34. (a) Vosburgh, W. C.; Cooper, G. R. *J. Am. Chem. Soc.* **1941**, *63*, 437–442; (b) Likussar, W.; Boltz, D. F. *Anal. Chem.* **1971**, *43*, 1265–1272; (c) Atkinson, G. F. *Anal. Chem.* **1972**, *44*, 1098; (d) Gil, V. M. S.; Oliveira, N. C. *J. Chem. Educ.* **1990**, *67*, 473–478.

35. (a) Rose, N. J.; Drago, R. S. *J. Am. Chem. Soc.* **1959**, *81*, 6138–6145; (b) Wachter, H. N.; Fried, V. *J. Chem. Educ.* **1974**, *51*, 798–799; (c) *Analytical Methods in Supramolecular Chemistry*; Schalley, C. A., Ed.; Wiley-VCH: Weinheim, Germany, **2007**; pp 17–54.

Appendix

List of NMR Spectra

List of X-Ray Crystal Data

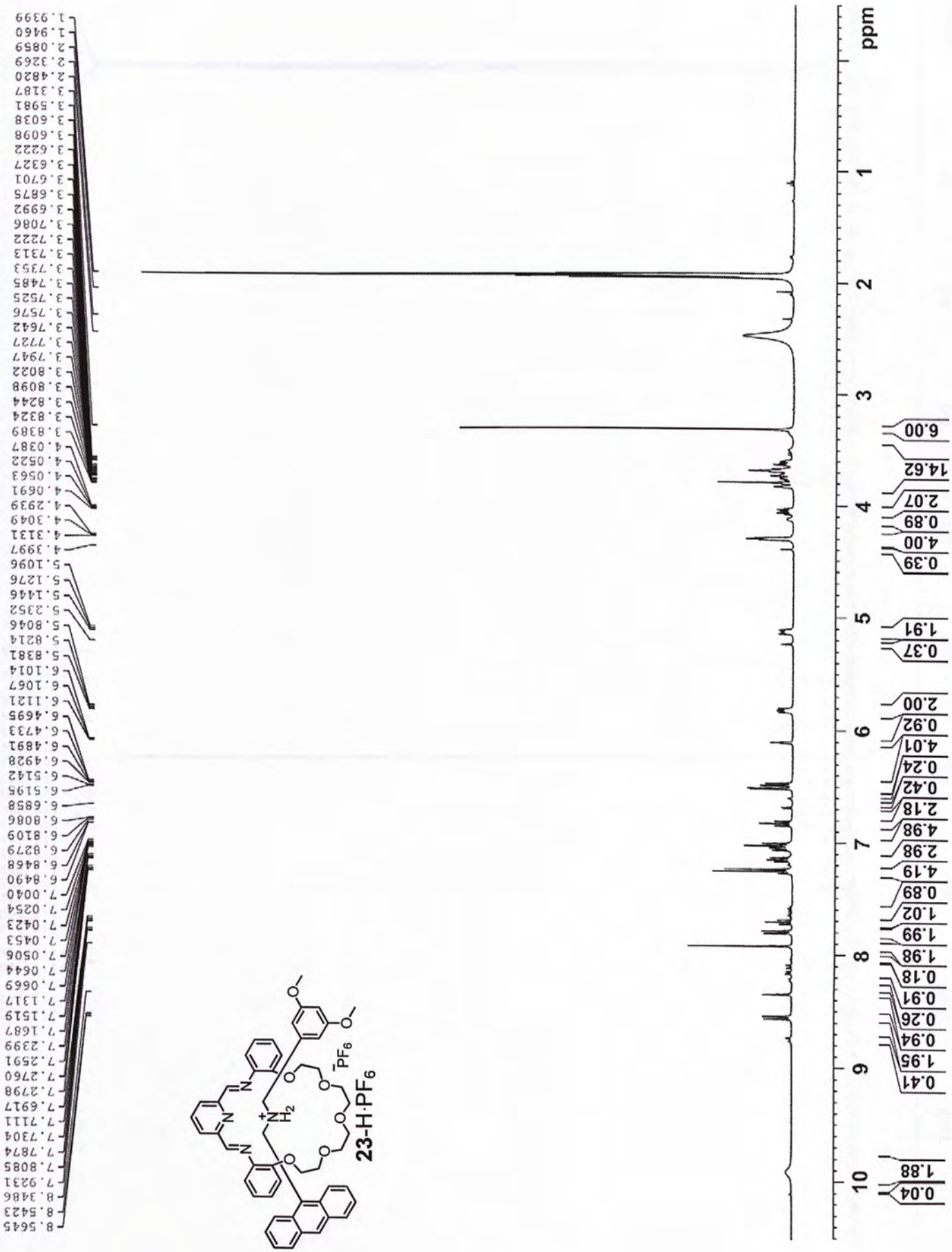
8.5645
8.5423
8.3486
7.9231
7.8085
7.7874
7.7304
7.7111
7.6917
7.2799
7.2760
7.2591
7.2399
7.1687
7.1519
7.1317
7.0669
7.0644
7.0506
7.0453
7.0423
7.0254
7.0040
6.8490
6.8468
6.8279
6.8109
6.8086
6.6858
6.5195
6.5142
6.4928
6.4891
6.4733
6.4695
6.1121
6.1067
6.1014
5.8381
5.8214
5.8046
5.2352
5.1446
5.1276
5.1096
4.3997
4.3131
4.3049
4.2939
4.0691
4.0563
4.0522
4.0387
3.8389
3.8324
3.8244
3.8098
3.8022
3.7947
3.7727
3.7642
3.7576
3.7525
3.7485
3.7353
3.7313
3.7222
3.7086
3.6992
3.6875
3.6701
3.6327
3.6222
3.6098
3.6038
3.5981
3.3187
3.2820
3.2269
3.0859
1.9460
1.9399
ppm
10
9
8
7
6
5
4
3
2
1
0.04
1.88
0.41
1.95
0.94
0.26
0.91
0.18
1.98
1.99
1.02
0.89
4.19
2.98
4.98
2.18
0.42
0.24
4.01
0.92
2.00
0.37
1.91
0.39
4.00
0.89
2.07
14.62
6.00
$^{+}NH_2$
$^{-}PF_6$
23-H·PF$_6$

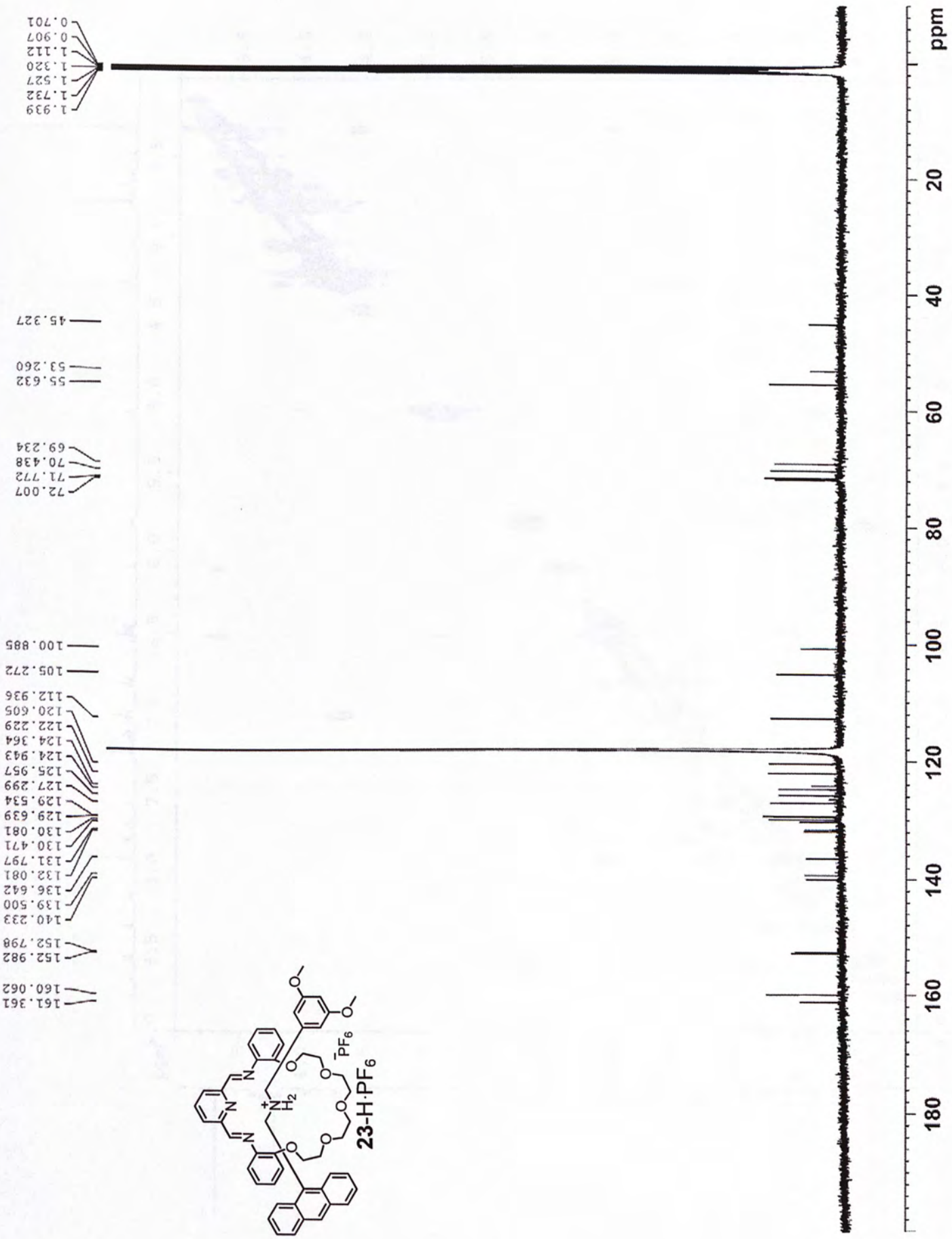
ppm
20
40
60
80
100
120
140
160
180
0.701
0.907
1.112
1.320
1.527
1.732
1.939
45.327
53.260
55.632
69.234
70.438
71.772
72.007
100.885
105.272
112.936
120.605
122.229
124.364
124.943
125.957
127.299
129.534
129.639
130.081
130.471
131.797
132.081
136.642
139.500
140.233
152.798
152.982
160.062
161.361
$^{+}NH_2$
$^{-}PF_6$
23-H·PF$_6$

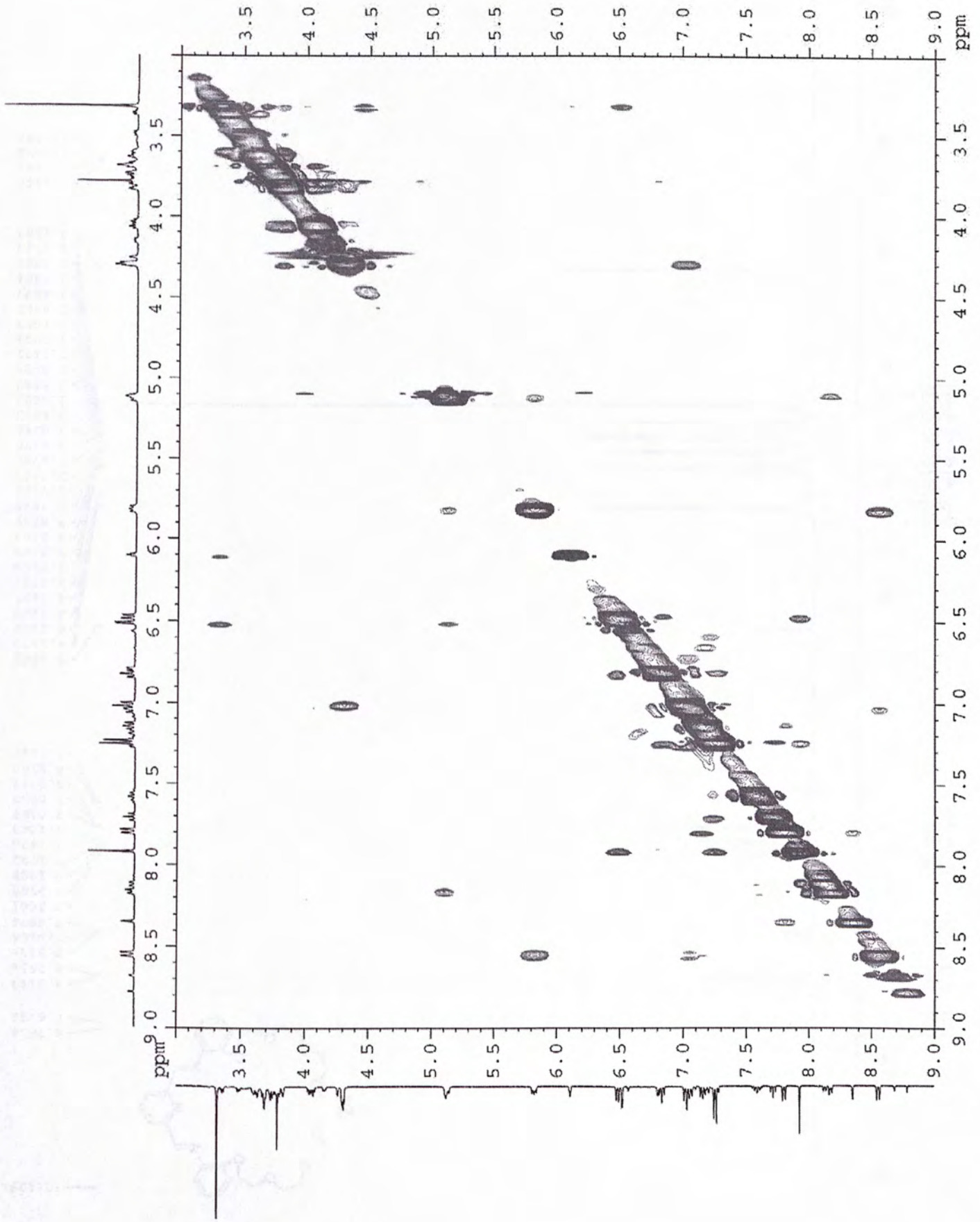
ppm
9.0
8.5
8.0
7.5
7.0
6.5
6.0
5.5
5.0
4.5
4.0
3.5

ppm
1
2
3
4
5
6
7
8
9
10
6.00
4.09
8.20
4.09
4.09
3.73
1.79
1.73
0.91
1.88
1.92
3.73
24

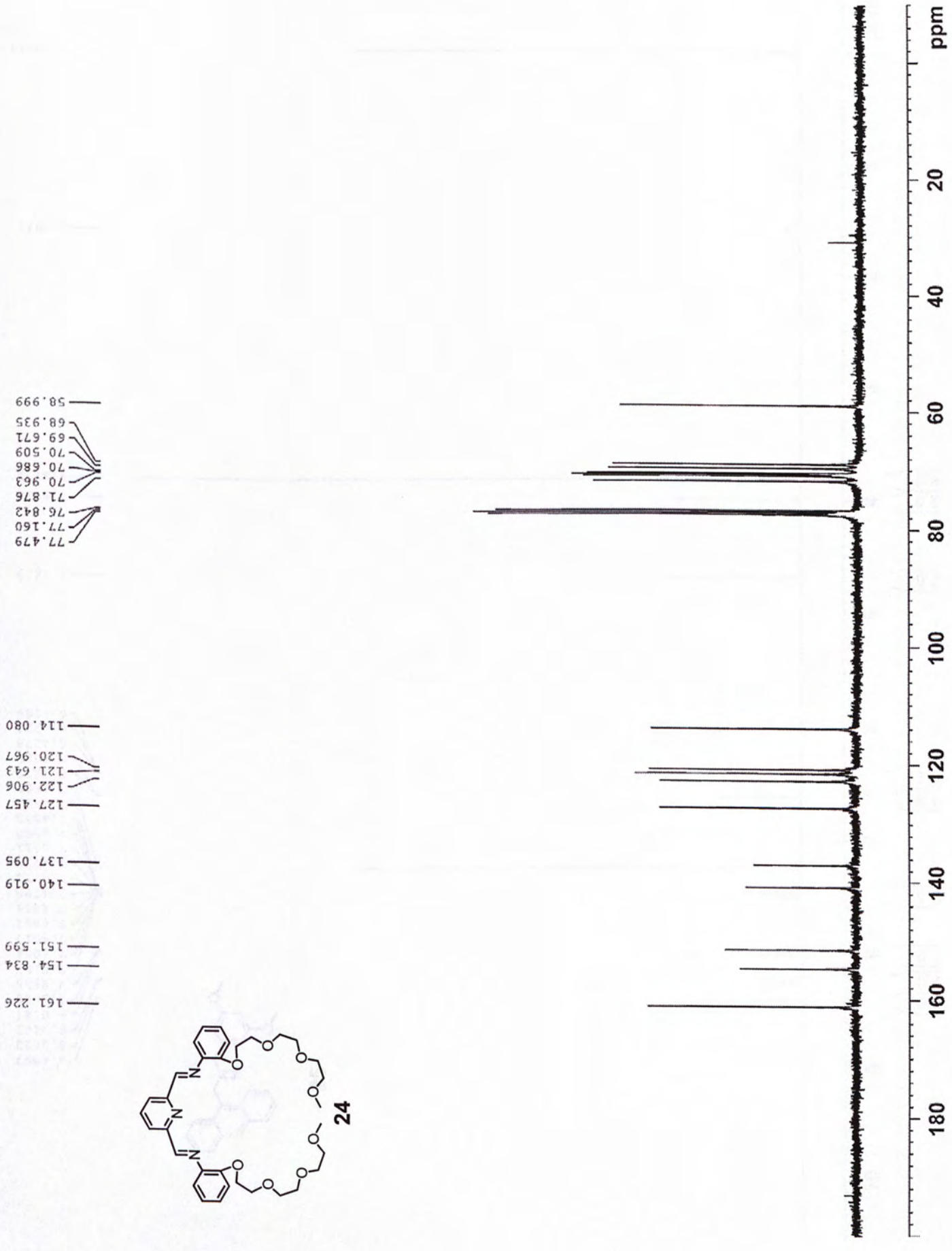
ppm
20
40
60
80
100
120
140
160
180
58.999
68.935
69.671
70.509
70.686
70.963
71.876
76.842
77.160
77.479
114.080
120.967
121.643
122.906
127.457
137.095
140.919
151.599
154.834
161.226
24

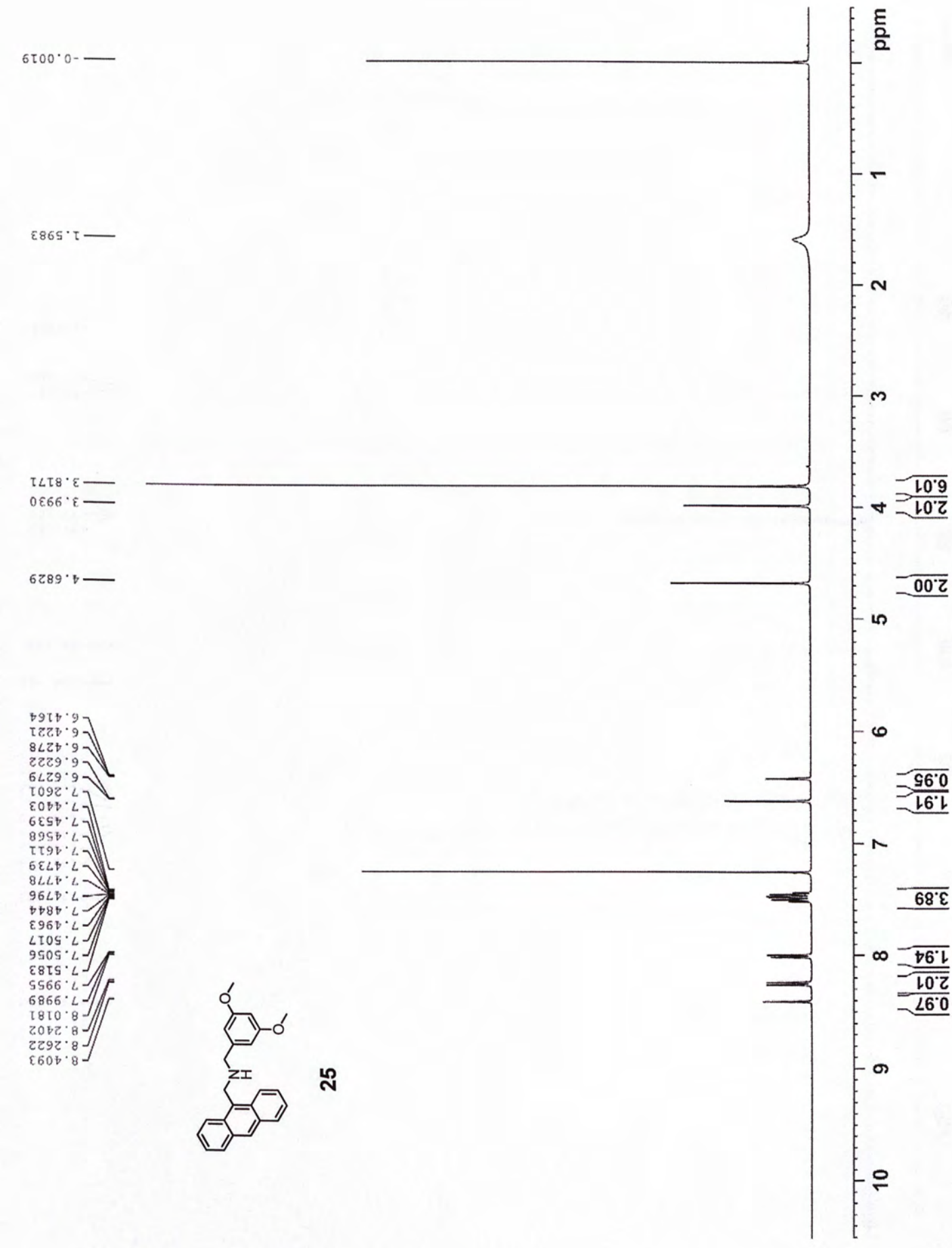
ppm
10
9
8
7
6
5
4
3
2
1
0.97
2.01
1.94
3.89
1.91
0.95
2.00
2.01
6.01
3.8171
3.9930
4.6829
1.5983
-0.0019
8.4093
8.2622
8.2402
8.0181
7.9989
7.9955
7.5183
7.5056
7.5017
7.4963
7.4844
7.4796
7.4778
7.4739
7.4611
7.4568
7.4539
7.4403
7.2601
6.6279
6.6222
6.4278
6.4221
6.4164
25

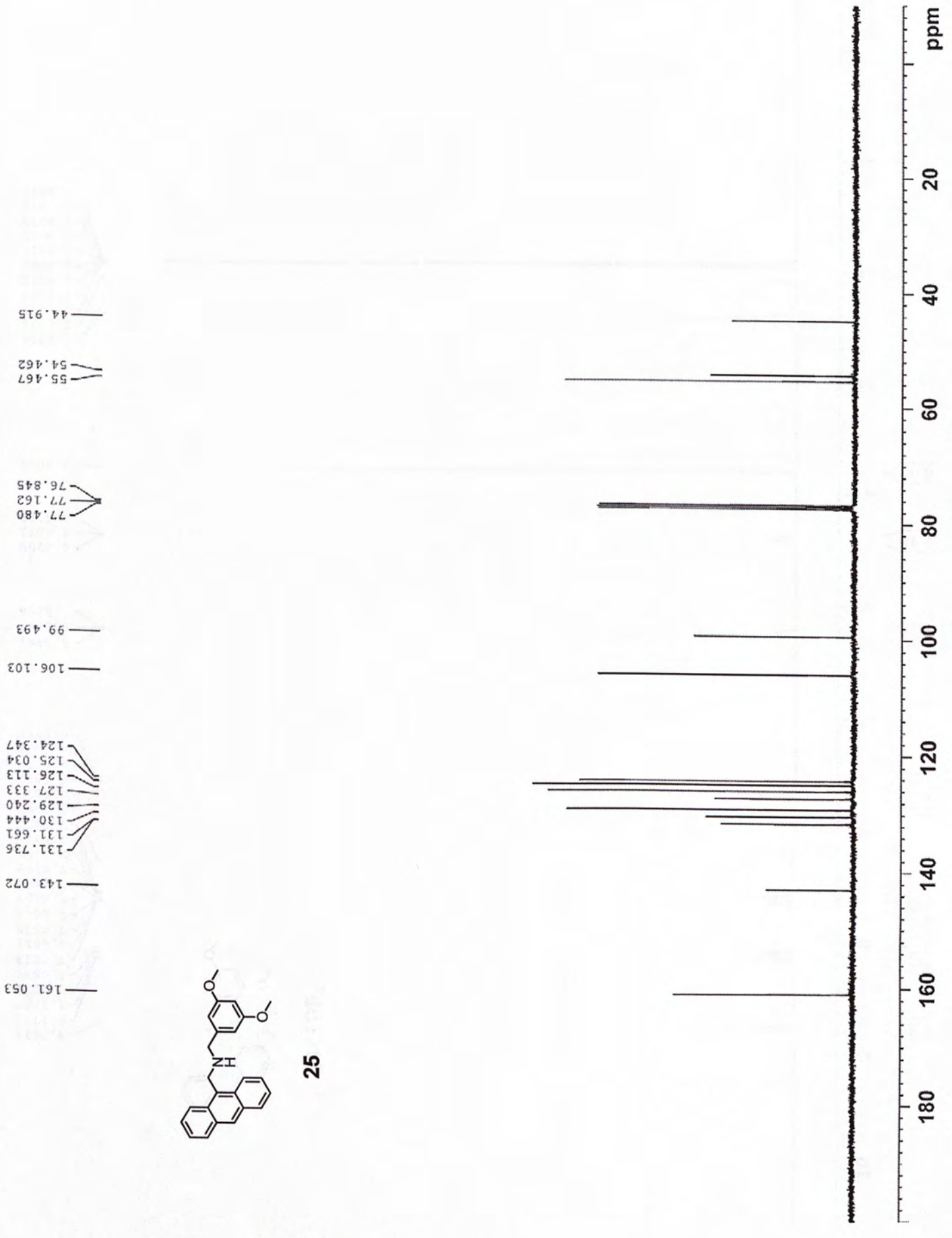
ppm
20
40
60
80
100
120
140
160
180
44.915
54.462
55.467
76.845
77.162
77.480
99.493
106.103
124.347
125.034
126.113
127.333
129.240
130.444
131.661
131.736
143.072
161.053
25

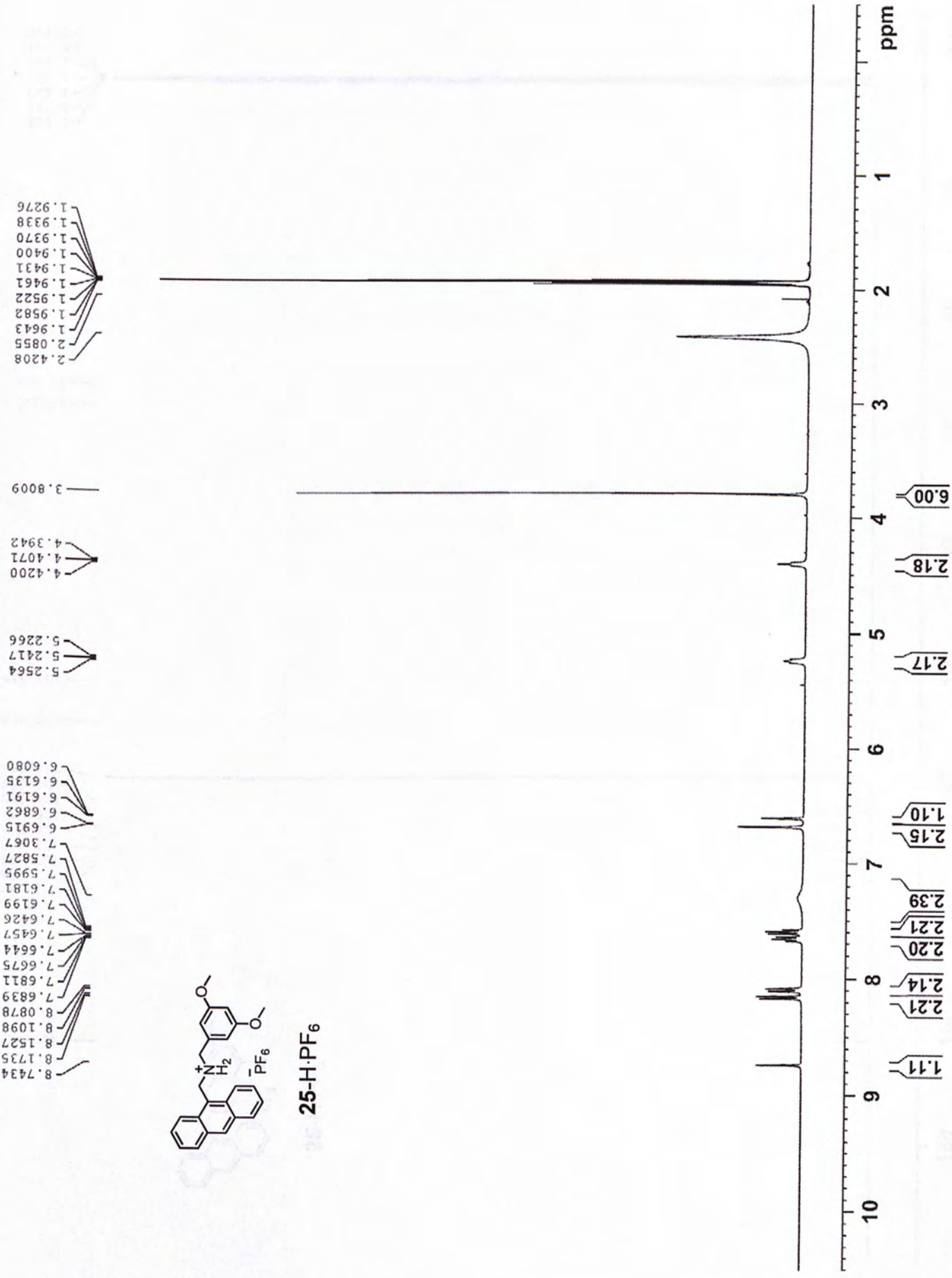
ppm
1
2
3
4
5
6
7
8
9
10
1.11
2.21
2.14
2.20
2.21
2.39
2.15
1.10
2.17
2.18
6.00
3.8009
8.7434
8.1735
8.1527
8.1098
8.0878
7.6839
7.6811
7.6675
7.6644
7.6457
7.6426
7.6199
7.6181
7.5995
7.5827
7.3067
6.6915
6.6862
6.6191
6.6135
6.6080
5.2564
5.2417
5.2266
4.4200
4.4071
4.3942
2.4208
2.0855
1.9643
1.9582
1.9522
1.9461
1.9431
1.9400
1.9370
1.9338
1.9276

25-H·PF_6

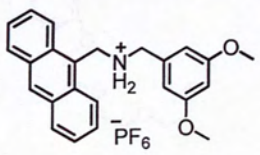
N
H2
PF6
O
O

25-H·PF_6

162.452
133.413
132.274
131.805
130.468
128.578
126.631
124.139
122.085
118.343
109.052
102.338
56.271
52.805
43.924
1.941
1.733
1.527
1.321
1.113
0.907
0.702
180
160
140
120
100
80
60
40
20
ppm

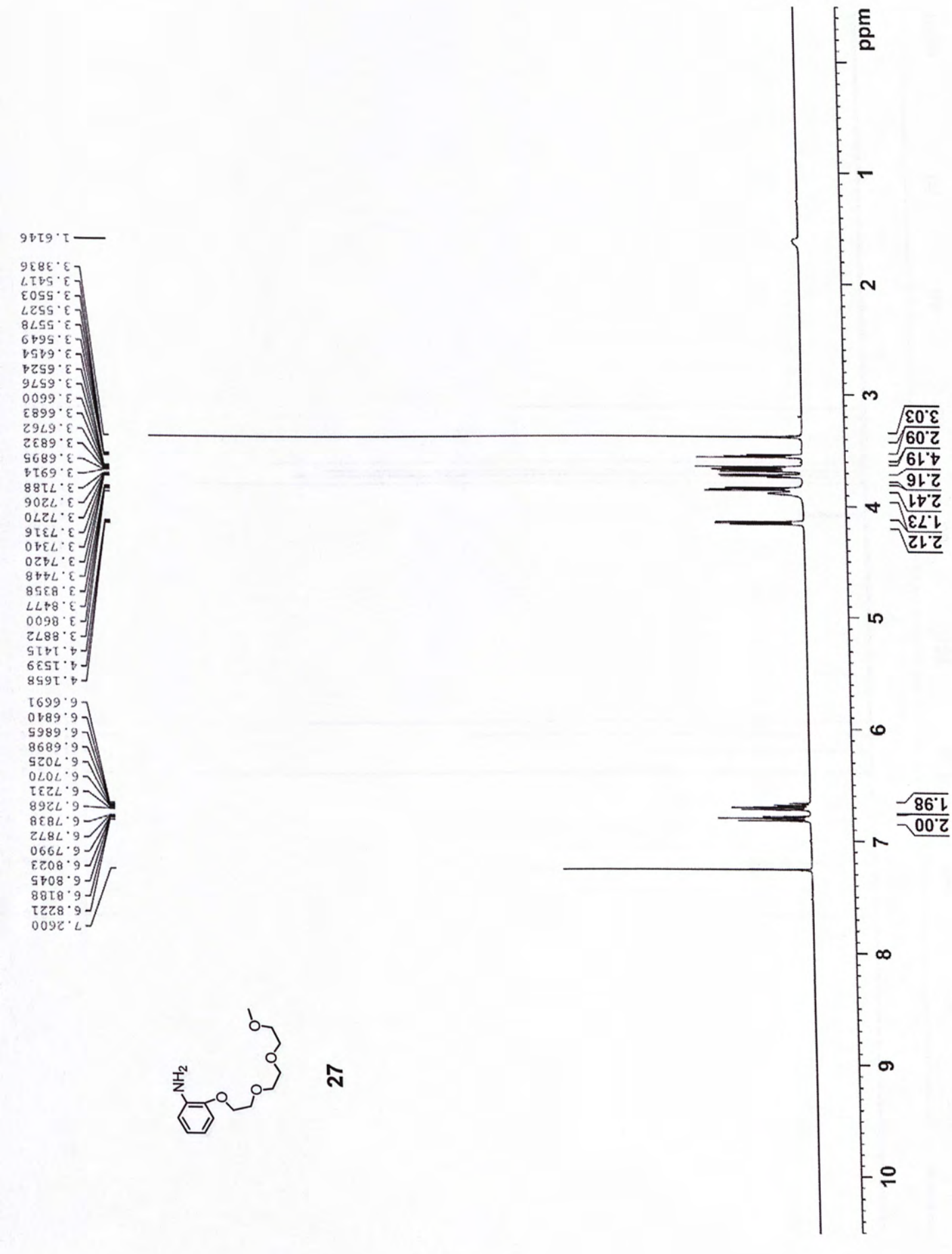
ppm
1
2
3
4
5
6
7
8
9
10
2.00
1.98
2.12
1.73
2.41
2.16
4.19
2.09
3.03
NH2
O
O
O
O
O
27
7.2600
6.8221
6.8188
6.8045
6.8023
6.7990
6.7872
6.7838
6.7268
6.7231
6.7070
6.7025
6.6898
6.6865
6.6840
6.6691
4.1658
4.1539
4.1415
3.8872
3.8600
3.8477
3.8358
3.7448
3.7420
3.7340
3.7316
3.7270
3.7206
3.7188
3.6914
3.6895
3.6832
3.6762
3.6683
3.6600
3.6576
3.6524
3.6454
3.5649
3.5578
3.5527
3.5503
3.5417
3.3836
1.6146

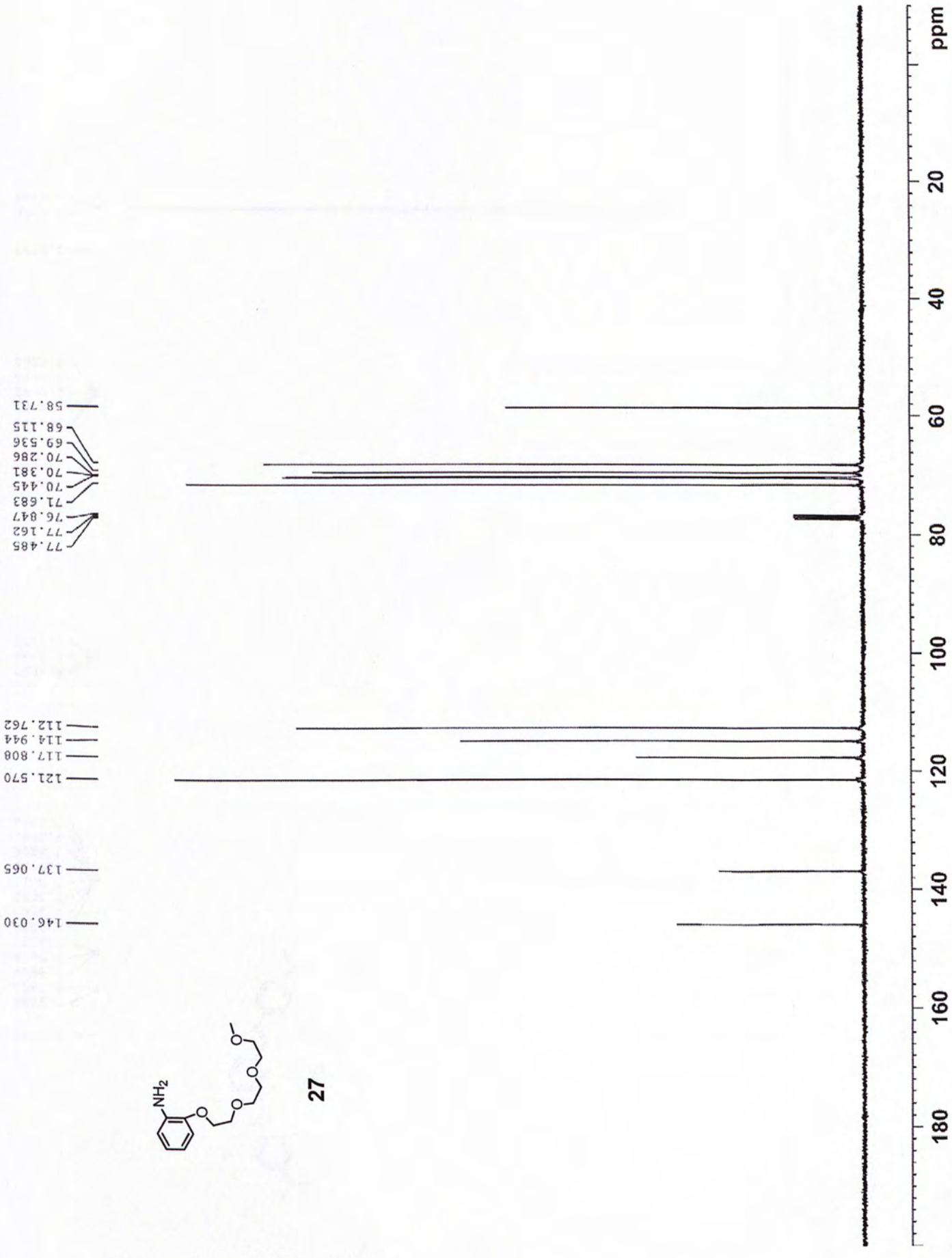
ppm
20
40
60
80
100
120
140
160
180
58.731
68.115
69.536
70.286
70.381
70.445
71.683
76.847
77.162
77.485
112.762
114.944
117.808
121.570
137.065
146.030
NH2
27

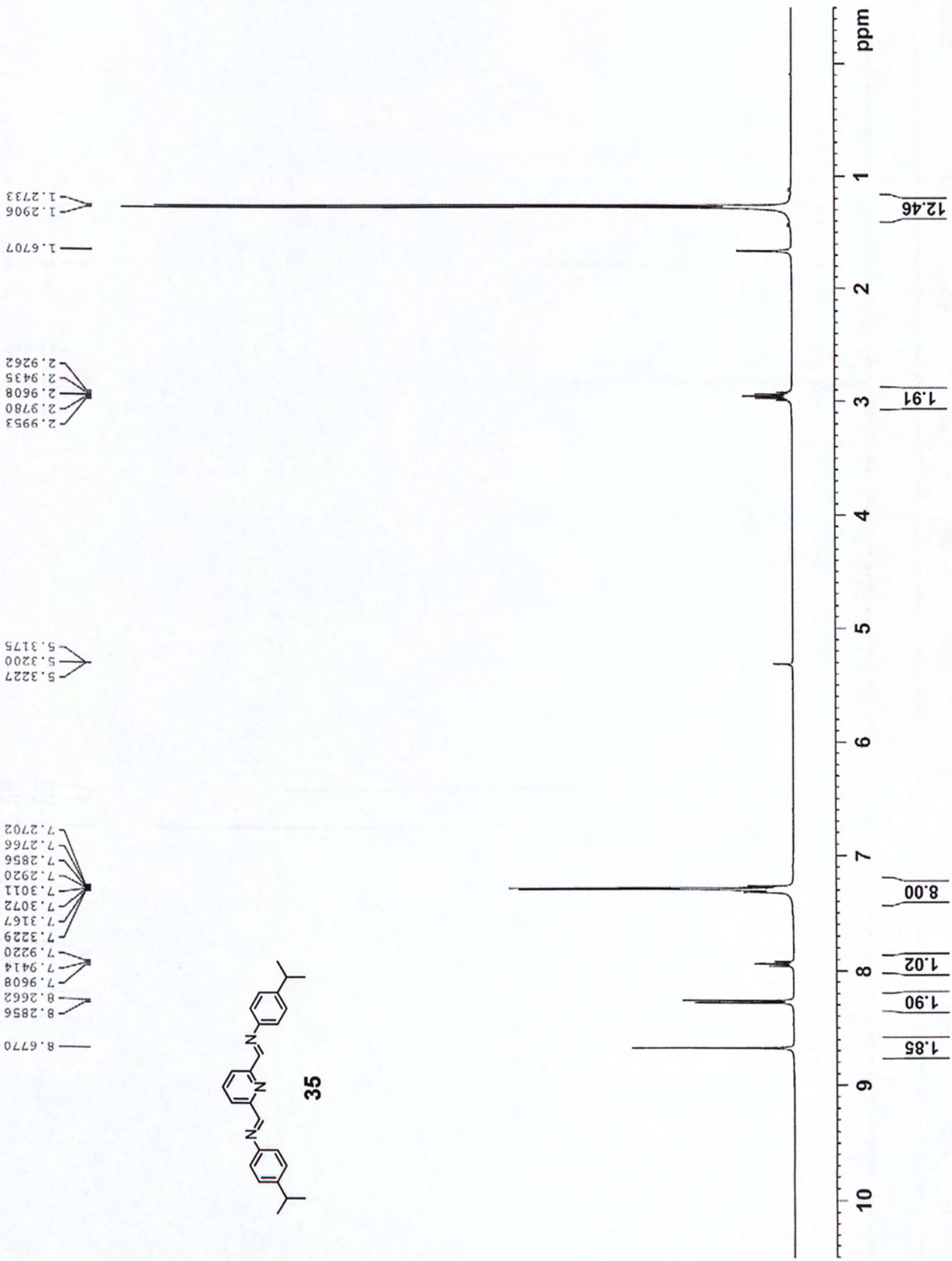
ppm
1
2
3
4
5
6
7
8
9
10
12.46
1.91
8.00
1.02
1.90
1.85
1.2733
1.2906
1.6707
2.9262
2.9435
2.9608
2.9780
2.9953
5.3227
5.3200
5.3175
7.2702
7.2766
7.2856
7.2920
7.3011
7.3072
7.3167
7.3229
7.9220
7.9414
7.9608
8.2662
8.2856
8.6770
35

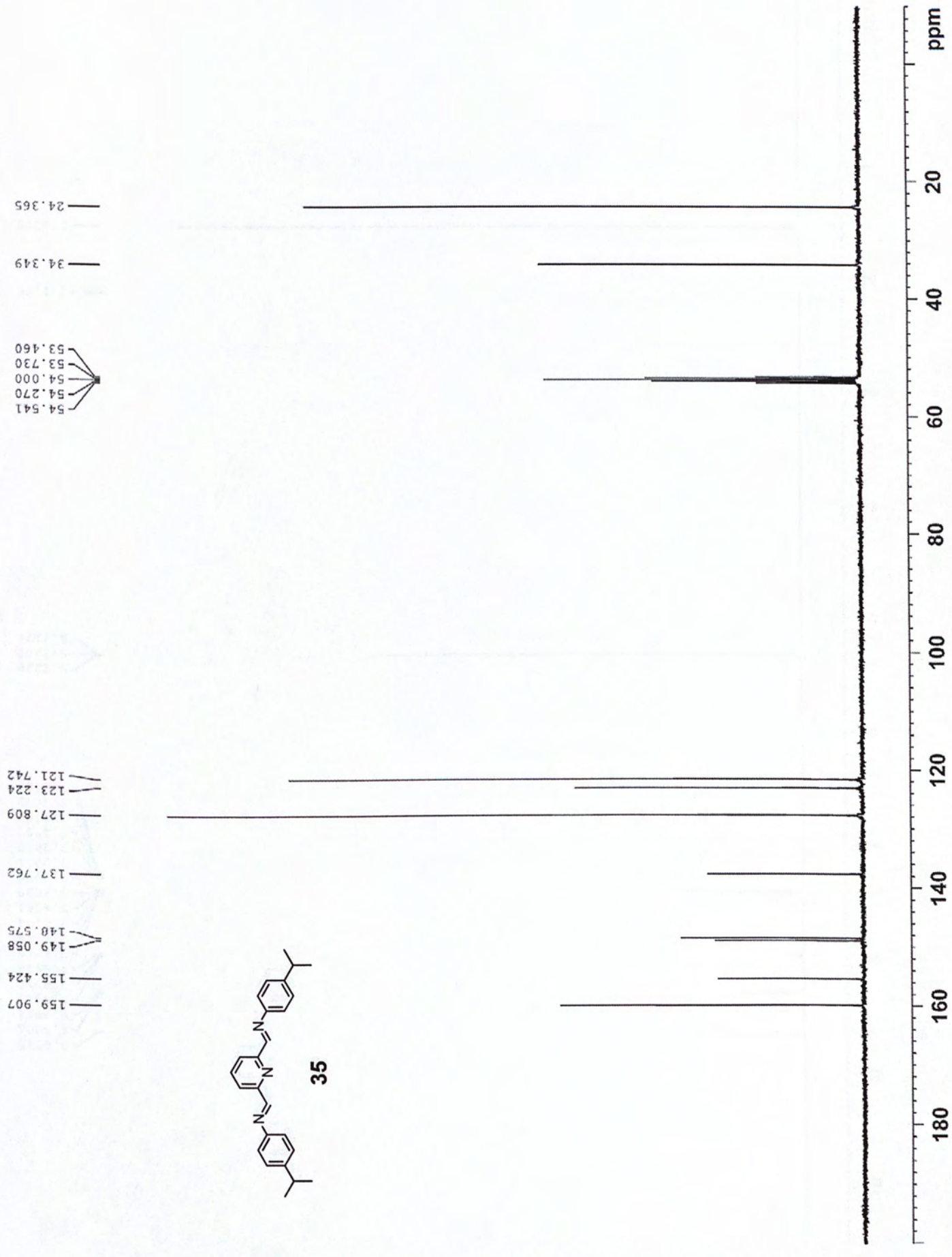
ppm
20
40
60
80
100
120
140
160
180
24.365
34.349
53.460
53.730
54.000
54.270
54.541
121.742
123.224
127.809
137.762
148.575
149.058
155.424
159.907
35

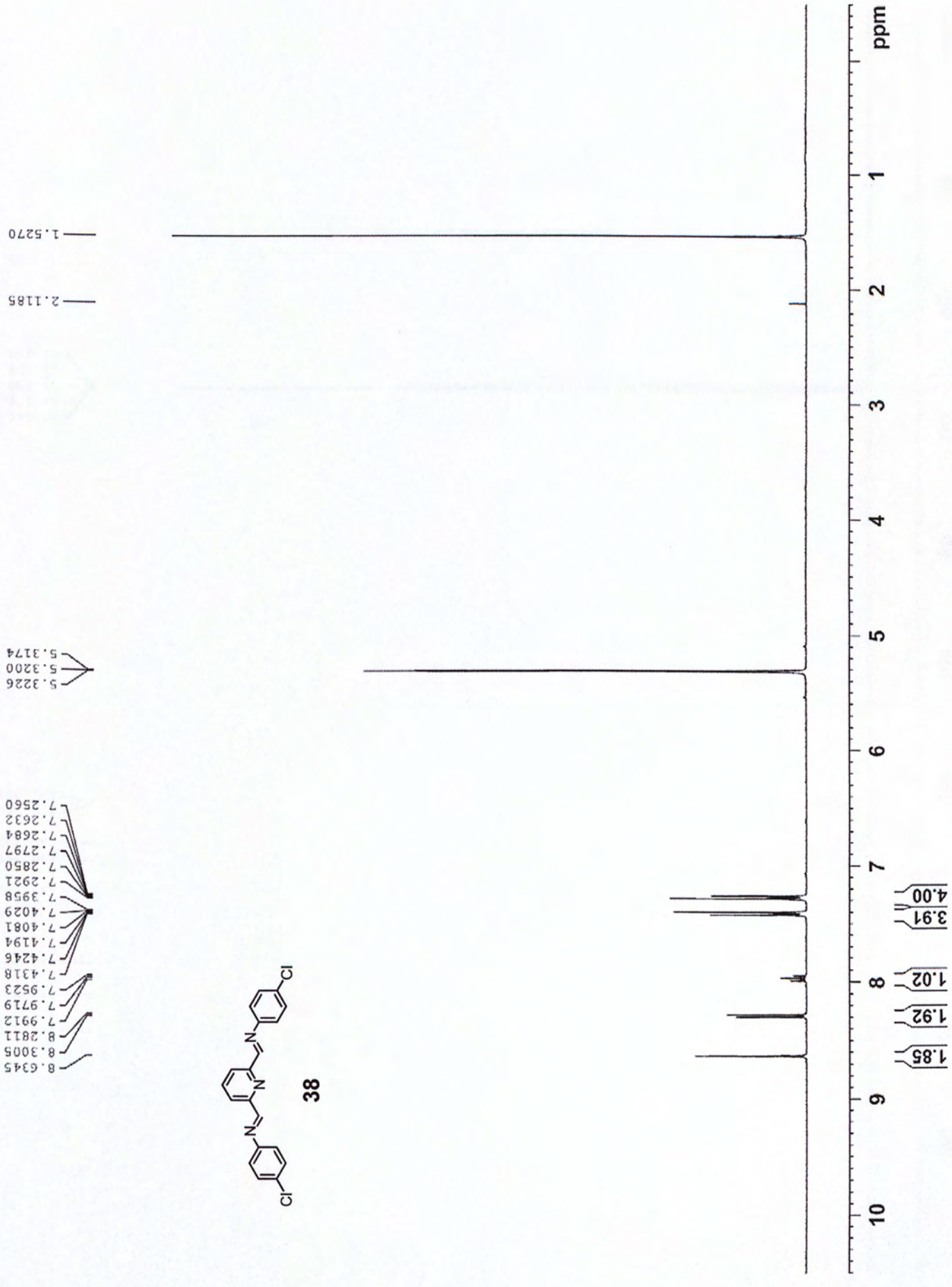
ppm
1
2
3
4
5
6
7
8
9
10
1.85
1.92
1.02
3.91
4.00
1.5270
2.1185
5.3226
5.3200
5.3174
8.6345
8.3005
8.2811
7.9912
7.9719
7.9523
7.4318
7.4246
7.4194
7.4081
7.4029
7.3958
7.2921
7.2850
7.2797
7.2684
7.2632
7.2560
Cl
Cl
N
N
N
38

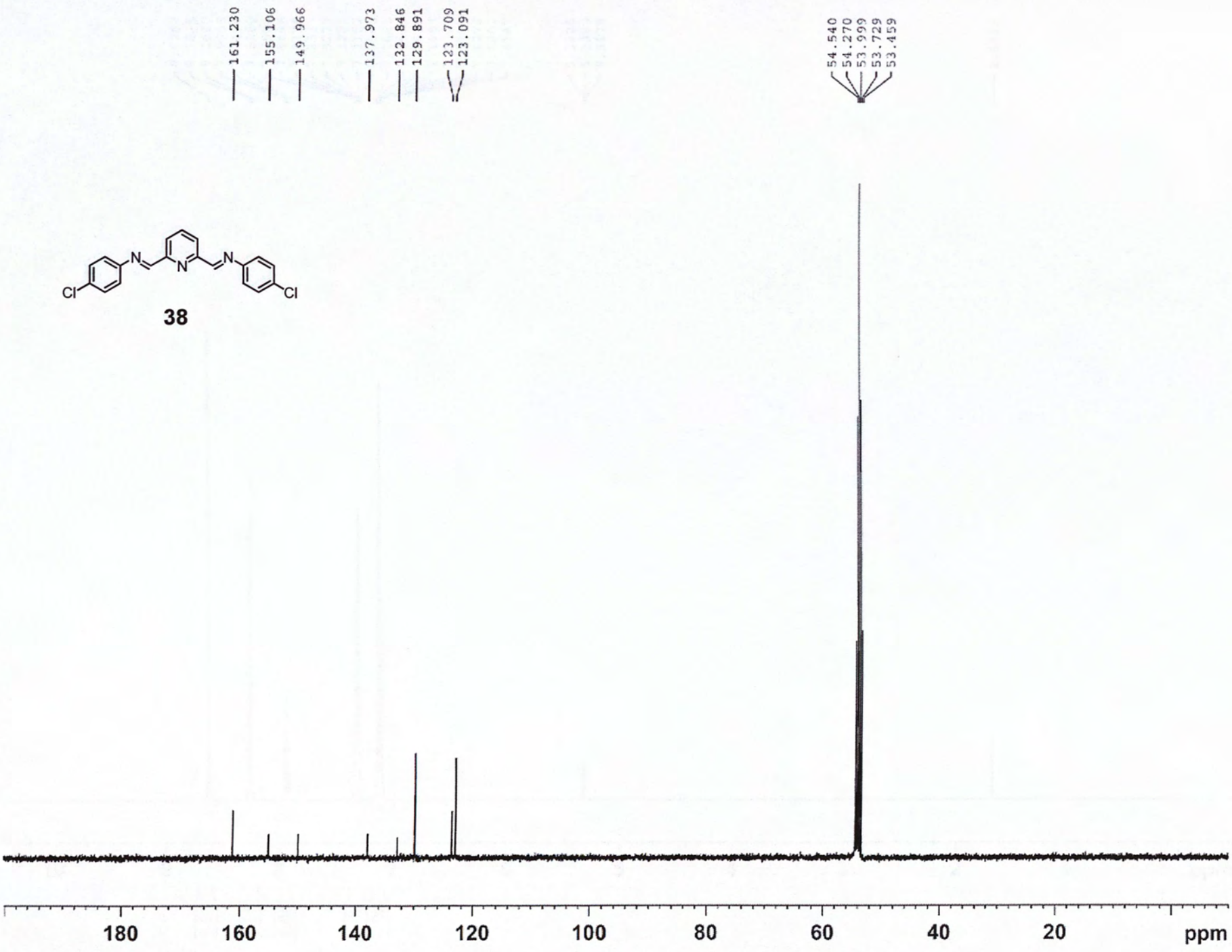
161.230
155.106
149.966
137.973
132.846
129.891
123.709
123.091
54.540
54.270
53.999
53.729
53.459
Cl
N
N
N
Cl
38
180
160
140
120
100
80
60
40
20
ppm

8.6367
8.2825
8.2630
7.9669
7.9476
7.9280
7.3500
7.3446
7.3375
7.3327
7.3277
7.3207
7.3152
7.3068
7.1665
7.1582
7.1526
7.1453
7.1367
7.1317
7.1278
7.1202
7.1147
5.3226
5.3200
5.3175
1.6833
39
F
N
N
N
F
1.93
2.00
1.06
4.09
4.00
ppm
10
9
8
7
6
5
4
3
2
1

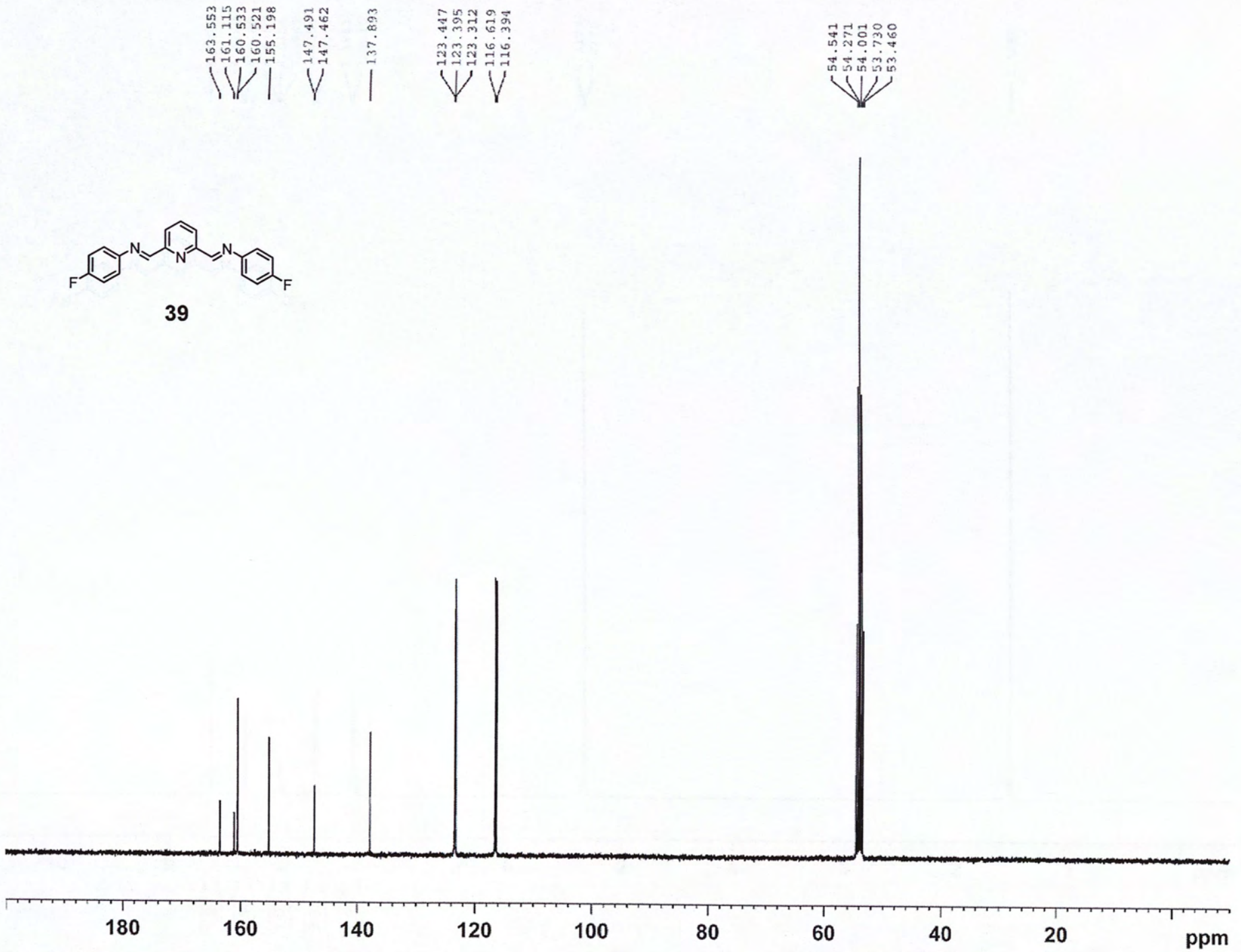
163.553
161.115
160.533
160.521
155.198
147.491
147.462
137.893
123.447
123.395
123.312
116.619
116.394
54.541
54.271
54.001
53.730
53.460
F
N
N
N
F
39
180
160
140
120
100
80
60
40
20
ppm

ppm
1
2
3
4
5
6
7
8
9
10
1.87
1.95
1.07
3.98
4.00
8.6354
8.3462
8.3268
8.0351
8.0156
7.9961
7.7159
7.6951
7.3843
7.3636
5.3199
5.3179
1.5280
40

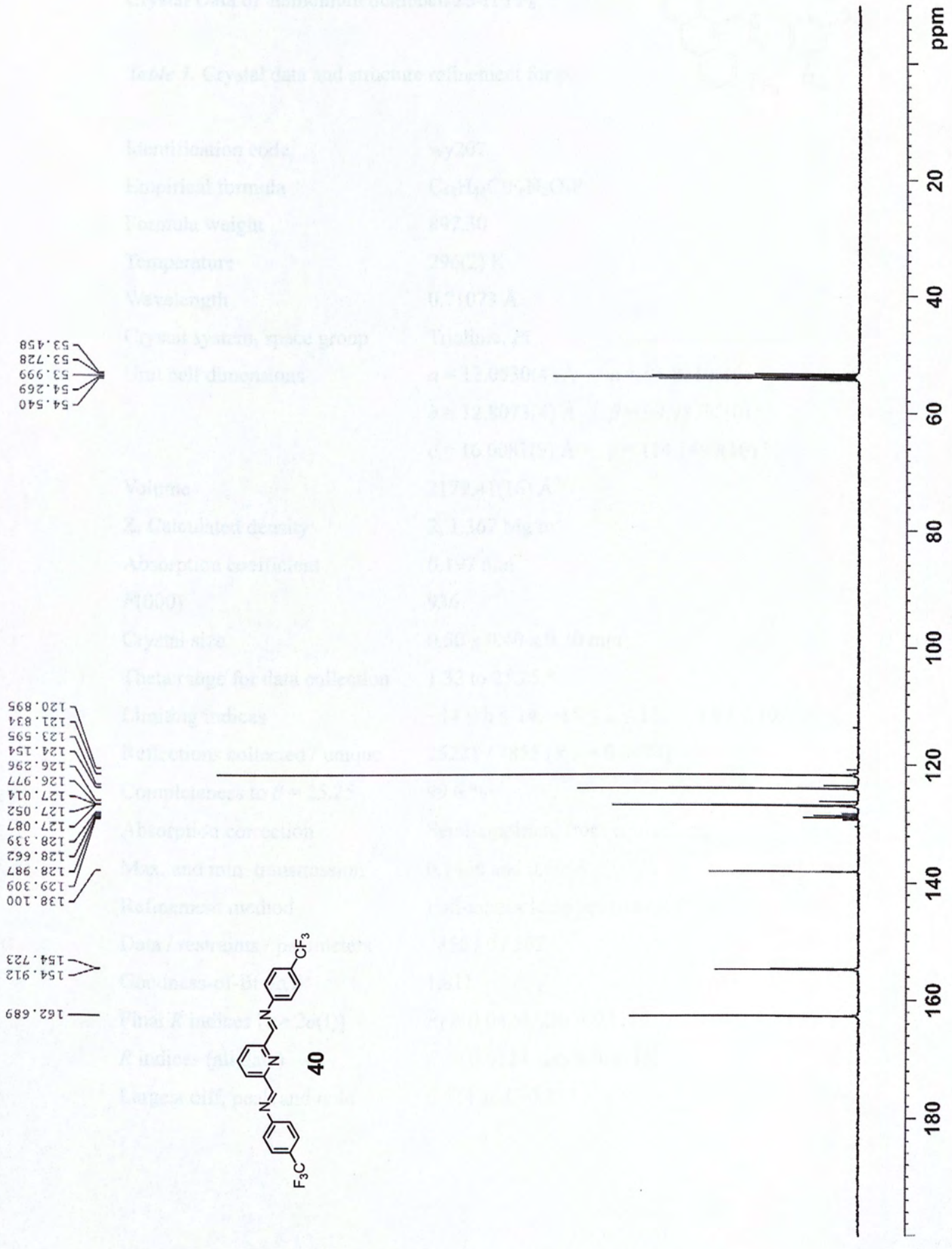
ppm
20
40
60
80
100
120
140
160
180
53.458
53.728
53.999
54.269
54.540
120.895
121.834
123.595
124.154
126.296
126.977
127.014
127.052
127.087
128.339
128.662
128.987
129.309
138.100
154.723
154.912
162.689
CF_3
F_3C
N
N
N
40

Crystal Data of ammonium dumbbell **25**-H·PF_6

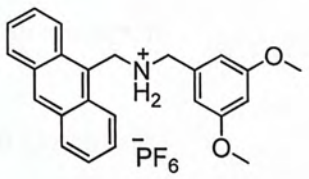

Table 1. Crystal data and structure refinement for p.

Identification code	wy207
Empirical formula	$C_{48}H_{48}ClF_6N_2O_4P$
Formula weight	897.30
Temperature	296(2) K
Wavelength	0.71073 Å
Crystal system, space group	Triclinic, $P\bar{1}$
Unit cell dimensions	a = 12.0530(4) Å α = 95.8310(10) °
	b = 12.8073(4) Å β = 99.9830(10) °
	c = 16.0081(9) Å γ = 114.1490(10) °
Volume	2179.41(16) $Å^3$
Z, Calculated density	2, 1.367 Mg/m^3
Absorption coefficient	0.197 mm^{-1}
F(000)	936
Crystal size	0.50 x 0.40 x 0.30 mm
Theta range for data collection	1.32 to 25.25 °
Limiting indices	$-14 \leq h \leq 14$, $-15 \leq k \leq 15$, $-19 \leq l \leq 19$
Reflections collected / unique	25221 / 7855 [R_{int} = 0.0434]
Completeness to θ = 25.25	99.6 %
Absorption correction	Semi-empirical from equivalents
Max. and min. transmission	0.7456 and 0.6068
Refinement method	Full-matrix least-squares on F^2
Data / restraints / parameters	7855 / 0 / 562
Goodness-of-fit on F^2	1.011
Final R indices [$I > 2\sigma(I)$]	R_1 = 0.0420, ${}_wR_2$ = 0.1117
R indices (all data)	R_1 = 0.0524, ${}_wR_2$ = 0.1235
Largest diff. peak and hole	0.424 and −0.327 e.$Å^{-3}$

Table 2. Atomic coordinates (x 10^4) and equivalent isotropic displacement parameters (A^2 x 10^3) for p.

U(eq) is defined as one third of the trace of the orthogonalized Uij tensor.

	x	y	z	U(eq)
N(1')	1202(1)	2060(1)	3018(1)	37(1)
N(1)	−1444(1)	869(1)	−508(1)	37(1)
O(1')	5916(1)	5342(1)	4176(1)	61(1)
O(2')	4352(2)	4790(1)	1159(1)	64(1)
C(1)	−971(2)	1418(2)	−1239(1)	43(1)
C(2)	−1986(2)	971(2)	−2061(1)	39(1)
C(3)	−2374(2)	1735(2)	−2444(1)	46(1)
C(4)	−3283(2)	1305(2)	−3209(1)	50(1)
C(5)	−3826(2)	131(2)	−3598(1)	45(1)
C(6)	−3433(2)	−609(2)	−3210(1)	41(1)
C(7)	−2519(2)	−193(2)	−2439(1)	42(1)
C(8)	−3163(4)	3183(3)	−3341(2)	116(1)
C(9)	−4867(2)	−2273(2)	−4293(2)	65(1)
C(10)	−2498(2)	1118(2)	−319(1)	39(1)
C(11)	−3074(2)	516(2)	363(1)	38(1)
C(12)	−3942(2)	−670(2)	130(1)	42(1)
C(13)	−4230(2)	−1354(2)	−709(2)	52(1)
C(14)	−5087(2)	−2485(2)	−914(2)	69(1)
C(15)	−5719(2)	−3020(2)	−301(2)	78(1)
C(16)	−5475(2)	−2423(2)	503(2)	67(1)
C(17)	−4586(2)	−1223(2)	752(2)	49(1)
C(18)	−4371(2)	−573(2)	1559(1)	53(1)
C(19)	−3530(2)	599(2)	1796(1)	47(1)
C(20)	−3346(2)	1281(2)	2617(1)	62(1)
C(21)	−2531(2)	2408(3)	2848(2)	69(1)
C(22)	−1830(2)	2953(2)	2270(2)	63(1)
C(23)	−1972(2)	2358(2)	1474(1)	52(1)
C(24)	−2840(2)	1158(2)	1194(1)	41(1)
C(1')	1452(2)	3314(2)	3048(1)	45(1)
C(2')	2733(2)	3985(2)	2902(1)	40(1)
C(3')	3758(2)	4415(2)	3596(1)	42(1)
C(4')	4955(2)	4957(2)	3458(1)	44(1)
C(5')	5117(2)	5078(2)	2636(1)	48(1)

C(6')	4085(2)	4646(2)	1943(1)	46(1)
C(7')	2884(2)	4103(2)	2070(1)	44(1)
C(8')	7114(2)	5535(3)	4042(2)	74(1)
C(9')	3360(2)	4169(2)	415(2)	70(1)
C(10')	91(2)	1336(2)	3351(1)	46(1)
C(11')	169(2)	235(2)	3550(1)	43(1)
C(12')	−555(2)	−844(2)	2979(1)	43(1)
C(13')	−1469(2)	−1019(2)	2215(2)	55(1)
C(14')	−2136(2)	−2080(2)	1689(2)	63(1)
C(15')	−1931(2)	−3047(2)	1874(2)	67(1)
C(16')	−1083(2)	−2935(2)	2585(2)	60(1)
C(17')	−383(2)	−1851(2)	3170(1)	48(1)
C(18')	473(2)	−1743(2)	3914(1)	52(1)
C(19')	1175(2)	−692(2)	4488(1)	49(1)
C(20')	2055(2)	−593(2)	5251(2)	63(1)
C(21')	2749(3)	435(3)	5796(2)	73(1)
C(22')	2610(2)	1440(2)	5625(2)	69(1)
C(23')	1787(2)	1388(2)	4914(1)	56(1)
C(24')	1028(2)	323(2)	4305(1)	46(1)
O(1)	−3733(2)	1958(2)	−3656(1)	84(1)
O(2)	−3854(2)	−1768(1)	−3543(1)	59(1)
P(1')	0	5000	5000	50(1)
P(1)	0	5000	0	68(1)
F(1')	1400(1)	5794(2)	4984(1)	86(1)
F(1)	−565(3)	5182(2)	766(2)	167(1)
F(2')	133(2)	3864(1)	4635(1)	83(1)
F(2)	1338(2)	5874(2)	512(2)	152(1)
F(3')	−472(2)	5134(1)	4045(1)	80(1)
F(3)	185(2)	3934(2)	318(2)	109(1)
Cl(1)	689(1)	1239(1)	1054(1)	53(1)

Table 3. Bond lengths [Å] and angles [°] for p.

N(1')-C(1')	1.502(2)
N(1')-C(10')	1.506(2)
N(1)-C(10)	1.501(2)
N(1)-C(1)	1.502(2)
O(1')-C(4')	1.364(2)
O(1')-C(8')	1.420(3)
O(2')-C(6')	1.361(2)
O(2')-C(9')	1.420(3)
C(1)-C(2)	1.508(3)
C(2)-C(7)	1.378(3)
C(2)-C(3)	1.396(3)
C(3)-C(4)	1.381(3)
C(4)-O(1)	1.365(2)
C(4)-C(5)	1.393(3)
C(5)-C(6)	1.376(3)
C(6)-O(2)	1.370(2)
C(6)-C(7)	1.391(3)
C(8)-O(1)	1.423(3)
C(9)-O(2)	1.427(3)
C(10)-C(11)	1.504(2)
C(11)-C(24)	1.409(3)
C(11)-C(12)	1.410(3)
C(12)-C(13)	1.430(3)
C(12)-C(17)	1.434(3)
C(13)-C(14)	1.354(3)
C(14)-C(15)	1.407(4)
C(15)-C(16)	1.347(4)
C(16)-C(17)	1.431(3)
C(17)-C(18)	1.385(3)
C(18)-C(19)	1.389(3)
C(19)-C(20)	1.431(3)
C(19)-C(24)	1.437(3)
C(20)-C(21)	1.338(4)
C(21)-C(22)	1.405(4)
C(22)-C(23)	1.362(3)
C(23)-C(24)	1.427(3)

C(1')-C(2')	1.503(3)
C(2')-C(3')	1.382(3)
C(2')-C(7')	1.390(3)
C(3')-C(4')	1.391(3)
C(4')-C(5')	1.378(3)
C(5')-C(6')	1.386(3)
C(6')-C(7')	1.388(3)
C(10')-C(11')	1.512(3)
C(11')-C(12')	1.410(3)
C(11')-C(24')	1.411(3)
C(12')-C(13')	1.427(3)
C(12')-C(17')	1.441(3)
C(13')-C(14')	1.356(3)
C(14')-C(15')	1.408(4)
C(15')-C(16')	1.342(4)
C(16')-C(17')	1.422(3)
C(17')-C(18')	1.387(3)
C(18')-C(19')	1.386(3)
C(19')-C(20')	1.430(3)
C(19')-C(24')	1.433(3)
C(20')-C(21')	1.344(4)
C(21')-C(22')	1.411(4)
C(22')-C(23')	1.350(3)
C(23')-C(24')	1.430(3)
P(1')-F(1')#1	1.5801(15)
P(1')-F(1')	1.5802(15)
P(1')-F(3')#1	1.5886(14)
P(1')-F(3')	1.5886(14)
P(1')-F(2')#1	1.5924(13)
P(1')-F(2')	1.5924(13)
P(1)-F(1)	1.543(2)
P(1)-F(1)#2	1.543(2)
P(1)-F(2)	1.5505(19)
P(1)-F(2)#2	1.5505(19)
P(1)-F(3)#2	1.5882(17)
P(1)-F(3)	1.5882(17)
C(1')-N(1')-C(10')	115.38(14)
C(10)-N(1)-C(1)	111.79(14)
C(4')-O(1')-C(8')	116.97(17)

C(6')-O(2')-C(9')	117.20(17)
N(1)-C(1)-C(2)	111.54(14)
C(7)-C(2)-C(3)	120.10(18)
C(7)-C(2)-C(1)	119.74(17)
C(3)-C(2)-C(1)	120.15(17)
C(4)-C(3)-C(2)	118.83(18)
O(1)-C(4)-C(3)	124.79(19)
O(1)-C(4)-C(5)	113.64(19)
C(3)-C(4)-C(5)	121.57(18)
C(6)-C(5)-C(4)	118.76(18)
O(2)-C(6)-C(5)	124.49(18)
O(2)-C(6)-C(7)	114.94(16)
C(5)-C(6)-C(7)	120.54(17)
C(2)-C(7)-C(6)	120.19(17)
N(1)-C(10)-C(11)	114.14(14)
C(24)-C(11)-C(12)	120.76(17)
C(24)-C(11)-C(10)	120.15(16)
C(12)-C(11)-C(10)	118.80(16)
C(11)-C(12)-C(13)	122.94(18)
C(11)-C(12)-C(17)	119.33(18)
C(13)-C(12)-C(17)	117.73(18)
C(14)-C(13)-C(12)	121.3(2)
C(13)-C(14)-C(15)	120.6(2)
C(16)-C(15)-C(14)	120.8(2)
C(15)-C(16)-C(17)	120.9(2)
C(18)-C(17)-C(16)	122.0(2)
C(18)-C(17)-C(12)	119.27(18)
C(16)-C(17)-C(12)	118.7(2)
C(17)-C(18)-C(19)	122.17(18)
C(18)-C(19)-C(20)	122.1(2)
C(18)-C(19)-C(24)	119.39(18)
C(20)-C(19)-C(24)	118.5(2)
C(21)-C(20)-C(19)	122.1(2)
C(20)-C(21)-C(22)	119.6(2)
C(23)-C(22)-C(21)	121.2(2)
C(22)-C(23)-C(24)	121.3(2)
C(11)-C(24)-C(23)	123.80(17)
C(11)-C(24)-C(19)	119.01(18)
C(23)-C(24)-C(19)	117.16(18)

N(1')-C(1')-C(2')	109.31(14)
C(3')-C(2')-C(7')	120.73(17)
C(3')-C(2')-C(1')	119.04(17)
C(7')-C(2')-C(1')	120.10(17)
C(2')-C(3')-C(4')	119.51(18)
O(1')-C(4')-C(5')	123.86(18)
O(1')-C(4')-C(3')	115.83(17)
C(5')-C(4')-C(3')	120.31(18)
C(4')-C(5')-C(6')	119.89(18)
O(2')-C(6')-C(5')	115.05(17)
O(2')-C(6')-C(7')	124.44(18)
C(5')-C(6')-C(7')	120.51(18)
C(6')-C(7')-C(2')	119.05(18)
N(1')-C(10')-C(11')	110.11(14)
C(12')-C(11')-C(24')	120.54(18)
C(12')-C(11')-C(10')	121.15(18)
C(24')-C(11')-C(10')	118.25(18)
C(11')-C(12')-C(13')	124.29(18)
C(11')-C(12')-C(17')	118.90(18)
C(13')-C(12')-C(17')	116.81(18)
C(14')-C(13')-C(12')	121.6(2)
C(13')-C(14')-C(15')	120.8(2)
C(16')-C(15')-C(14')	120.3(2)
C(15')-C(16')-C(17')	121.3(2)
C(18')-C(17')-C(16')	121.2(2)
C(18')-C(17')-C(12')	119.55(19)
C(16')-C(17')-C(12')	119.2(2)
C(19')-C(18')-C(17')	122.13(19)
C(18')-C(19')-C(20')	121.5(2)
C(18')-C(19')-C(24')	119.22(19)
C(20')-C(19')-C(24')	119.3(2)
C(21')-C(20')-C(19')	121.1(2)
C(20')-C(21')-C(22')	120.2(2)
C(23')-C(22')-C(21')	120.8(2)
C(22')-C(23')-C(24')	121.8(2)
C(11')-C(24')-C(23')	123.49(19)
C(11')-C(24')-C(19')	119.64(18)
C(23')-C(24')-C(19')	116.9(2)
C(4)-O(1)-C(8)	117.5(2)

C(6)-O(2)-C(9)	117.73(16)
F(1')#1-P(1')-F(1')	180.000(1)
F(1')#1-P(1')-F(3')#1	90.56(9)
F(1')-P(1')-F(3')#1	89.44(9)
F(1')#1-P(1')-F(3')	89.44(9)
F(1')-P(1')-F(3')	90.56(9)
F(3')#1-P(1')-F(3')	180.00(12)
F(1')#1-P(1')-F(2')#1	90.62(9)
F(1')-P(1')-F(2')#1	89.38(9)
F(3')#1-P(1')-F(2')#1	90.66(8)
F(3')-P(1')-F(2')#1	89.34(8)
F(1')#1-P(1')-F(2')	89.38(9)
F(1')-P(1')-F(2')	90.62(9)
F(3')#1-P(1')-F(2')	89.34(8)
F(3')-P(1')-F(2')	90.66(8)
F(2')#1-P(1')-F(2')	180.000(1)
F(1)-P(1)-F(1)#2	180.0
F(1)-P(1)-F(2)	91.91(18)
F(1)#2-P(1)-F(2)	88.09(18)
F(1)-P(1)-F(2)#2	88.09(18)
F(1)#2-P(1)-F(2)#2	91.91(18)
F(2)-P(1)-F(2)#2	179.999(1)
F(1)-P(1)-F(3)#2	88.23(13)
F(1)#2-P(1)-F(3)#2	91.77(13)
F(2)-P(1)-F(3)#2	88.33(11)
F(2)#2-P(1)-F(3)#2	91.67(11)
F(1)-P(1)-F(3)	91.77(13)
F(1)#2-P(1)-F(3)	88.23(13)
F(2)-P(1)-F(3)	91.67(11)
F(2)#2-P(1)-F(3)	88.33(11)
F(3)#2-P(1)-F(3)	180.0

Symmetry transformations used to generate equivalent atoms:

#1 −x, −y+1, −z+1 #2 –x, −y+1, −z

Table 4. Anisotropic displacement parameters ($A^2 \times 10^3$) for p.

The anisotropic displacement factor exponent takes the form:

$-2\pi^2 [h^2 a^{*2} U11 + ... + 2 h k a^* b^* U12]$

	U11	U22	U33	U23	U13	U12
N(1')	37(1)	35(1)	39(1)	7(1)	11(1)	16(1)
N(1)	31(1)	46(1)	35(1)	5(1)	5(1)	18(1)
O(1')	44(1)	78(1)	52(1)	8(1)	2(1)	23(1)
O(2')	64(1)	70(1)	46(1)	16(1)	17(1)	16(1)
C(1)	37(1)	50(1)	43(1)	9(1)	16(1)	17(1)
C(2)	40(1)	48(1)	36(1)	11(1)	18(1)	22(1)
C(3)	55(1)	39(1)	50(1)	12(1)	20(1)	22(1)
C(4)	60(1)	48(1)	53(1)	18(1)	15(1)	33(1)
C(5)	51(1)	49(1)	40(1)	11(1)	9(1)	26(1)
C(6)	51(1)	42(1)	38(1)	10(1)	15(1)	25(1)
C(7)	54(1)	49(1)	39(1)	13(1)	15(1)	33(1)
C(8)	170(4)	59(2)	119(3)	17(2)	−12(2)	68(2)
C(9)	72(2)	53(1)	58(1)	−1(1)	1(1)	24(1)
C(10)	38(1)	46(1)	41(1)	11(1)	14(1)	23(1)
C(11)	33(1)	46(1)	41(1)	13(1)	11(1)	22(1)
C(12)	34(1)	46(1)	52(1)	13(1)	9(1)	23(1)
C(13)	43(1)	52(1)	61(1)	4(1)	8(1)	23(1)
C(14)	60(1)	53(1)	86(2)	−3(1)	2(1)	28(1)
C(15)	62(2)	40(1)	121(3)	14(1)	10(2)	16(1)
C(16)	56(1)	51(1)	101(2)	34(1)	23(1)	24(1)
C(17)	39(1)	49(1)	68(1)	26(1)	16(1)	24(1)
C(18)	47(1)	70(1)	61(1)	36(1)	26(1)	33(1)
C(19)	41(1)	66(1)	45(1)	20(1)	15(1)	31(1)
C(20)	63(1)	96(2)	43(1)	21(1)	22(1)	47(1)
C(21)	68(2)	98(2)	45(1)	−2(1)	8(1)	44(2)
C(22)	53(1)	68(2)	60(1)	−7(1)	4(1)	26(1)
C(23)	43(1)	57(1)	52(1)	7(1)	12(1)	19(1)
C(24)	35(1)	53(1)	42(1)	13(1)	10(1)	24(1)
C(1')	43(1)	37(1)	60(1)	11(1)	17(1)	20(1)
C(2')	40(1)	30(1)	51(1)	9(1)	12(1)	17(1)
C(3')	48(1)	38(1)	44(1)	12(1)	14(1)	21(1)
C(4')	41(1)	40(1)	47(1)	5(1)	5(1)	17(1)
C(5')	40(1)	45(1)	55(1)	11(1)	14(1)	13(1)

C(6')	51(1)	40(1)	45(1)	12(1)	14(1)	17(1)
C(7')	44(1)	38(1)	46(1)	9(1)	6(1)	15(1)
C(8')	48(1)	93(2)	75(2)	0(1)	0(1)	35(1)
C(9')	76(2)	86(2)	45(1)	19(1)	11(1)	32(1)
C(10')	42(1)	42(1)	60(1)	14(1)	22(1)	18(1)
C(11')	39(1)	43(1)	54(1)	16(1)	23(1)	18(1)
C(12')	37(1)	43(1)	56(1)	15(1)	24(1)	17(1)
C(13')	46(1)	58(1)	66(1)	14(1)	17(1)	26(1)
C(14')	48(1)	66(2)	68(2)	3(1)	8(1)	22(1)
C(15')	63(1)	51(1)	74(2)	1(1)	18(1)	13(1)
C(16')	66(1)	44(1)	72(2)	14(1)	28(1)	21(1)
C(17')	46(1)	44(1)	60(1)	17(1)	28(1)	18(1)
C(18')	57(1)	49(1)	65(1)	26(1)	29(1)	29(1)
C(19')	50(1)	54(1)	53(1)	23(1)	26(1)	24(1)
C(20')	68(2)	76(2)	60(1)	30(1)	24(1)	39(1)
C(21')	71(2)	92(2)	56(1)	21(1)	9(1)	34(2)
C(22')	71(2)	71(2)	52(1)	7(1)	14(1)	20(1)
C(23')	64(1)	52(1)	53(1)	13(1)	21(1)	21(1)
C(24')	45(1)	48(1)	49(1)	17(1)	24(1)	18(1)
O(1)	114(2)	56(1)	85(1)	16(1)	−11(1)	52(1)
O(2)	83(1)	44(1)	48(1)	3(1)	0(1)	33(1)
P(1')	52(1)	56(1)	45(1)	4(1)	9(1)	30(1)
P(1)	56(1)	38(1)	106(1)	11(1)	30(1)	11(1)
F(1')	58(1)	97(1)	99(1)	23(1)	22(1)	27(1)
F(1)	243(3)	150(2)	179(3)	57(2)	142(2)	112(2)
F(2')	98(1)	76(1)	83(1)	−5(1)	13(1)	55(1)
F(2)	82(1)	72(1)	247(3)	8(2)	−18(2)	8(1)
F(3')	97(1)	94(1)	51(1)	13(1)	5(1)	48(1)
F(3)	98(1)	65(1)	168(2)	40(1)	34(1)	34(1)
Cl(1)	62(1)	54(1)	41(1)	1(1)	−6(1)	32(1)

Table 5. Hydrogen coordinates (x 10^4) and isotropic displacement parameters (A^2 x 10^3) for p.

	x	y	z	U(eq)
H(1'A)	1887	2037	3330	44
H(1'D)	1087	1729	2468	44
H(1A)	−1709	93	−645	45
H(1D)	−813	1145	−31	45
H(1B)	−282	1250	−1335	52
H(1C)	−656	2258	−1083	52
H(3A)	−2026	2519	−2189	55
H(5A)	−4442	−147	−4110	54
H(7A)	−2268	−702	−2178	51
H(8A)	−3564	3541	−3707	174
H(8B)	−2291	3500	−3342	174
H(8C)	−3251	3336	−2763	174
H(9A)	−5074	−3085	−4458	98
H(9B)	−4627	−1881	−4757	98
H(9C)	−5582	−2193	−4167	98
H(10A)	−3144	878	−848	47
H(10B)	−2190	1952	−134	47
H(13A)	−3820	−1016	−1122	63
H(14A)	−5259	−2912	−1464	82
H(15A)	−6311	−3795	−453	93
H(16A)	−5891	−2795	903	80
H(18A)	−4804	−933	1956	64
H(20A)	−3807	930	3003	74
H(21A)	−2430	2829	3387	83
H(22A)	−1258	3734	2435	76
H(23A)	−1494	2740	1106	62
H(1'B)	1402	3642	3606	54
H(1'C)	827	3367	2606	54
H(3'A)	3649	4343	4152	51
H(5'A)	5919	5450	2547	58
H(7'A)	2191	3822	1605	53
H(8'A)	7712	5806	4590	111
H(8'B)	7363	6112	3687	111
H(8'C)	7078	4820	3761	111

H(9'A)	3659	4348	−95	105
H(9'B)	2693	4392	434	105
H(9'C)	3056	3347	404	105
H(10C)	−675	1135	2921	56
H(10D)	71	1783	3870	56
H(13B)	−1611	−390	2074	66
H(14B)	−2735	−2169	1201	76
H(15B)	−2384	−3766	1503	80
H(16B)	−952	−3580	2696	72
H(18B)	579	−2397	4031	63
H(20B)	2150	−1251	5372	76
H(21B)	3322	485	6287	88
H(22B)	3090	2147	6007	83
H(23B)	1713	2062	4816	68

Crystal Data of diimine **34** (R = OMe)

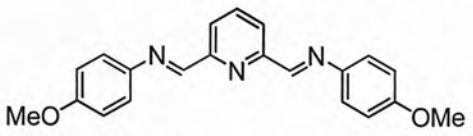

Table 1. Crystal data and structure refinement for p.

Identification code	WY206
Empirical formula	$C_{21}H_{19}N_3O_2$
Formula weight	345.39
Temperature	296(2) K
Wavelength	0.71073 Å
Crystal system, space group	Orthorhombic, *A*ba2
Unit cell dimensions	a = 7.1660(6) Å α = 90 °
	b = 40.204(3) Å β = 90 °
	c = 6.3427(5) Å γ = 90 °
Volume	1827.4(3) Å^3
Z, Calculated density	4, 1.255 Mg/m^3
Absorption coefficient	0.083 mm^{-1}
F(000)	728
Crystal size	0.40 x 0.30 x 0.20 mm
Theta range for data collection	1.01 to 27.95 °
Limiting indices	$-7 \le h \le 9$, $-52 \le k \le 52$, $-8 \le l \le 6$
Reflections collected / unique	6680 / 2019 [R_{int} = 0.0504]
Completeness to θ = 27.95	99.5 %
Absorption correction	multi-scan
Max. and min. transmission	0.7456 and 0.6521
Refinement method	Full-matrix least-squares on F^2
Data / restraints / parameters	2019 / 1 / 119
Goodness-of-fit on F^2	1.000
Final R indices [I > 2σ(I)]	R_1 = 0.0439, $_wR_2$ = 0.0920
R indices (all data)	R_1 = 0.0926, $_wR_2$ = 0.1147
Absolute structure parameter	1(2)
Largest diff. peak and hole	0.123 and −0.230 e.Å^{-3}

Table 2. Atomic coordinates (x 10^4) and equivalent isotropic displacement parameters (A^2 x 10^3) for p.

U(eq) is defined as one third of the trace of the orthogonalized Uij tensor.

	x	y	z	U(eq)
O(1)	−94(2)	2110(1)	4471(3)	53(1)
C(1)	−30(4)	285(1)	154(4)	48(1)
C(2)	−43(4)	293(1)	−2011(5)	60(1)
C(3)	0	0	−3110(7)	70(1)
C(4)	−85(4)	593(1)	1405(5)	55(1)
C(5)	−68(3)	1173(1)	1698(4)	41(1)
C(6)	−872(3)	1449(1)	739(4)	44(1)
C(7)	−881(3)	1754(1)	1708(4)	42(1)
C(8)	−28(3)	1795(1)	3653(4)	41(1)
C(9)	821(3)	1526(1)	4624(4)	47(1)
C(10)	769(3)	1218(1)	3649(4)	47(1)
C(11)	842(5)	2173(1)	6407(5)	70(1)
N(1)	0	0	1255(5)	52(1)
N(2)	−84(3)	874(1)	531(4)	46(1)

Table 3. Bond lengths [Å] and angles [°] for p.

O(1)-C(8)	1.371(2)
O(1)-C(11)	1.422(3)
C(1)-N(1)	1.343(3)
C(1)-C(2)	1.374(4)
C(1)-C(4)	1.469(3)
C(2)-C(3)	1.369(3)
C(3)-C(2)#1	1.369(3)
C(4)-N(2)	1.258(3)
C(5)-C(10)	1.387(4)
C(5)-C(6)	1.391(3)
C(5)-N(2)	1.413(3)
C(6)-C(7)	1.371(3)
C(7)-C(8)	1.387(4)
C(8)-C(9)	1.383(3)
C(9)-C(10)	1.385(3)
N(1)-C(1)#1	1.343(3)
C(8)-O(1)-C(11)	118.31(18)
N(1)-C(1)-C(2)	122.6(2)
N(1)-C(1)-C(4)	116.0(2)
C(2)-C(1)-C(4)	121.4(2)
C(3)-C(2)-C(1)	119.3(3)
C(2)#1-C(3)-C(2)	118.8(4)
N(2)-C(4)-C(1)	121.2(2)
C(10)-C(5)-C(6)	117.7(2)
C(10)-C(5)-N(2)	125.6(2)
C(6)-C(5)-N(2)	116.6(2)
C(7)-C(6)-C(5)	121.3(2)
C(6)-C(7)-C(8)	120.1(2)
O(1)-C(8)-C(9)	124.7(2)
O(1)-C(8)-C(7)	115.5(2)
C(9)-C(8)-C(7)	119.9(2)
C(8)-C(9)-C(10)	119.2(2)
C(9)-C(10)-C(5)	121.8(2)
C(1)#1-N(1)-C(1)	117.3(3)
C(4)-N(2)-C(5)	122.3(2)

Symmetry transformations used to generate equivalent atoms: #1 −x, −y, z

Table 4. Anisotropic displacement parameters (A^2 x 10^3) for p.

The anisotropic displacement factor exponent takes the form:

$-2\pi^2$ [h^2 a^{*2} U11 + ... + 2 h k a* b* U12]

	U11	U22	U33	U23	U13	U12
O(1)	71(1)	36(1)	53(1)	−1(1)	−6(1)	4(1)
C(1)	67(2)	36(2)	41(2)	0(1)	1(1)	−2(1)
C(2)	97(2)	40(1)	44(2)	7(1)	−4(2)	0(1)
C(3)	123(4)	55(2)	33(2)	0	0	−1(2)
C(4)	82(2)	40(1)	42(2)	1(1)	5(2)	−4(1)
C(5)	47(1)	34(1)	41(2)	2(1)	−1(2)	−2(1)
C(6)	50(2)	43(1)	37(1)	4(1)	−5(1)	1(1)
C(7)	48(1)	34(1)	44(2)	8(1)	−3(2)	3(1)
C(8)	44(1)	32(1)	46(2)	3(1)	6(1)	1(1)
C(9)	56(1)	42(1)	42(1)	3(1)	−6(1)	0(1)
C(10)	55(2)	35(1)	51(2)	7(1)	−7(2)	3(1)
C(11)	98(2)	48(2)	63(2)	−14(2)	−16(2)	0(2)
N(1)	80(2)	36(2)	40(2)	0	0	−5(1)
N(2)	56(1)	37(1)	47(1)	−1(1)	−3(1)	−2(1)

Table 5. Hydrogen coordinates (x 10^4) and isotropic displacement parameters (A^2 x 10^3) for p.

	x	y	z	U(eq)
H(2A)	−81	495	−2723	72
H(3)	0	0	−4577	84
H(4A)	−121	579	2868	66
H(6A)	−1415	1427	−585	52
H(7A)	−1460	1934	1059	51
H(9A)	1418	1553	5915	56
H(10A)	1310	1037	4322	56
H(11A)	669	2402	6801	104
H(11B)	2150	2128	6242	104
H(11C)	339	2032	7486	104

Crystal Data of diimine **36** (R = Me)

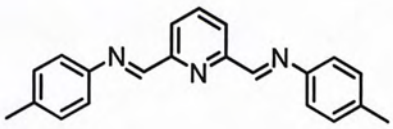

Table 1. Crystal data and structure refinement for p.

Identification code	wy201
Empirical formula	$C_{21}H_{19}N_3$
Formula weight	313.39
Temperature	296(2) K
Wavelength	0.71073 Å
Crystal system, space group	Monoclinic, *P*2/*c*
Unit cell dimensions	a = 4.7249(7) Å α = 90 °
	b = 6.2811(9) Å β = 94.639(3) °
	c = 28.965(4) Å γ = 90 °
Volume	856.8(2) Å^3
Z, Calculated density	2, 1.215 Mg/m^3
Absorption coefficient	0.073 mm^{-1}
F(000)	332
Crystal size	0.50 x 0.40 x 0.30 mm
Theta range for data collection	1.41 to 25.25 °
Limiting indices	$-5 \le h \le 5, -7 \le k \le 7, -34 \le l \le 34$
Reflections collected / unique	11557 / 1566 [R_{int} = 0.0405]
Completeness to θ = 25.25	99.7 %
Absorption correction	multi-scan
Max. and min. transmission	0.7456 and 0.5906
Refinement method	Full-matrix least-squares on F^2
Data / restraints / parameters	1566 / 0 / 111
Goodness-of-fit on F^2	3.356
Final *R* indices [I > 2σ(I)]	R_1 = 0.1742, $_wR_2$ = 0.6124
R indices (all data)	R_1 = 0.1810, $_wR_2$ = 0.6184
Extinction coefficient	0.31(18)
Largest diff. peak and hole	0.544 and −0.451 e.Å^{-3}

Table 2. Atomic coordinates (x 10^4) and equivalent isotropic displacement parameters (A^2 x 10^3) for p.

U(eq) is defined as one third of the trace of the orthogonalized Uij tensor.

	x	y	z	U(eq)
N(1)	0	6305(10)	2500	48(2)
N(2)	5501(10)	6935(8)	3400(2)	53(2)
C(1)	0	10724(13)	2500	60(3)
C(2)	1842(12)	9622(10)	2801(2)	56(2)
C(3)	1797(11)	7400(9)	2795(2)	45(2)
C(4)	3709(12)	6109(9)	3107(2)	50(2)
C(5)	7361(12)	5638(9)	3683(2)	48(2)
C(6)	8606(15)	6494(11)	4085(2)	63(2)
C(7)	10497(14)	5365(12)	4369(2)	68(2)
C(8)	11291(13)	3287(12)	4268(2)	61(2)
C(9)	10077(14)	2446(11)	3848(2)	64(2)
C(10)	8197(14)	3556(10)	3563(2)	59(2)
C(11)	13379(17)	2040(15)	4572(3)	86(3)

Table 3. Bond lengths [Å] and angles [°] for p.

N(1)-C(3)	1.344(6)
N(1)-C(3)#1	1.344(6)
N(2)-C(4)	1.260(6)
N(2)-C(5)	1.411(7)
C(1)-C(2)	1.369(7)
C(1)-C(2)#1	1.369(7)
C(2)-C(3)	1.396(9)
C(3)-C(4)	1.470(7)
C(5)-C(6)	1.372(8)
C(5)-C(10)	1.417(9)
C(6)-C(7)	1.363(8)
C(7)-C(8)	1.396(11)
C(8)-C(9)	1.404(9)
C(8)-C(11)	1.491(8)
C(9)-C(10)	1.356(8)
C(3)-N(1)-C(3)#1	118.4(6)
C(4)-N(2)-C(5)	120.4(5)
C(2)-C(1)-C(2)#1	119.3(7)
C(1)-C(2)-C(3)	119.2(5)
N(1)-C(3)-C(2)	121.9(5)
N(1)-C(3)-C(4)	115.7(5)
C(2)-C(3)-C(4)	122.3(5)
N(2)-C(4)-C(3)	122.2(5)
C(6)-C(5)-N(2)	118.1(5)
C(6)-C(5)-C(10)	117.4(5)
N(2)-C(5)-C(10)	124.3(5)
C(7)-C(6)-C(5)	121.5(6)
C(6)-C(7)-C(8)	122.3(6)
C(7)-C(8)-C(9)	115.8(6)
C(7)-C(8)-C(11)	122.9(6)
C(9)-C(8)-C(11)	121.3(7)
C(10)-C(9)-C(8)	122.4(6)
C(9)-C(10)-C(5)	120.5(6)

Symmetry transformations used to generate equivalent atoms: #1 −x, y, −z+1/2

Table 4. Anisotropic displacement parameters (A^2 x 10^3) for p.

The anisotropic displacement factor exponent takes the form:

$-2\pi^2$ [h^2 a^{*2} U11 + ... + 2 h k a* b* U12]

	U11	U22	U33	U23	U13	U12
N(1)	49(4)	39(3)	52(4)	0	−12(3)	0
N(2)	61(3)	48(3)	49(3)	−3(2)	−6(2)	−4(2)
C(1)	70(6)	38(4)	71(6)	0	−3(4)	0
C(2)	64(4)	46(4)	57(4)	−5(2)	2(3)	−4(2)
C(3)	52(4)	41(3)	43(3)	−2(2)	3(2)	−10(2)
C(4)	53(4)	44(3)	51(4)	4(2)	−7(3)	−9(2)
C(5)	47(3)	49(3)	48(3)	4(2)	−1(2)	−4(2)
C(6)	75(4)	56(4)	55(4)	2(3)	−4(3)	1(3)
C(7)	65(4)	80(5)	54(4)	1(3)	−17(3)	−4(3)
C(8)	49(4)	74(4)	59(4)	14(3)	−2(3)	−1(3)
C(9)	65(4)	59(4)	67(4)	5(3)	−1(3)	7(3)
C(10)	62(4)	62(4)	51(3)	−7(3)	−6(3)	−1(3)
C(11)	86(5)	98(6)	71(5)	23(4)	−12(4)	24(4)

Table 5. Hydrogen coordinates (x 10^4) and isotropic displacement parameters (A^2 x 10^3) for p.

	x	y	z	U(eq)
H(1)	0	12205	2500	72
H(2B)	3109	10346	3008	67
H(4A)	3592	4633	3088	60
H(6A)	8150	7878	4166	75
H(7A)	11286	6001	4639	81
H(9A)	10580	1079	3763	77
H(10A)	7450	2947	3287	71
H(11A)	13978	2867	4841	129
H(11B)	14996	1703	4405	129
H(11C)	12506	747	4666	129